7-12-2014

A TECHNIQUE FOR MEASURING THE TIME RESPONSE AND THROUGH-PUT DELAY OF NEUTRON TIME-OF-FLIGHT (nTOF) SCINTILLATION DETECTORS USING COSMIC RADIATION IN A COINCIDENCE SYSTEM

Michael Bonura

Michael Andrew Bonura
Candidate

Chemical and Nuclear Engineering
Department

This thesis is approved, and it is acceptable in quality and form for publication:

Approved by the Thesis Committee:

Gary W. Cooper, Chairperson

Robert D. Busch

Carlos L. Ruiz

A TECHNIQUE FOR MEASURING THE TIME RESPONSE AND THROUGH-PUT DELAY OF NEUTRON TIME-OF-FLIGHT (nTOF) SCINTILLATION DETECTORS USING COSMIC RADIATION IN A COINCIDENCE SYSTEM

by

MICHAEL A BONURA

B.S. HISTORY
UNITED STATES MILITARY ACADEMY, 1997
M.A. HISTORY
THE FLORIDA STATE UNIVERSITY, 2006
PH.D. HISTORY
THE FLORIDA STATE UNIVERSITY, 2008

THESIS

Submitted in Partial Fulfillment of the
Requirements for the Degree of

Master of Science
Nuclear Engineering

The University of New Mexico
Albuquerque, New Mexico

May, 2014

DEDICATION

I would like to dedicate this work to my family. Over the course of the last 4 years, my family has supported me through all of the late night homework and study sessions and the time I had to be away from them both while I was working full time and when I transitioned to being a student full time. They picked up the slack at home and made it possible for me to keep going and become a Nuclear Engineer.

I would like to thank my mother-in-law Sandra for entertaining the kids so that I could work and for covering the housework that I usually did when the requirements of my graduate study prevented me from pitching in. I would like to thank my kids Kyra and Erik for being very supportive throughout this process. They often wished me well and that I should have fun at school. They helped me do my homework and even began to do ñhomeworkò themselves. I hope my example showed them that learning can be fun even while it is hard work.

Of course, the most important person in my life is my wife Kimberlee. Without her support none of my success would have been possible. She is my best friend and an excellent sounding board for ideas both personal and academic. While I dedicate this mastersô thesis to my whole family, it is really dedicated to her. I literally could not have done it without her.

ACKNOWLEDGEMENTS

Just as the support of my family was crucially important to my success, there are many people who contributed to my academic success. First and foremost, I would like to acknowledge the help and support of Dr. Gary Cooper. He has been teaching and mentoring me since I started taking undergraduate nuclear engineering classes in preparation for doing graduate studies. He graciously accepted me as a graduate student late in the game and has gone out of his way to make me successful. I would also like to thank Dr. Carlos Ruiz for his help, guidance, and example. I am honored that he took an active interest in my development and handed off to me the cosmic radiation experiments that he had been planning for some time. If I have become a nuclear engineer, it is in large part due to his mentorship. He spent a lot of his time answering questions and discussing nuclear physics with me so that I thoroughly understood all of the principles that went into my experiments. I would also like to thank the members of Department 1677 Dr. Gordon Chandler, Dr. Alan Nelson, Dr. Kelly Hahn, Jed Styron, Mr. José Torres and Ms. Ruth Smelser for all of their help, advice, and support. This impressive team of scientists and technicians are dedicated to their profession and committed to doing good experimental science. I would also like to thank the Sandia National Laboratories management that has supported my research, in particular Dr. Greg Rochau and Dr. Joel Lash.

My academic success began at the Department of Chemical and Nuclear Engineering even before I was admitted into the graduate program. I took a large number of undergraduate courses in preparation for doing graduate work, and my undergraduate peers were vital to that success. I would also like to thank Dr. Robert Busch and Mr. Ken

Carpenter for their constant support throughout my studies. Both in the classroom and out, they spent countless hours ensuring that I understood the nuclear reactor physics and the basics of nuclear engineering. They bent over backwards to make sure I had the support I needed to be successful, and I am a better student, nuclear engineer, and man because of it. I would also like to thank the department staff for helping me to navigate the often obtuse university policy each and every semester for the past four and a half years. In particular, I would like to thank Ms. Jocelyn White, Ms. Jasmine Torres, and Ms. Cheryl Brozena. I need a lot of help, and they always made time to square me away.

A TECHNIQUE FOR MEASURING THE TIME RESPONSE AND THROUGH-PUT DELAY OF NEUTRON TIME-OF-FLIGHT (nTOF) SCINTILLATION DETECTORS USING COSMIC RADIATION IN A COINCIDENCE SYSTEM

By

Michael Andrew Bonura

B.S., History, United States Military Academy, 1997

M.A., History, Florida State University, 2006

Ph.D., History, Florida State University, 2008

M.S., Nuclear Engineering, University of New Mexico, 2014

ABSTRACT

Plastic scintillator-based neutron time-of-flight (nTOF) detectors are used to measure neutron signals from fusion experiments. These nTOF signals yield a temporal pulse width that is used to determine ion temperatures after the de-convolution of the experimentally determined detector time response and shifted to account for the detector through-put delay. Typically, time response and through-put delays are measured at an accelerator or laser facility. However, an alternative method can use cosmic radiation to measure time response and through-put delay. Two plastic scintillator detectors in a coincidence system can detect an incident cosmic ray. If a third nTOF detector is placed between these coincident detectors, the output cosmic ray signal in the nTOF detector can be analyzed to produce the time response and through-put delay. Measurements taken using cosmic radiation were mostly within one standard deviation of data taken on the same detectors at an electron accelerator.

TABLE OF CONTENTS

TABLE OF FIGURES

LIST OF TABLES

CHAPTER 1: INTRODUCTION

As a cleaner alternative to fission nuclear reactors, scientists and engineers have spent the last seventy years attempting to create energy from fusion. To produce energy from fusion, nuclear fuels must be confined long enough at a sufficiently high temperature to achieve high enough rates of exothermic reactions. The two most readily attainable fusion reactions, which release large amounts of energy, are the deuterium and tritium reactions that make up Equations 1 through 3.

$$d + T \rightarrow {}^{4}He + n + 17.6\ MeV \quad (1)$$

$$d + d \rightarrow p + T + 4.03\ MeV \quad (2)$$

$$d + d \rightarrow {}^{3}He + n + 3.27\ MeV \quad (3)$$

where d is deuterium, T is tritium and n is a neutron. As indicated, there is only one significant reaction pathway for deuterium reacting with tritium but, there are two possible reaction pathways for deuterium reacting with itself. The two deuterium-on-deuterium reactions occur with almost equal probability.[1]

To create the right conditions for these fusion reactions to occur, there has to be an external confinement mechanism to overcome the electrostatic repulsion of the fusion reactants in the fuel. Among these is the inertial confinement mechanism. Over the past few decades, extensive research on inertial confinement fusion has been conducted at facilities such as the National Ignition Facility (NIF) at Lawrence Livermore Laboratories and the Z Machine at Sandia National Laboratories. In inertial confinement fusion (ICF), a small spherical shell of fuel, proportional to its radius, is rapidly compressed to

[1] A. A. Harms, et al., *Principles of Fusion Energy: An Introduction to Fusion Energy for Students of Science and Engineering* (London: World Scientific, 2000), 8, 47.

extremely high densities achieving a thousand times solid density. This compression creates a ñhot spotò at the center of the compressed fuel, which results in a fusion burn wave that propagates to the outer regions of the fuel. The entire process takes place so rapidly that the inertia of the fuel mass keeps the fuel together long enough that more fusion energy can be produced than was required to create the fusion conditions.[2]

Because neutrons are the only fusion product that escapes the ICF fuel largely unperturbed, measuring the properties of the emitted neutrons can provide important information about the fusion conditions in an experiment. Most fundamentally, measuring the number of neutrons emitted corresponds directly to the number of fusion reactions that occurred. The measured emitted neutron energy spectrum provides two critically important parameters about the fusing plasma. As a result of the energy released in the deuterium-tritium or deuterium-deuterium reactions, neutrons are produced with with an energy spectrum centered at 14.1 MeV or 2.45 MeV, respectively. Knowing these energies and the arrival time at a distant detector, the time of the fusion burn (the ñbangò time) can be measured. This measurement is particularly important in Sandia National LaboratoriesôZ experiments because, unlike the case of laser driven fusion, no ñtime equals zeroò of the fusion burn is otherwise available.

In addition, these neutrons will carry energy contributions from the kinetic energies of the reacting ions. If the reacting ions have a Maxwellian distribution (*i.e.* a ñthermalò plasma), there will be a Gaussian distribution of the neutron energy spectrum.[3] Thus, if the energy spectrum or converted time-of-flight spectrum can be measured, the

[2] Denis Keefe, "Inertial Confinement Fusion," *The Annual Review of Nuclear Particle Science* 32 (1982), 393.
[3] T.J. Murphy, et al., "Neutron Time-of-Flight and Emission Time Diagnostics for the National Ignition Facility," *Review of Scientific Instruments* 72 (2001): 6-9.

temperature of the Maxwellian distributed ions is determined. Further, if the density of the fuel is substantial, there will be significant down scattering of neutrons in the fuel itself. Measuring this ñdown-scattered fractionò allows one to determine the fuel density, another important parameter in ICF. The differences in neutron energies, particularly for the temperature measurement, are so small that they cannot be measured directly. Instead a neutron time-of-flight (nTOF) measurement technique is used, in which the dd or dT neutron spectrum is converted to a time spectrum by taking advantage of the fact that the neutrons are born almost instantaneously in time (sub-nanosecond). Then neutrons are allowed to propagate over a long distance (6-25 meters) to a detector that time resolves the signal. For practical source-to-detector distances, the broadening due to a Gaussian distribution is typically on the order of at most a few tens of nanoseconds for deuterium-deuterium reactions, and only a few nanoseconds for deuterium-tritium reactions. In either case, precise knowledge of the detectorôs time response is essential, because it is used to unfold the full width at half maximum (FWHM) of the time-distributed signal, which yields the temperature of the fusion plasma. The observed signal width will include in addition to the thermal broadening of interest, the fundamental time response of the detector (a delta function input pulse will give an output signal of finite width) and the variation in possible interaction times as the neutrons propagate through the detector. These time responses must be known and unfolded from the total output signal to obtain the desired thermal broadening and subsequent determination of temperature.

Knowing the through-put time of the detector is also essential to accurately determine the bang time that the neutrons are produced. The through-put of this detector consists of the time between the interaction of the neutron with a proton in the scintillator

and the creation of an output signal. In this work, an inexpensive method is investigated which uses cosmic radiation as a signal source to accurately determine the time response and through-put of nTOF detectors.

SECTION 1: Directly Detecting Neutrons

Neutron Time-of-Flight (nTOF) Spectrometry

A common method of neutron spectrometry for neutrons of energies below 15 MeV is neutron time of flight spectrometry in which the time-of-flight of a neutron is measured using a scintillation detector. If the time of flight of the incident neutron is known and the distance between the origin and the detector is known, then the relationship between the neutron time-of-flight and the neutron energy is determined using Equation 4.

$$t_F = \frac{72.3\,D}{\sqrt{E_n}} \tag{4}$$

Where t_F is the neutron time-of-flight in nanoseconds, D is the distance between the scintillation detector and the origin in meters, and E_n is the neutron energy in MeV.[4] Because of the precise nature of laser-generated implosions (sub-picosecond) where the bang time is very precisely determined, NIF scientists utilize this technique to measure neutron energies.[5]

Pulsed power fusion experiments do not have an accurate way of determining the fusion bang time. To do so, a system of two or more nTOF detectors at different distances determines the neutron energy spectrum. The Z Facility at Sandia National Laboratories

[4] J. B. Birks, *The Theory and Practice of Scintillation Counting* (New York: Pergamon Press, 1964), 409-410.
[5] M. Gatu Johnson, et al., "Neutron spectrometry- An essential tool for diagnosing implosions at the National Ignition Facility," *The Review of Scientific Instruments* 83, number 10 (2012): 10D308-4.

utilizes nTOF detectors at several distances from the neutron sources.[6] As the neutron interacts with the scintillator in a pair of detectors, Equation 4 can still be used to determine the neutron energy. The time of flight becomes the time between the signal from the first detector and the corresponding signal from the second detector. The distance between the detectors must also be known to determine neutron velocity and subsequent neutron energy at a discrete point in time. Plastic scintillator detectors afford the necessary timing accuracy needed to determine the energy of neutrons.

Proton Recoil Spectrometry

Because the neutron has no charge, it is difficult to detect them using the techniques applied to ionizing radiation. One of the most effective ways of directly detecting neutrons is through the elastic scattering of neutrons by target nuclei of low atomic number. Of the possible targets for neutron scattering, the most efficient is that of protons, thus leading to proton recoil detectors. This is because in a collision with a proton, the spectrum of energy transferred from the incident neutron to the recoil proton ranges from zero to the incident neutron energy.[7] This relationship is described by Equation 5:

$$E_R = \frac{2A}{(1+A)^2}(1 - \cos\Theta)E_n \qquad (5)$$

where A is the target nucleus mass number divided by the neutron mass, E_n is the neutron kinetic energy, E_R is the recoil nucleus, $\bar{U}$ is the scattering angle of the neutron. In situations where the incident neutron only grazes the proton, Equation 5 shows that the

[6] A. J. Nelson, et al., "A novel method for modeling the neutron time of flight detector response in current mode to inertial confinement fusion experiments," *The Review of Scientific Instruments* 83 (2012): 10D915-2.

[7] Glenn F. Knoll, *Radiation Detection and Measurement,* 4th ed. (New York: John Wiley & Sons, Inc., 2010), 570-575.

recoil energy would be near zero and the change in the neutron energy would be similarly negligible. This allows two proton recoil detectors to provide accurate neutron time-of-flight data, and thus accurate neutron energy measurements.

Because of the large amount of hydrogen relative to other constituents, organic (plastic) scintillators can be used in proton recoil detection. With a high cross section for scattering of neutrons, the hydrogen produces a relatively high efficiency neutron detector with a relatively thin scintillator thickness.[8] Plastic scintillators, thus, are widely used for time-of-flight spectroscopy due to their relative inexpensiveness, high efficiency, and the ability to make them in a wide variety of geometries.

Section 2: Scintillation Detectors

Scintillator Time Resolution

Another characteristic of plastic scintillators is their relatively short time resolution. The time resolution of the plastic scintillator itself is quite small, normally from 1 to 4 ns.[9] Thus the theoretically shortest resolving time of a plastic scintillator is given by Equation 6:

$$\bar{t} \cong \frac{\tau}{R} \tag{6}$$

where Űis the scintillator decay constant of the scintillator light and R is the number of photo-electrons released from the photo-cathode of the light collecting photo-multiplier tube (PMT).[10] However, to measure the output signal of a scintillation detector requires a PMT and there are statistical properties of the PMT that makes recording detector output

[8] J. A. Harvey and N.W. Hill, "Scintillation Detectors for Neutron Physics Research," *Nuclear Instruments and Methods* 162 (1979): 508.
[9] P. B. Lyons and J. Stevens, "Time Response of Plastic Scintillators," *Nuclear Instruments and Methods* 114 (1974): 317.
[10] M. A. El-Wahab and J. V. Kane, "An Analytic Treatment for Scintillation Counter Time Resolution Functions," *Nuclear Instruments and Methods* 15 (1962): 15.

signals with the theoretically shortest time resolution of the system difficult. There are two main sources of these properties: the first is the photo-electronic emission from the cathode, and the second is the single electron response of the PMT electron multiplier. The statistical property of the photo-cathode emission is dependent on the time law of the photo-cathodeôs illumination combined with Poisson statistics (assumed for the electrons) to create an illumination function described by Equation 7:

$$I(t) = \frac{R}{\tau} exp\left(-\frac{t}{\tau}\right) \qquad (7)$$

where R is the average number of photoelectrons due to scintillation and Ű is the decay time constant of the light pulse. The statistical properties of the single electron response have three elements: the average pulse shape $(\mathring{U}_{\partial})^2$, the average charge A or $(\mathring{U}_A)^2$, and an average time position h with respect to the time emission of the photo-electron $(\mathring{U}_{ph})^2$. Each of these properties has individual variances. These variances are quoted as $(\mathring{U}_{\partial})^2$ = 1/200; $(\mathring{U}_A)^2$ = 1/3 and $(\mathring{U}_{ph})^2$ = (5E-10)^2 sec^2.[11] These variances constitute the difference between the analytical calculations of time resolution and the experimentally measured time resolution.

Detector Time Response Function

The time resolution of the scintillator-light guide-PMT system is the time response of the detector, and the time history of that response is important when unfolding the time-of-flight data to ensure the measurement of an accurate neutron energy spectrum.[12] This is because when the time-of-flight signal is measured, it includes

[11] E. Gatti and V. Svelto, "Time resolution in scintillation counters," in J. B. Birks, editor, *Proceedings of the Symposium on Nuclear Instruments* (Manchester: Victoria University of Manchester, 1962),35-37.; R. F. Post and L. I. Schiff, "Statistical Limitations on the Resolving Time of a Scintillation Counter," *Physical Review* 80 (1950): 1113.

[12] D. J. Thomas, "Neutron spectrometry," *Radiation Measurements* 45 (2010): 1179.

the true neutron signal along with the detector response function. If the detector response function is known, then a Fourier de-convolution technique can be used to unfold the data to yield the real time-of-flight signal.[13] The most accurate way to determine the detector time response function is to experimentally measure that time response function. These studies often use accelerator-based gamma-ray (bremsstrahlung) producing reactions as a source of radiation impinging on the detector.[14] However, these studies are expensive and the requires the availability of an accelerator facility. As an alternative, cosmic radiation energetic enough charged particles that can be used as a source required to measure a detector time response function.

Scintillation Detectors and Cosmic Radiation

Briefly, the cosmic radiation originating in outer space that is incident on the Earthôs surface undergoes interactions in the upper Earth atmosphere. The primary cosmic radiation consists of protons, alpha particles, and heavier nuclei. This radiation interacts with the interplanetary magnetic field, is affected by solar activity, and interacts with the electrons, molecules, and nuclei in the Earthôs atmosphere.[15] These interactions create cosmic particle air showers.[16] These cosmic air showers contain non-ionizing particles such as neutrons, hadrons, and gamma rays and ionizing particles such as

[13] T. J. Murphy, R. A. Lerche, and C. Bennett, G. Howe, "Ion Temperature Measurements of Indirectly Driven Implosions Using a Geometry Compensated Neutron Time-Of-Flight Detector," *The Review of Scientific Instruments* 66, (1995): 931.

[14] E. Gatti, V. Svelto, "Time resolution in scintillation counters," in J. B. Birks, editor, *Proceedings of the Symposium on Nuclear Instruments* (Manchester: Victoria University of Manchester, 1962), 313; W. Bartl, P. Weinzierl, "Experimental Investigation on the Limits of Time Resolution of Scintillation Counters," *The Review of Scientific Instruments* 34 (1963): 253; A. Fallu-Labruyere, H. Tan, W. Hennig, and W. K. Wardurton, "Time resolution studies using digital constant fraction discrimination," *Nuclear Instruments and Methods in Physics Research A* 579 (2007): 248; B. Bengtson, M. Moszynski, "Timing Properties of Scintillation Counters," *Nuclear Instruments and Methods* 81 (1970): 110.

[15] K. Peter and F. Grieder, *Cosmic Rays at Earth: Researcher's Reference Manual and Data Book*, (New York: Elsevier, 2001), 2-3.

[16] Todor Stanev, *High Energy Cosmic Rays*, 2nd edition (Chichester: Springer, 2010), 179-221.

electrons, pions, and muons.[17] Electrons make up the bulk of these charged particles because they are created by pair production from decaying pions, decaying muons, and knock-on electrons ejected by primary and secondary cosmic radiation. Muons constitute the primary decay products of pions. Protons and the heavy nuclei from the primary cosmic radiation are attenuated in the upper atmosphere and often do not penetrate to sea level.[18] Because of their mass is over 200 times that of electrons, the cosmic air shower muons are the most abundant cosmic radiation that penetrates from the upper atmosphere to sea level.[19]

These muons are heavy charged particles and lose energy mostly through ionization. It has been demonstrated that plastic scintillators provide a simple and effective way of detecting relativistic heavy charged particles.[20] Plastic scintillator detectors are currently being used to detect cosmic ray muons, and are considered to have the most effective combination of muon sensitivity of a cost effective detector that has a long lifespan.[21] Recently, there have been a number of experiments that have used cosmic ray muons to calibrate plastic scintillator detectors. In 2009, experiments at the Swedish National Electron Accelerator Facility in coordination with the University of Lund, Sweden demonstrated that it was possible to energy calibrate plastic scintillator detectors using cosmic ray muons.[22] Additionally, calibration experiments at the National Key

[17] A. D. Bray, et al., "Response of Plastic Scintillators to Cosmic Ray Air Showers," *The Review of Scientific Instruments* 36 (1965): 588.
[18] Stanev, *High Energy Cosmic Rays*, 198, 231, 275.
[19] Bogdan Mitrica, "20 years of cosmic muons research performed in IFIN-HH," *Exotic Nuclei and Nuclear/Particle Astrophysics (IV) From Nuclei to Stars AIP Conference Proceedings* (2010): 291-293.
[20] C. L. Ruiz, R. W. Huggett, P. N. Kirk, "Response of Plastic Scintillation Counters to Relativistic Heavy Ions," *Nuclear Instruments and Methods* 159 (1979): 59.
[21] M. Platino, et. al., "Fabrication and testing system for plastic scintillator muon counters used in cosmic showers detection," *32nd International Cosmic Ray Conference, Beijing* vol. 4 (2011): 330.
[22] David Jacobsson, "Calibration of plastic-scintillator detectors at MAX-lab in preparation for ($\supset$, $\acute{}^{+}$) experiments" (thesis, Lund University, 2009), 1-31.

Laboratory of Laser Fusion of the China Academy of Engineering Physics compared the detector time response functions using photon, cosmic rays, and pulsed 14,1 MeV dT neutron sources.[23] Although they found that the time response using cosmic radiation was 18% less than the pulsed neutron source, it was closer to the time response using the neutron source than photon sources. Thus cosmic radiation may be a better calibration source than accelerator-produced photons.

[23] J. B. Chen, *et al*., "Calibration of the time response functions of a quenched plastic scintillator for neutron time of flight," *Nuclear Instruments and Methods in Physics Research A* 491 (2002): 476-477.

CHAPTER 2: EXPERIMENTAL SET-UP

This experiment was designed to investigate the use of cosmic rays to measure the time response function of a nTOF detector. The relativistic cosmic rays are energetic enough to pass through and deposit energy in several stacked scintillation detectors. Thus, it is possible to use a coincidence system with two scintillation detectors placed in line. These detectors will respond to cosmic rays from a wide variety of directions. However, some cosmic rays will travel through both detectors recording a coincident signal from a single cosmic ray. This coincident ray can be used to determine the time when the incident ray passes through the detectors. If a nTOF detector of interest is then placed between these two coincidence detectors, the time response of the nTOF detector can be measured. This experimental arrangement is displayed in Figure 1.

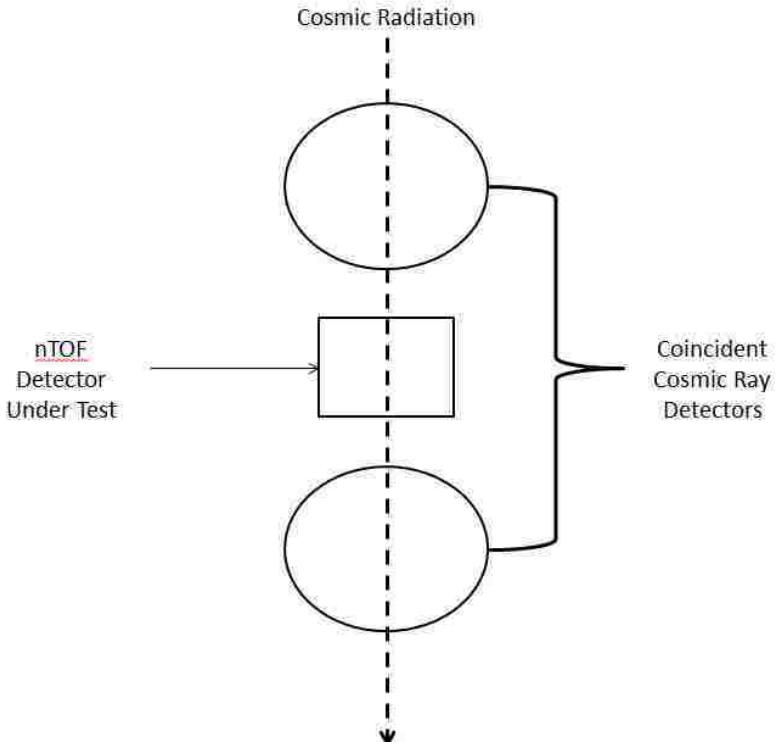

Figure 1: General Cosmic Radiation Experimental System

If the coincident signal from the two cosmic detectors is used to externally trigger an oscilloscope connected to the nTOF detector, then the oscilloscope will record the simultaneous signal from the nTOF detector. This waveform contains both the through-put and the pulse width of the nTOF detector.

Section 1: Coincidence Detector Characterization

Coincidence Detector Design

The coincidence cosmic detectors in this system employ two identically designed plastic scintillator-PMT detectors. The diagram of the coincidence detectors is displayed in Figure 2. Each detector consists of a 7.62 cm diameter by 1.27 cm thick BC404 plastic scintillator coupled to a Hamamatsu R329 PMT via a Lucite light guide. The cosmic coincidence detectors are operated in single-event mode. The BC404 specifications are located in Appendix A. The specifications of the R329 PMT are located in Appendix B.

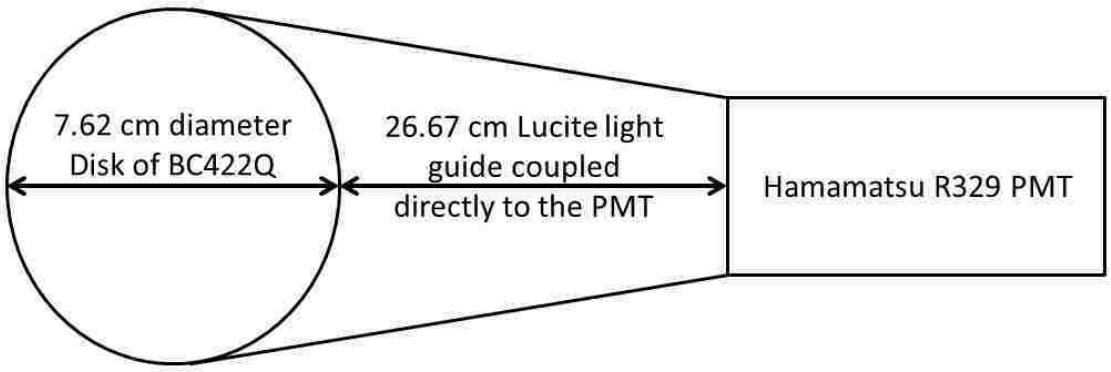

Figure 2: Plastic Scintillation-PMT Detector Design

Counting Plateaus with Scintillation Detectors

To determine the optimal operating PMT voltage bias for the coincidence detectors, a counting plateau must be measured. The counting plateau will identify the range of bias settings in which the output signals are most stable. This is accomplished by introducing a source that produces mono-energetic radiation at a constant rate and then measuring the

resulting outputs through the PMT and a counting system. There will be a steep slope at lower voltage settings as the pulse heights are too small to pass through the discriminator of the counting system, and an exponentially increasing slope at higher voltages due to the onset of regeneration effects in the PMT such as after-pulsing and saturation effects. Between these two phenomena there will be a plateau where the slope is relatively stable and less sensitive to changes in bias.[24] The bias setting that is between the first 30% and 50% of the plateau provides an operating bias that is most stable for the type of incident radiation used in creating the plateau. For scintillators, the plateau is much less pronounced than for other types of detectors as demonstrated by the plateau for a plastic scintillator detector using a ^{207}Bi source in Figure 3 as it appeared in *Techniques for Nuclear and Particle Physics Experiments*

.

[24] W. R. Leo, *Techniques for Nuclear and Particle Physics Experiments: A how to Approach,* 2nd ed. (New York: Springer-Verlag, 1994), 209.

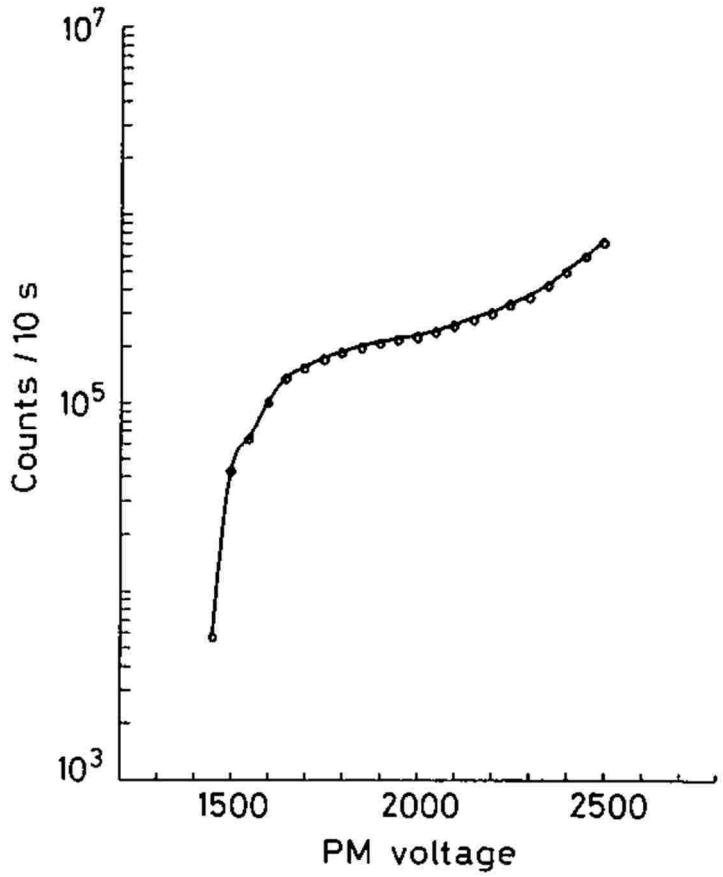

Figure 3: Measured Plateau Curve for Plastic Scintillator[25]

The plateau for the curve in Figure 3 is between 1800V and 2000V. This plateau depends on intrinsic factors of the scintillator as well as extrinsic factors of the discriminator and the PMT. The intrinsic factors depend on the spectrum of the radiation incident on the scintillator while the extrinsic factors include the threshold value of the discriminator and the gain-voltage characteristics of the PMT.[26]

For the coincidence detectors, counting plateaus were measured using cosmic rays, a 6.66 nCi Co-60 source and a 785.83 nCi Ba-133 source. The Co-60 and Ba-133 sources were used as a gamma sources with high activity of almost mono-energetic

[25] Ibid., 210.
[26] Ibid., 210.

photons. The two detectors were designated as cosmic detectors 10 and 11 respectively. The output signal of each detector was connected to an Ortec NIM Model 935 Quad 200-MHz Constant-Fraction Discriminator (CFD). The importance of constant fraction discrimination in measuring output signals of varying amplitudes is discussed in Appendix C, and the specifications of the Ortec NIM Model 935 are located in Appendix D. The discriminator threshold of the Ortec NIM Model 935 was set at the manufacturerôs minimum threshold recommendation of 50 mV. The negative output TTL pulse from the Ortec NIM Model 935 was then connected to an Ortec NIM Model 772 Counter. The specifications of the Ortec NIM Model 772 Counter are located in Appendix E. Each connection was done by employing 50-Ohm RG-223 coaxial cable. The experimental set-up for the counting plateaus is located in Figure 4.

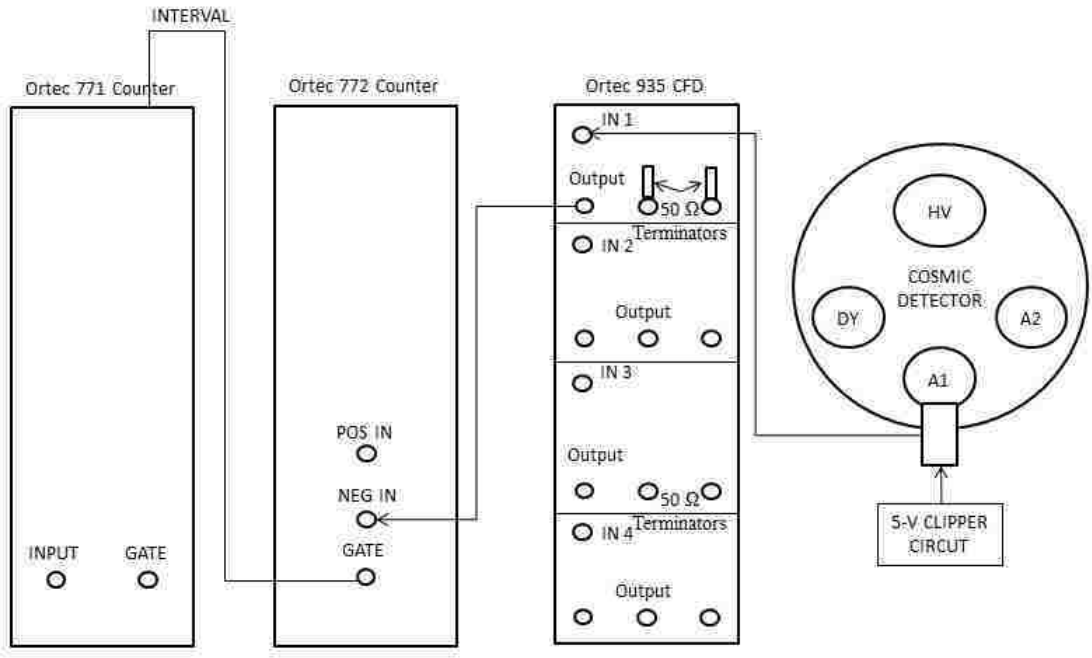

Figure 4: Counting Plateau Experimental Set-up

Measurements were taken over 300 second intervals. An Ortec NIM Model 771 Timer-Counter was used to set the 300 second interval. The specifications of the Ortec NIM Model 771 are located in Appendix O. A cable connected the interval output of the Ortec NIM Model 771 to the gate connecter of the Ortec NIM Model 772. Initial counting plateaus were determined with cosmic radiation for bias settings ranging from -1000 V to -2500 V on the PMT. The results from cosmic detector 10 and cosmic detector 11 are displayed in Figures 5 and 6, respectively. The plateaus for cosmic detectors 10 and 11 resembled the plateau as shown in Figure 3 but with a steeper slope and a plateau that was less sharp.

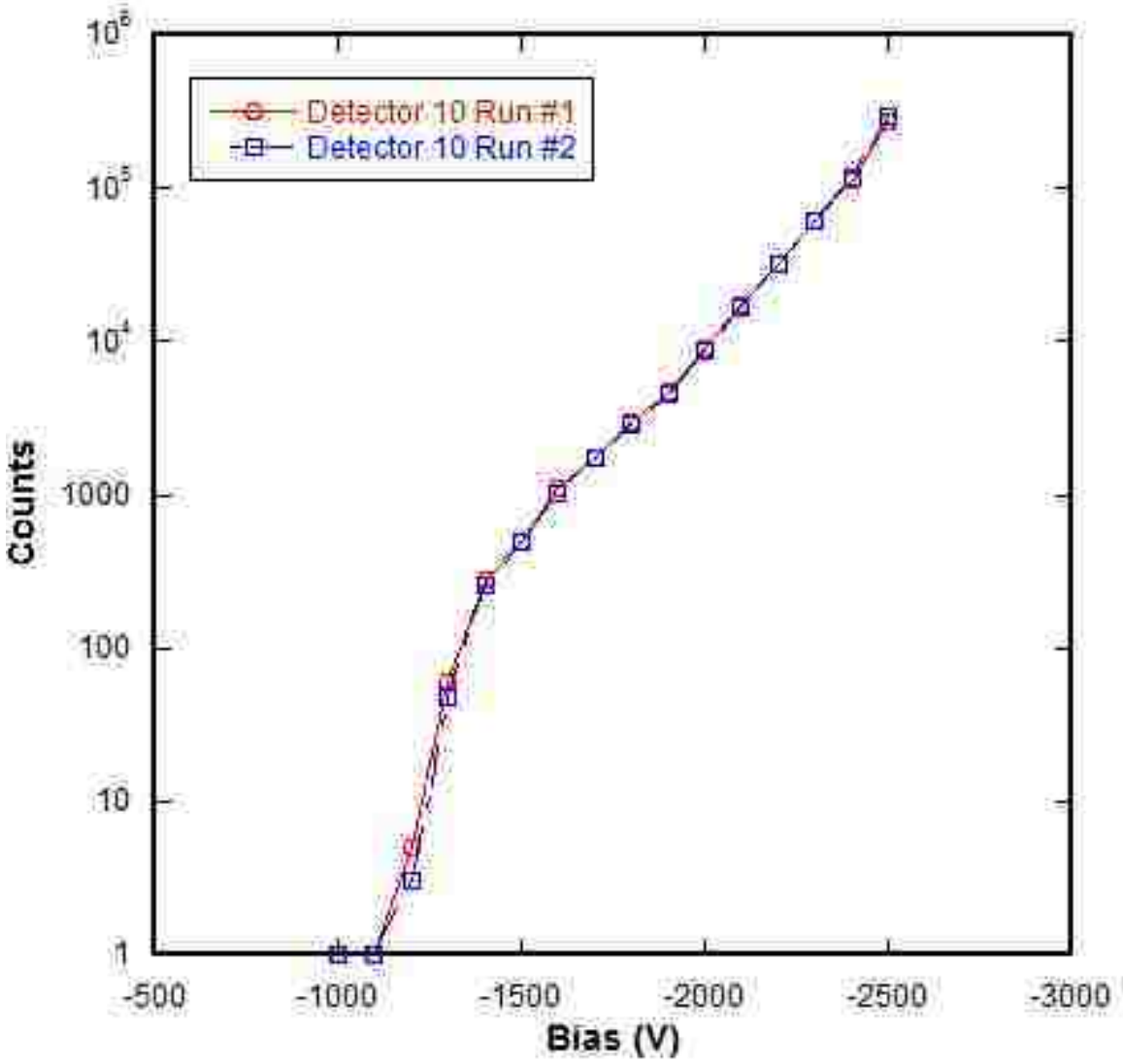

Figure 5: Cosmic Detector 10 Cosmic Radiation Counting Plateau at 50 mV Threshold

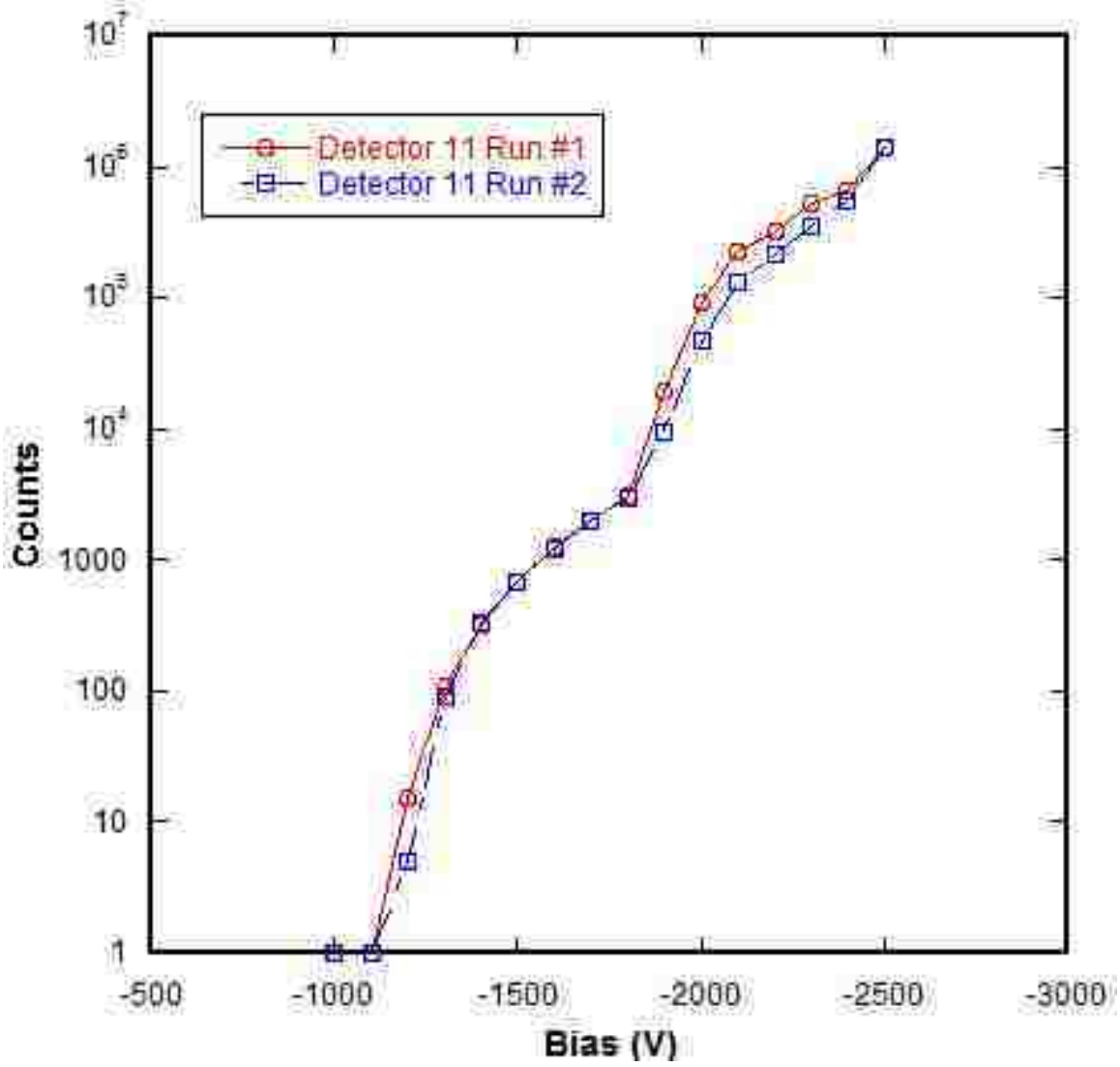

Figure 6: Cosmic Detector 11 Cosmic Radiation Counting Plateau at 50 mV Threshold

There was little evidence of real plateauing in either cosmic detector 10 or cosmic detector 11, although there seemed to be a stable area between -1700 V and -1800 V. The measurement of cosmic radiation at bias settings from -1000 V to -1300 V yielded extremely low count rates. Measurements taken at bias settings above -1900 V yielded count rates that increased with a steep slope and were the result of a saturated PMT due to the exponential increase in counts above -1900V. Therefore, the counting plateaus

using the Co-60 and Barium sources were measured with bias settings between -1300 V and -1800 V. The results for cosmic detector 10 and cosmic detector 11 are displayed in Figures 7 and 8 respectively.

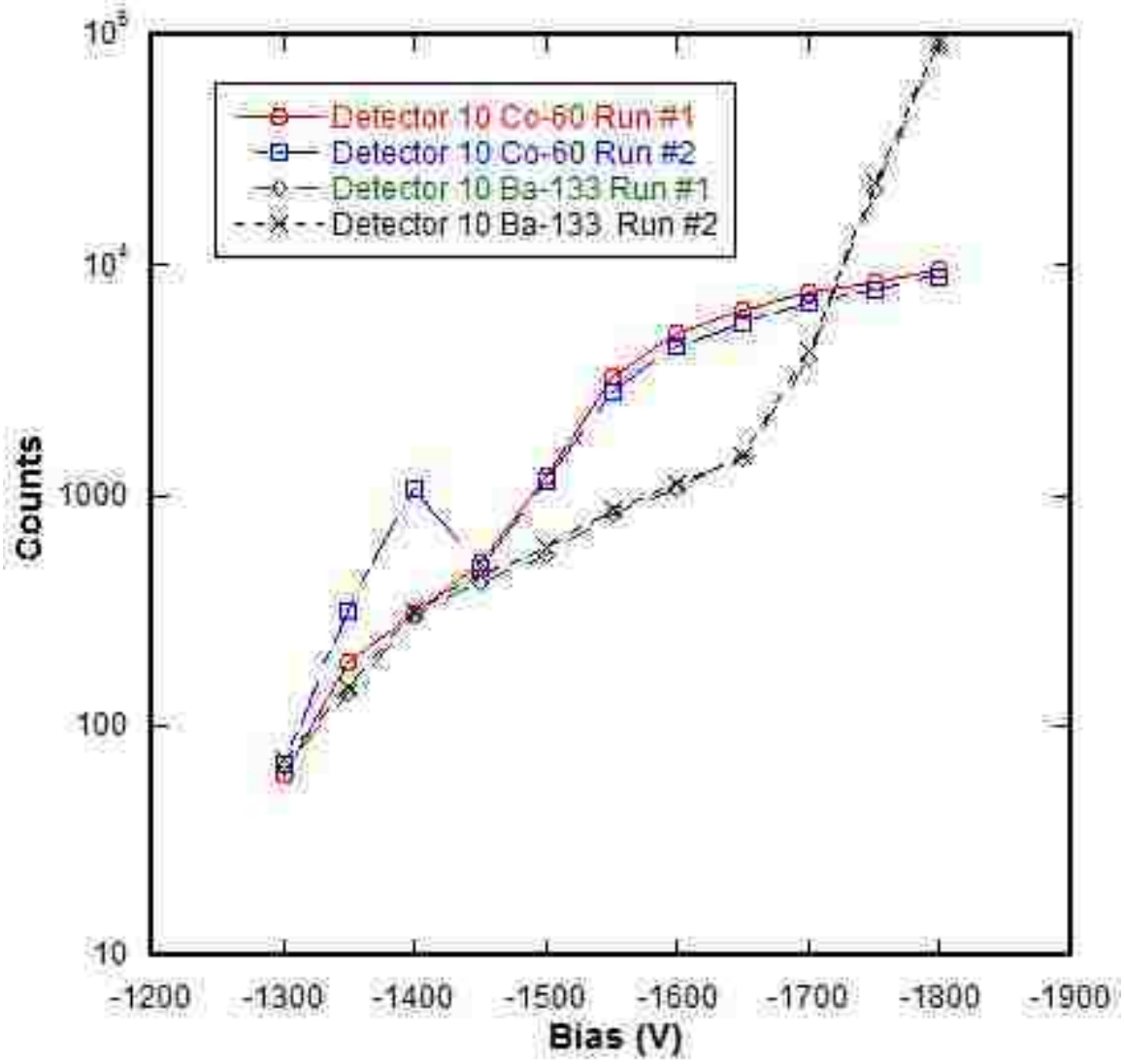

Figure 7: Cosmic Detector 10 Co-60 and Ba-133 Counting Plateaus

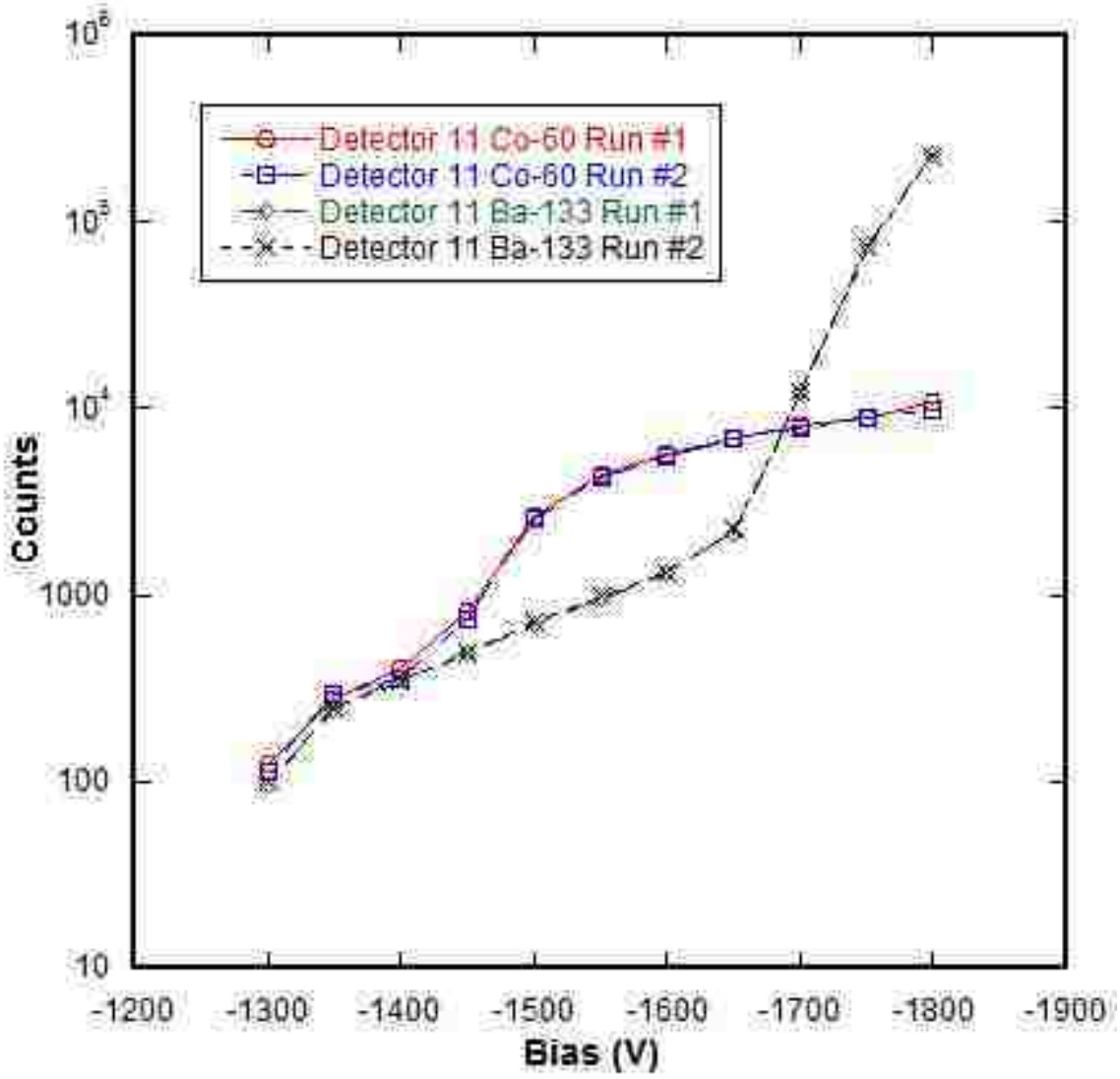

Figure 8: Cosmic Detector 11 Co-60 and Ba-133 Counting Plateaus

The counting plateaus for cosmic detectors 10 and 11 were consistent across the various experiments conducted with Co-60 and Ba-133. The only exceptions to this are the measurements for cosmic detector 10 in Figure 7 for the Co-60 plateau run #2 taken at -1350 V and -1400 V. As these measurements were not consistent with the results of Co-60 plateau run #1, they can be considered anomalous. The Co-60 plateaus for both cosmic detector 10 and cosmic detector 11 appeared to be in good agreement with each other, and were between -1600 V and -1800 V. This also agreed well with the cosmic

radiation plateaus. For both cosmic detectors there was no distinguishable plateau with the Ba-133 source. Overall, while there was a slight plateau between -1600 V and -1800 V, there was not a particularly clear plateau for both cosmic detectors across three different radiation sources.

Due to the lack of a defined plateau at the 50 mV discriminator threshold on the constant fraction discriminator, other threshold settings were used to determine if signal noise was disrupting the plateau measurements by counting spurious counts caused by signal noise. The discriminator setting on the Ortec NIM Model 935 prevents signals with amplitudes that fall below the discriminator threshold from producing an output signal. The experiments were conducted using cosmic radiation, the Co-60 source and the Ba-133 source at thresholds of 75 mV and 100 mV. The results for 50 mV, 75 mV, and 100 mV are displayed for cosmic detector 9 and 10 in Figures 10 and 11, respectively.

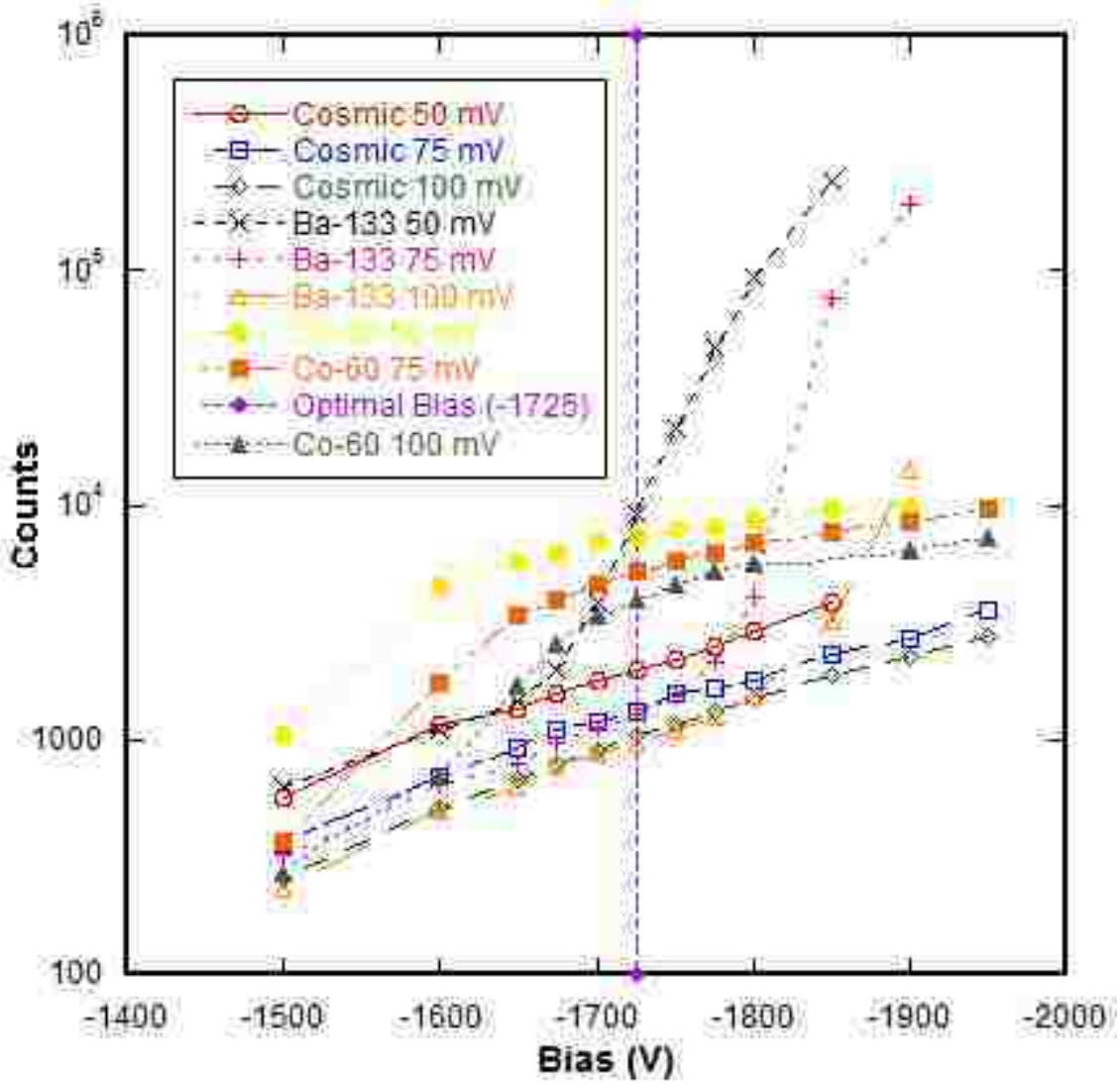

Figure 9: Cosmic Detector 10 Counting Plateaus at Varying Discriminator Thresholds

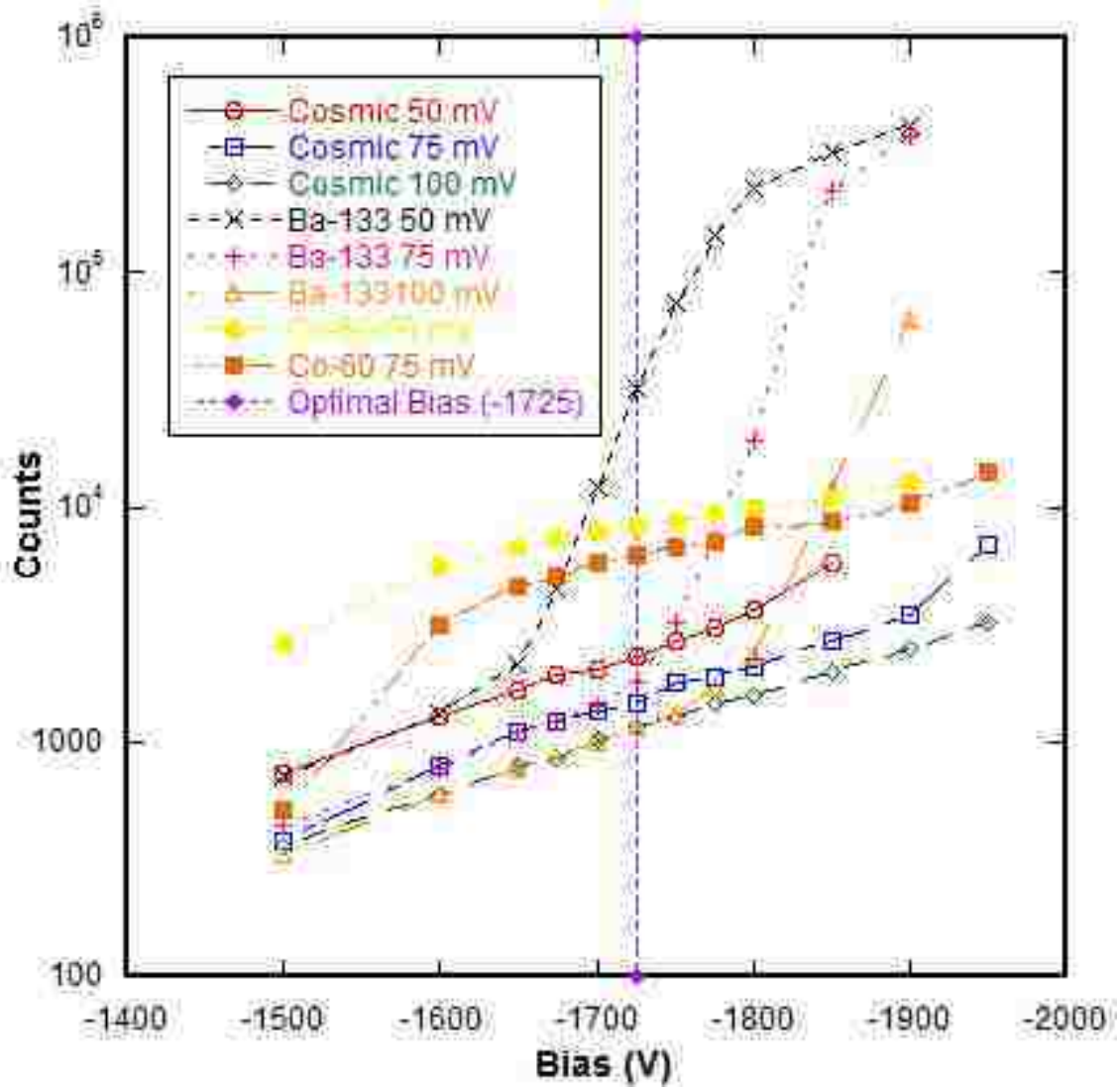

Figure 10: Cosmic Detector 11 Counting Plateaus at Varying Discriminator Thresholds

The curves appeared to be similar for both detectors in the sense that they all had plateaus over similar bias ranges. For all of the sources, as the threshold on the discriminator was increased, the total number of counts measured decreased as expected. For cosmic radiation, the counting plateau did smooth out, but so did the entire curve. However, there was still a recognizable plateau between -1700 V and -1800 V. For the Ba-133 source, the 50 mV curve showed no real plateau, but the 75 mV curve had a slight plateau right around -1700 V. The 100 mV threshold curve matched up almost

precisely with the 100 mV cosmic radiation curve and showed a plateau between -1700 V and -1775 V before increasing exponentially. For the Co-60 curves there was little difference from the 50 mV threshold to the 100 mV threshold and all three curves showed a stable area between -1700 V and -1850 V. This led to the determination to operate the detectors at -1725 V PMT bias.

Normalizing Pulse Shapes of the Coincidence Detectors

To optimize coincidence counting between the two coincidence cosmic detectors, it was important to ensure that the pulse shapes from both detectors were as normalized as possible. Normalizing the pulses from cosmic detectors 10 and 11 required matching both the amplitude and pulse shapes of the two detectors so that they are as similar as possible. This normalization ensured that the electronics used to determine coincident events between the two coincidence detectors identify true coincidences and not overlapping signals from each detector that are not coincident cosmic rays. The counting plateau experiments demonstrated that the PMT in cosmic detector 11 had a higher gain to bias ratio than cosmic detector 10. Using the -1725 V bias setting for both detectors, a series of experiments were conducted with the detectors aligned for coincidence events to compare the pulse shapes from cosmic radiation. The raw output signal was analyzed using a Tektronix Digital Phosphorus Oscilloscope (DPO) 4104. The specifications of the Tektronix DPO 4104 are located in Appendix F. These pulses are displayed in Figure 11 where the output from cosmic detector 11 is the yellow channel 1 and the output from cosmic detector 10 is the blue channel 2.

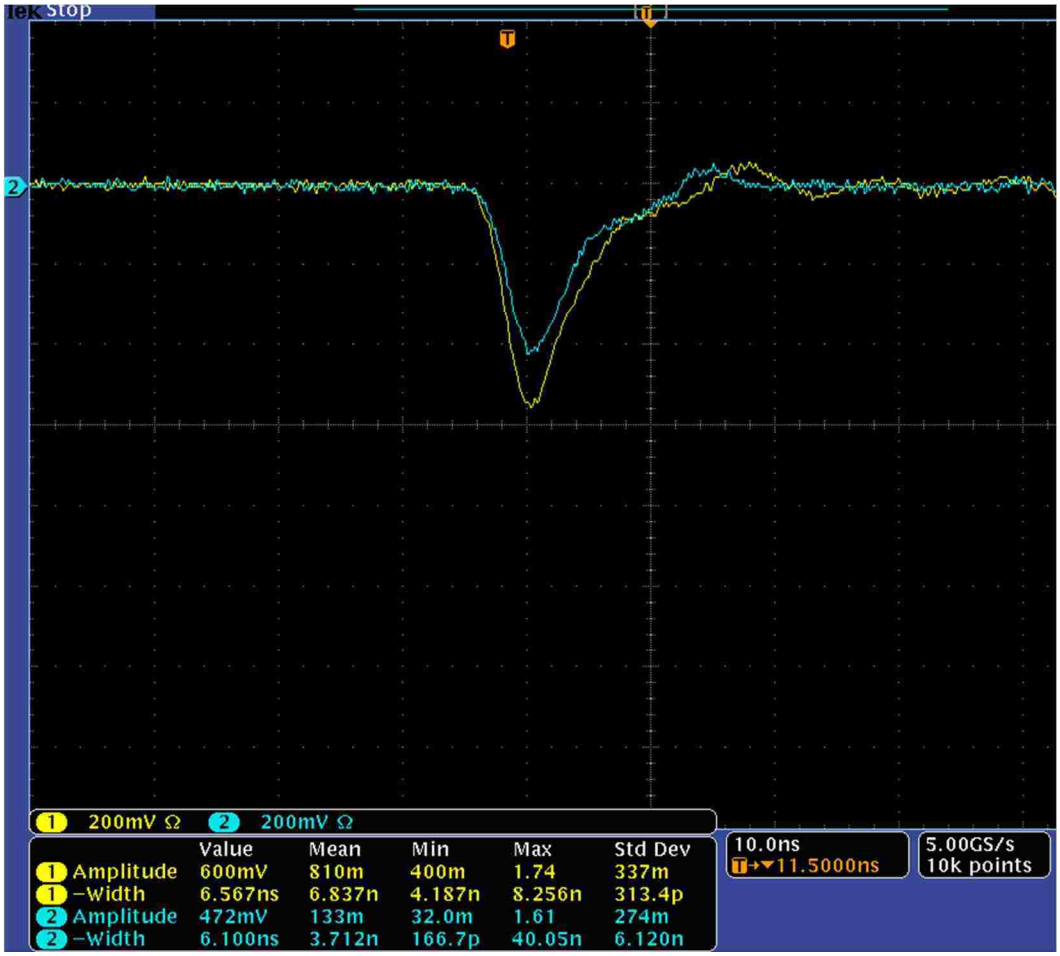

Figure 11: Un-Matched Pulse Shapes from Cosmic Detectors 10 and 11

Comparing the pulse shapes from cosmic detector 10 and cosmic detector 11 revealed that the pulse shapes of the output from cosmic detector 10 were smaller than the pulses from cosmic detector 11. The most straightforward method of changing the output pulse shape for cosmic detector 10 was to increase the bias. This was because the detectors were operating in a stable region of the R329 PMT and thus making small increases in bias would have no effect on PMT stability. Increasing the bias of cosmic detector 10 by increments of -5 V yielded larger pulses. It was determined that by biasing cosmic detector 10 to -1740 V the pulse shapes from cosmic detector 10 closely matched the pulse shapes from cosmic detector 11 in width and amplitude. This higher applied

bias was still nominally in the plateau region. The matched pulse shapes are displayed in Figure 12.

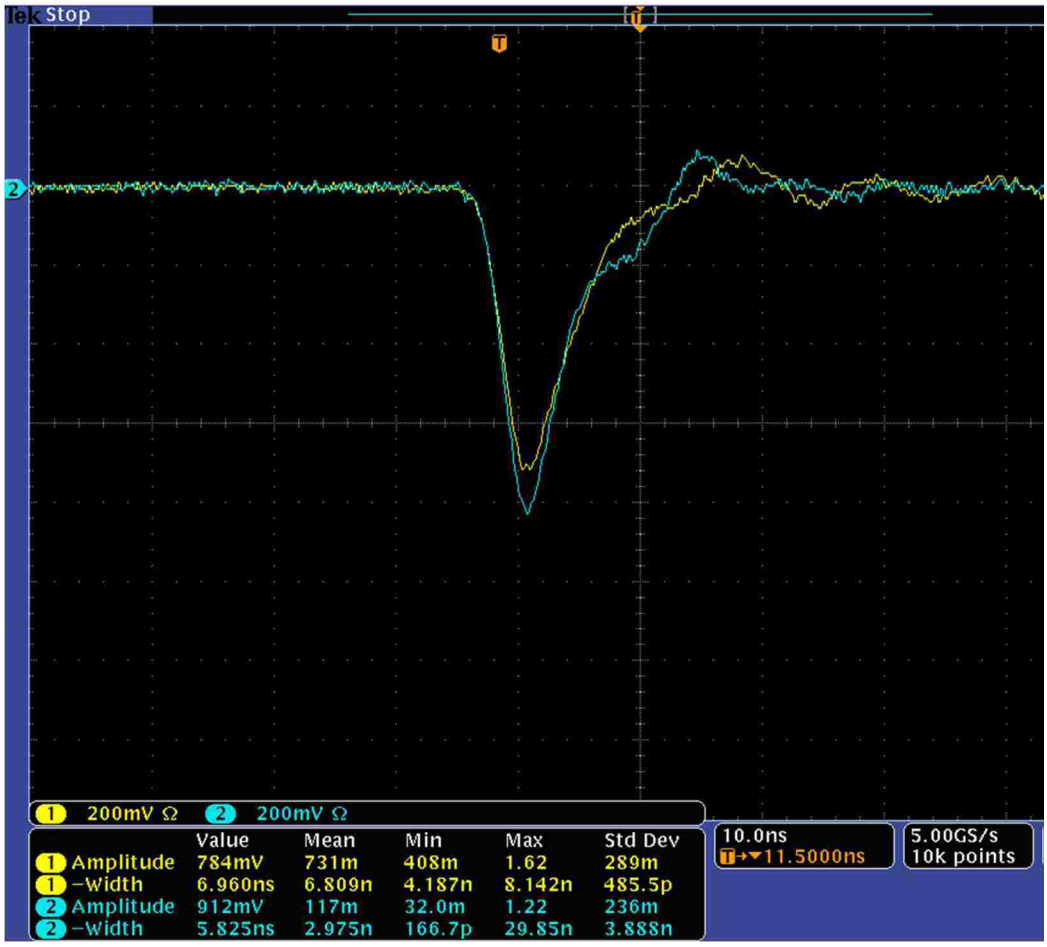

Figure 12: Matched Pulse Shapes from Cosmic Detectors 10 and 11

While the pulses were not an exact match, they seem to match very well the pulse shape, and leading edge and the falling edge. The leading edge and pulse shape is more important for the purpose of detecting coincident events because the logic electronics used to determine coincident events trigger off of the leading edge and centroid timing and not the absolute amplitude of the incoming signals. It was only the amplitudes and the structure post pulse that there seemed to be a discrepancy in the waveforms. These discrepancies will not adversely affect the ability to determine coincident events between

cosmic detectors 10 and 11. Although these matched pulse shapes occurred more often than any other pulse shapes displayed on the oscilloscope, they only occurred approximately half of the time that the coincidence electronics recorded pulses for both detectors.

Discriminator Threshold

The counting plateau measurement led to the conclusion that there was a large noise component of the signal with a constant fraction discriminator threshold at 50 mV, and perhaps even at 100 mV. An integral-pulse height spectrum was collected for both detectors at the operating bias settings determined from the pulse height matching of -1725 V for detector 11 and -1740 V for cosmic detector 10. Because the cosmic radiation was not a constant mono-energetic source, the spectrum did not yield any of the features usually found in an integral pulse height spectrum.[27] However, this experiment was conducted with the cosmic detectors aligned so that it was possible using the Ortec NIM Model 935 and the Ortec NIM Model CO4020 Quad Logic Unit to count coincident events between the two detectors. The specifications for the Ortec NIM Model CO4020 Quad Logic Unit are located in Appendix G. A graph of the number of coincident events as a function of discriminator setting is displayed in Figure 14.

[27] Knoll, 112-113.

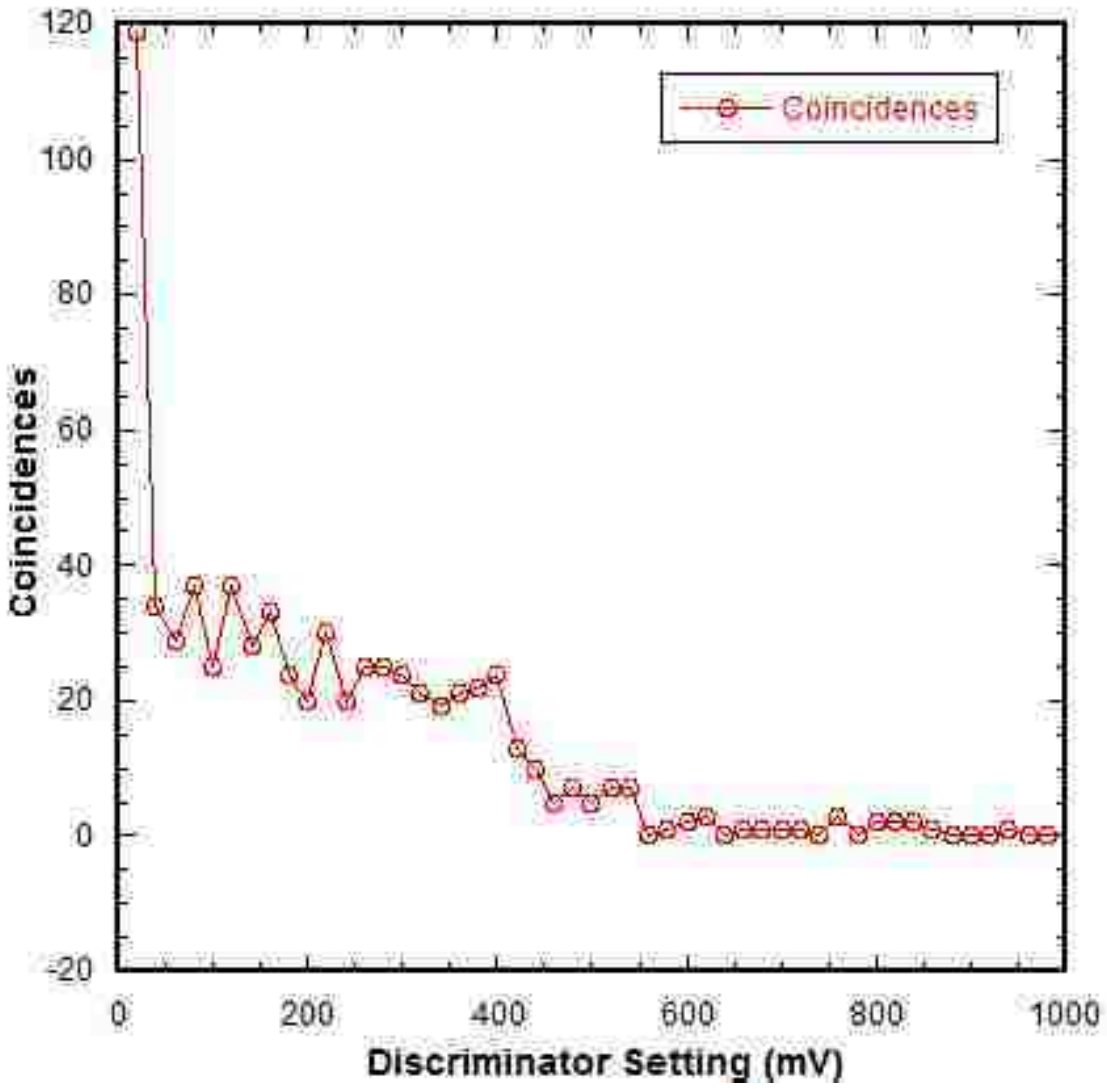

Figure 13: Coincident Counting versus Discriminator Setting

The purpose of this measurement of the coincident events as a function of discriminator setting was to determine if there was a discriminator setting that made sense to ensure that the maximum number of coincident events was counted. It appears that the first plateau of coincident events occurred between discriminator thresholds of 200 mV and 400 mV. The higher and less stable coincident counts from the lower discriminator settings indicated that discriminator settings below 200 mV may be dominated by signal noise. To ensure that only actual coincident events were counted by

this system, the discriminator setting on the Ortec NIM Model 935 will be set to 250 mV. This should ensure that the threshold is well above the majority of the signal noise for this system.

Section 2: Cosmic Ray Time Response Experimental Set-up

The Cosmic Radiation Experimental Set-up

The experimental electronics are triggered by the detection of a coincident cosmic ray from both cosmic detector 10 and cosmic detector 11. This begins with the output from cosmic detectors 10 and 11 going to the input of two of the four constant fraction discriminators in the Ortec NIM Model 935. Because the Ortec NIM Model 935 can only accept inputs less than 5 V, a 5 V clipper circuit was attached to the output of cosmic detectors 10 and 11 prior to connecting the signal cable into the Ortec NIM Model 935. Based on the results from Figure 13, the threshold setting on both constant fraction discriminators in the Ortec NIM Model 935 is set to 250 mV. The outputs from the constant fraction discriminators are then connected into separate logic units of the Ortec NIM Model CO4020. This was determined to be the optimal logic unit set-up because connecting the outputs of both cosmic detectors 10 and 11 into the same logic unit to measure coincidences resulted in non-logic output pulses. Because the logic output pulse will become the trigger for the entire system, it was important to ensure that the output logic pulse was as clean as possible. The two logic units in the Ortec NIM Model CO4020 were set to the ñORò position so that every incoming signal would register as an event. The negative output from each of these two logic units was connected to a third logic unit. This logic unit was set to ñANDò so that only coincident events produced an output signal. The output signal from the logic unit was then connected to the Tektronix

DPO 4104 and became the trigger for the nTOF detector. A diagram of this set-up is displayed in Figure 15. A series of pictures of the actual set-up is located in Appendix I.

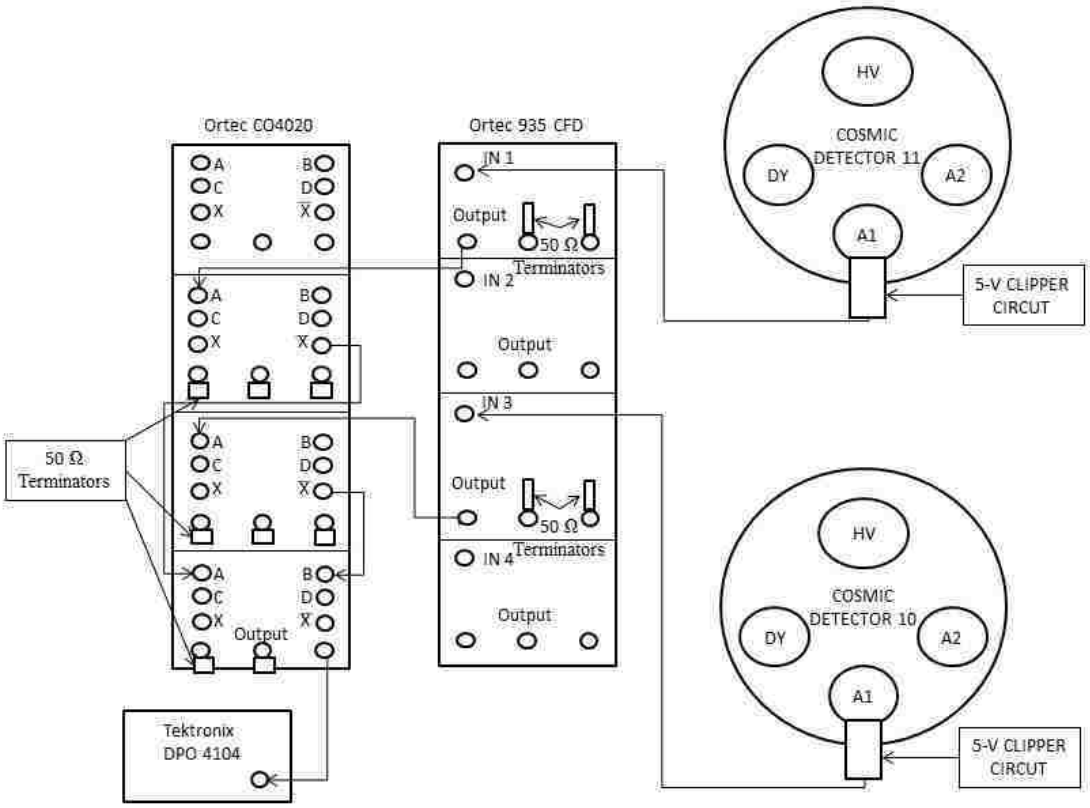

Figure 14: The Coincidence System with Cosmic Detectors 10 and 11

Measuring the Output from the nTOF detector

The output from the detector under test is connected to a series of Ortec NIM Model 425A Delay Units. The specifications of the Ortec NIM Model 425 Delay Unit are located in Appendix P. The output from the detector under test is delayed in reference to the coincidence detectors due to the through-put delay of the coincidence system that includes the time response of cosmic detectors 10 and 11 as well as the delay imparted by the coincidence electronics. This set-up is displayed in Figure 15. To record a clean time response from the nTOF, it must be delayed so that the 0 time on the digitizer is in fact the time the incident radiation interacted in the scintillator.

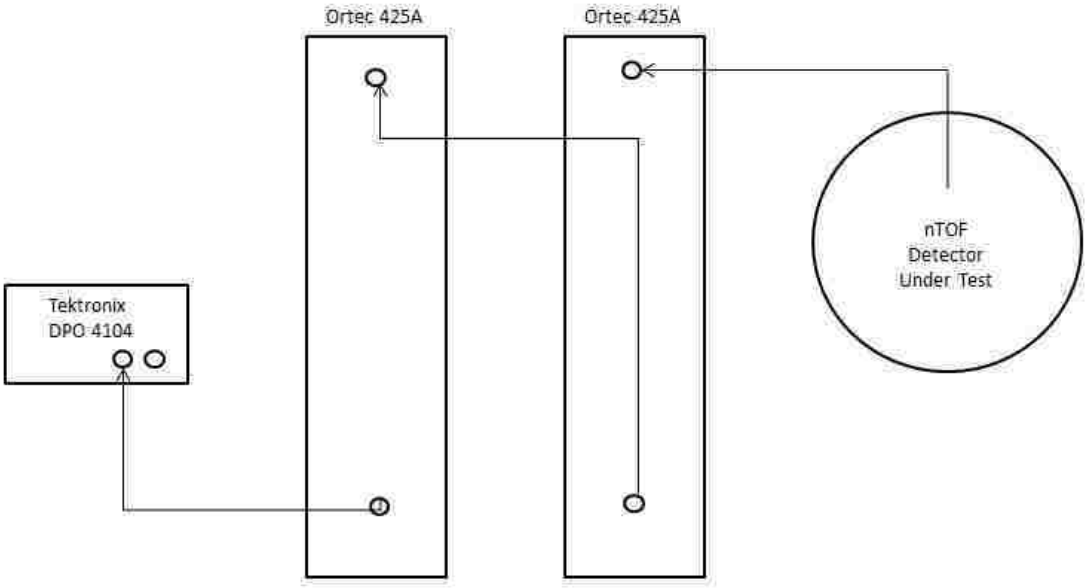

Figure 15: The nTOF Detector Experimental Set-up

Determining the Time Cosmic Rays Interact in the nTOF Detector

Measuring the through-put delay of cosmic detectors 10 and 11 to determine the entry time of the coincident cosmic radiation in the scintillator of the detector under test is non-trivial. It would require conducting an independent time response experiment on cosmic detectors 10 and 11 to determine their time response functions, and then a separate study on the delays through the electronics of the Ortec NIM Models 935 and CO4020. Ideally, these measurements should be done. However, for the work presented here, it was decided to use a reference detector whose time response function was independently determined through previous experiments using an accelerator to benchmark the through-put delay. The previous accelerator time response data on the reference nTOF detector D1 as well as the data on nTOF detector D2 is located in Appendix H. Detector D1 was used in the experimental set-up and the output of that detector was delayed until the centroid of the pulse from incident cosmic radiation was

adjusted to the previously determined average centroid position. D1 and D2 are nTOF detectors made up of a 7.62 cm by 2.54 cm piece of BC 422 1% Quenched scintillator coupled to a Lucite light guide and a Hamamatsu R5946 PMT. They are both operated in current mode. The specifications of detectors D1 and D2 are located in Appendix J. The design of D1 and D2 are similar to that displayed in Figure 2. The previously determined centroid average at -2500 V was 11.5 ns. A delayed signal from D1 whose centroid was located at 11.5 ns after the delay is displayed in Figure 16. The output from D1 in Figure 17 is designated with the blue channel 2 waveform while the yellow channel 1 waveform is the output from the coincidence logic unit.

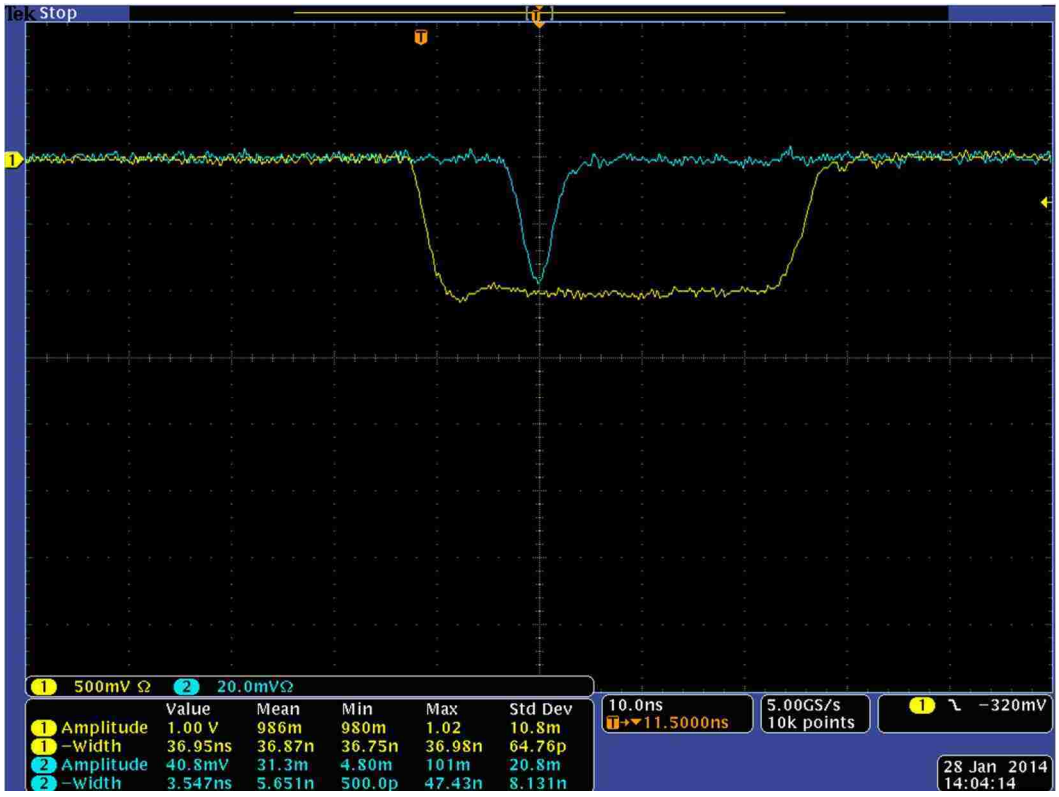

Figure 16: The Delayed Output Signal from Reference nTOF Detector D1

The Cosmic Radiation Experimental Set-up

The cosmic radiation experimental set-up combines the coincidence system described above with the set-up for the detector under test. This is accomplished by placing the detector under test in between the two coincidence system detectors and aligning it with the scintillation areas of those coincidence detectors. This creates a set-up where all three scintillation areas are aligned to detect cosmic radiation that passes between all three detectors. This complete set-up is displayed in Figure 17. All of the connections in Figure 17 are made using RG-223/U 50-Ohm coaxial cable.

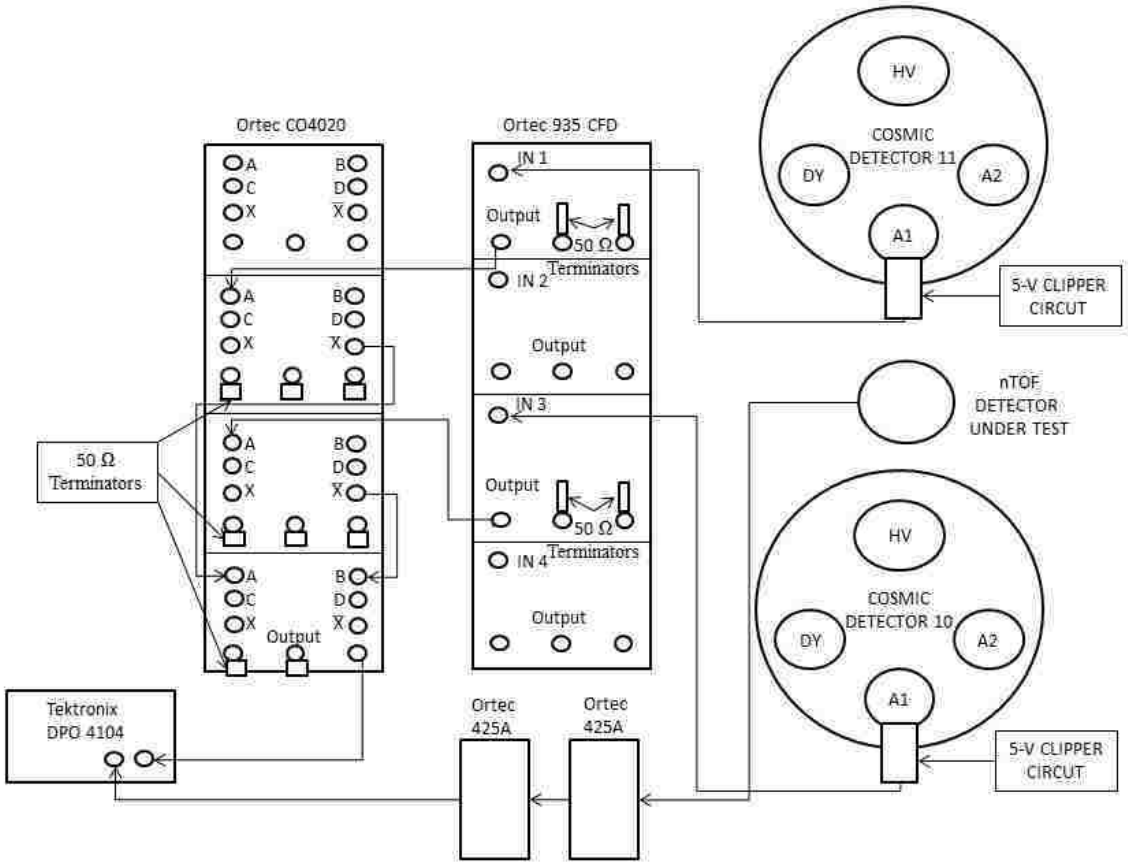

Figure 17: The Cosmic Radiation Experimental Set-up

CHAPTER 3: EXPERIMENTAL PROCEDURE

Section 1: Preparing the Experimental Electronics

With the experimental set-up described above, the experimental procedure begins with a burn-in process for the PMTs. According to the manufacturerôs specifications, the PMTs should be under bias for at least thirty minutes prior to taking data. The coincidence detectors should be set to -2500 V. The detector under test should be set to the maximum allowable bias setting according to the PMT specifications. Additionally, when the detectors are biased to -2500 V the coincidence electronics should also be turned on to allow the electronics to warm-up as well.

Once the detectors and electronics have been under bias for thirty minutes or more, the coincidence detectors should be set at the operating bias settings determined in the previous chapter. Cosmic detector 10 should be set to -1740 V and cosmic detector 11 should be set to -1725 V. The output from the logic unit should be set as the trigger for the Tektronix DPO 4104 Oscilloscope. The trigger should be set to -320 mV. This trigger level was chosen to be about thirty percent of the logic output pulse of the logic unit and appeared to be good point in the rise time of that pulse to provide stable triggers. After the trigger, the output from the detector under test is recorded on the DPO 4104 whenever there is a coincident cosmic ray that has passed between all three detectors.

Section 2: Experimental Measurements

As nTOF measurements require the use of a variety of different bias setting on the detector under test, it is important to determine the time response of the detector under test as a function of detector bias. To ensure that a wide range of bias settings are covered adequately, it was determined that measurements would begin at the maximum

recommended voltage of the detector under test. Measurements would then be taken at 100 V intervals down to -1000 V or until the PMT stops responding to the incoming cosmic radiation, whichever comes first.

For each bias setting, twenty waveforms were captured by the Tektronix DPO 4104 oscilloscope. For every captured waveform, a screen capture of the signal and a 10,000 point set of data were recorded. The screen capture will provide a history of the signal, the pulse shape, and the settings on the oscilloscope for future reference. The 10,000 point set of data will be used to analyze the waveform and determine the through-put delay and detector time response.

Section 3: Determining Acceptable Waveforms from the nTOF Detector Under Test

Not all of the waveforms that are recorded when the coincidence detectors register a cosmic ray are good waveforms. The expectation for a good waveform is a wave that exhibits the characteristics of a Gaussian function from the scintillator response combined with an exponential detector response function from the PMT (the combined Gaussian-exponential function is described in detail in the following chapter). An example of this kind of waveform is displayed in Figure 18.

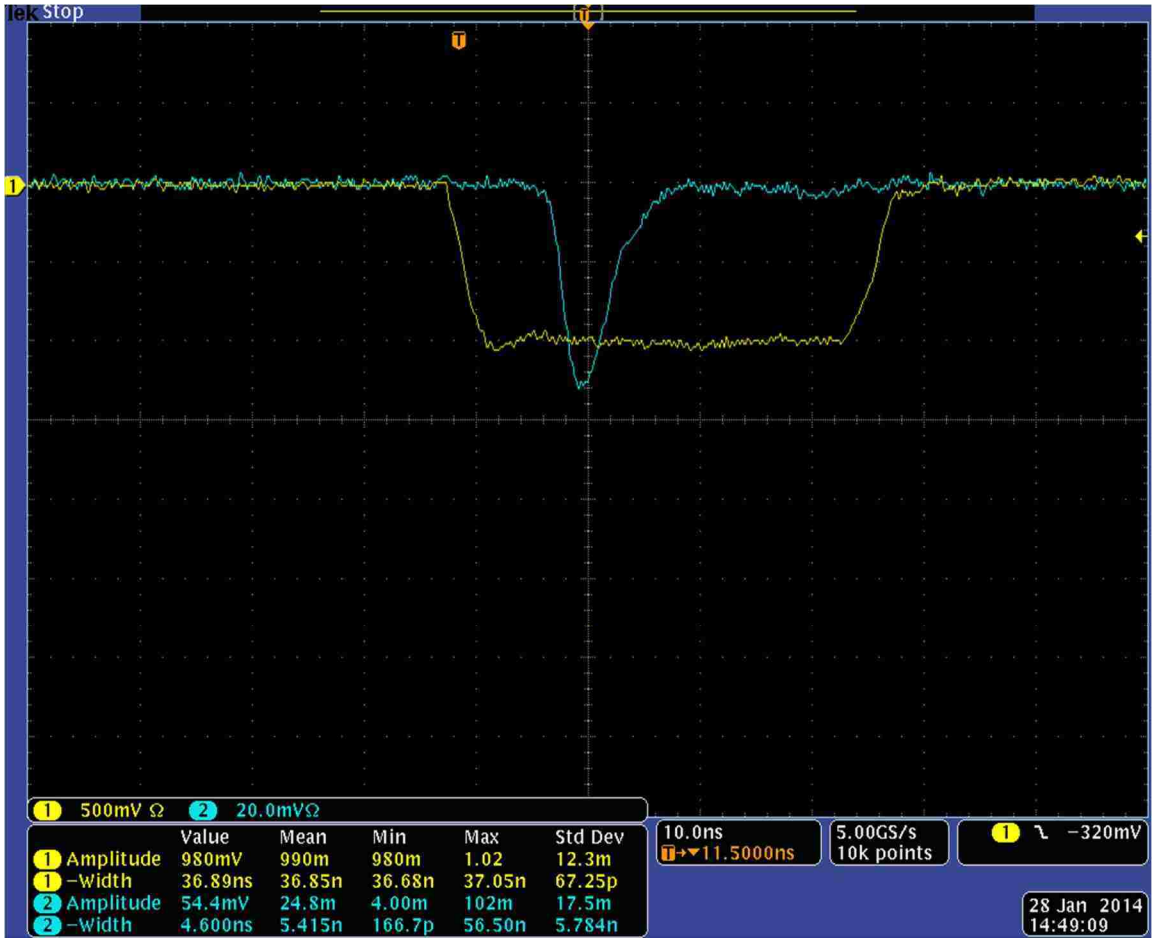

Figure 18: Combined Gaussian and Exponential Waveform

This combined wave is most likely a result of the ionizing radiation passing through the scintillator, and the most likely high energy cosmic ray to interact with the scintillator is the cosmic ray muon. However, there is a wide variety of cosmic radiation interacting with the scintillator. Therefore, some of the resulting waveforms triggered by the coincidence detectors are not viable waveforms for determining the time response of the detector under test. An example of this kind of wave is displayed in Figure 19.

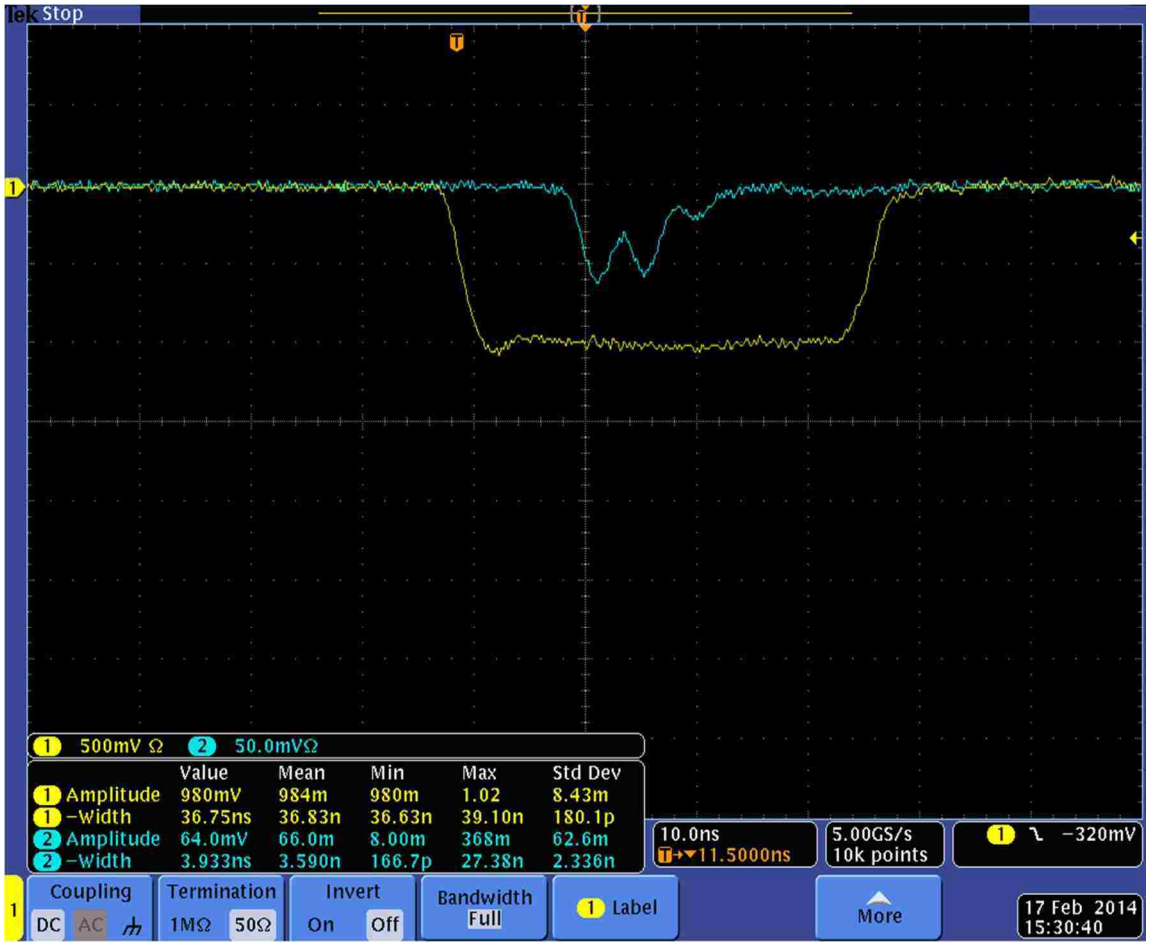

Figure 19: Non Combined Gaussian and Exponential Waveform

Waveforms like the ones displayed in Figure 20 are recorded by the oscilloscope approximately 40% of the time. Therefore, only waveforms that resemble the combined Gaussian and exponential waves similar to the shape of the waveform in Figure 19 are used to determine the time response of the detector under test. However, while the shape of the waveform used to determine the time response resembles that of the waveform in Figure 19, the amplitudes have a significant amount of variation.

CHAPTER 4: ANALYSIS AND RESULTS

Section 1: Analysis

Theoretical Treatment of the Exponentially Modified Gaussian Function

Because all of the different components of the scintillator-light guide-PMT system can be analytically understood, it is possible to calculate a time response function. The transit time of the radiation through the scintillator, the decay time of the scintillator, the transit time through the light guide, and the response of the PMT can be separately calculated and plotted. The resulting function has a shape of a Gaussian with an exponential tail. The shape of the time response function of a scintillation detector was established in the 1990s and has been used since then to analyze nTOF data.[28] This calculated time response function is displayed in Figure 20.

[28] T. J. Murphy, R. A. Lerche, "Development of a geometrically-compensated neutron time-of-flight detector for ICF applications with approximately 200 ps time response," *The Review of Scientific Instruments* 63, (1992), 4884.

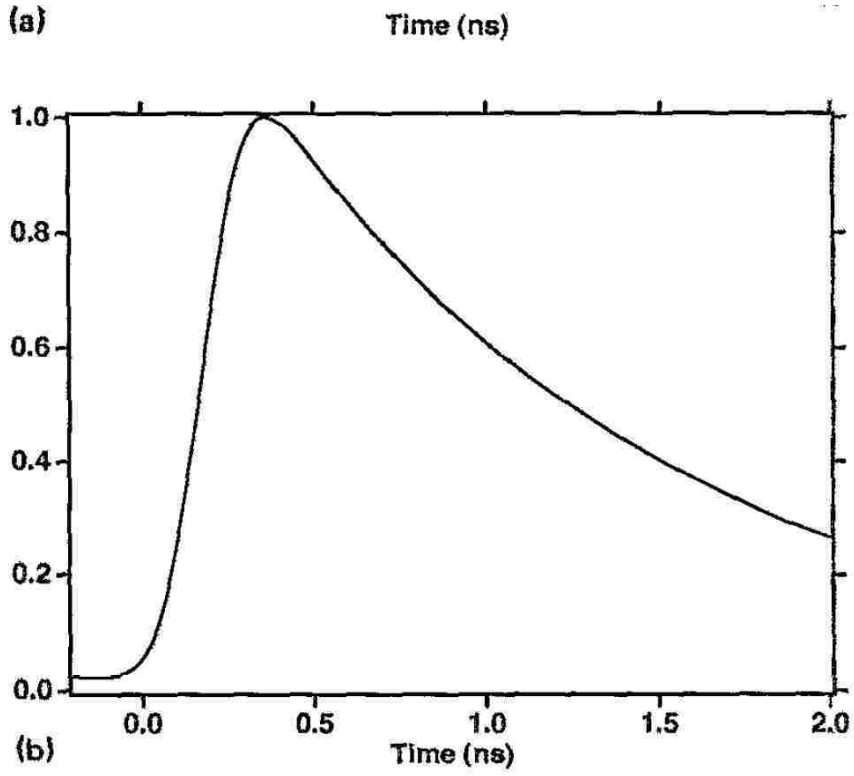

Figure 20: Calculated Time Response Function

This calculated time response function has the form of an exponentially modified Gaussian function. This function is displayed in Equation 8:

$$y(x; a, x_c, \sigma, \gamma) = \frac{a}{2\gamma} \exp\left(\frac{\sigma^2}{2\gamma^2} + \frac{x_c - x}{\gamma}\right)\left[\operatorname{erf}\left(\frac{x-a}{\sigma\sqrt{2}} - \frac{\sigma}{\gamma\sqrt{2}}\right) + \frac{\gamma}{|\gamma|}\right] \qquad 8$$

where a is the amplitude of the pulse, ů is the width of the pulse, x_c is the centroid location, and ɔ is the skewness variable.[29] It is readily apparent that the waveform displayed in Figure 18 is an inverted time response function of the same type as that displayed in Figure 20.

Analytical Methodology

[29] SASfit Manual, "Exponentially Modified Gaussian," accessed 17 March 2014, http://sasfit.ingobressler.net/manual/Exponentially_Modified_Gaussian.

The analytical methodology describes the process from capturing the data on an oscilloscope to fitting an exponentially modified Gaussian curve to the data points and then using that fitted curve to determine the through-put and time response of the detector under test. The waveform captured using the Tektronix DOP 4104 oscilloscope has 10,000 data points. A screen capture of the oscilloscope displays the trigger signal, the entire time history of the detector response, and the oscilloscope settings used during the experiment. This is displayed in Figure 21. A plot of just the 10,000 point waveform is displayed in Figure 22.

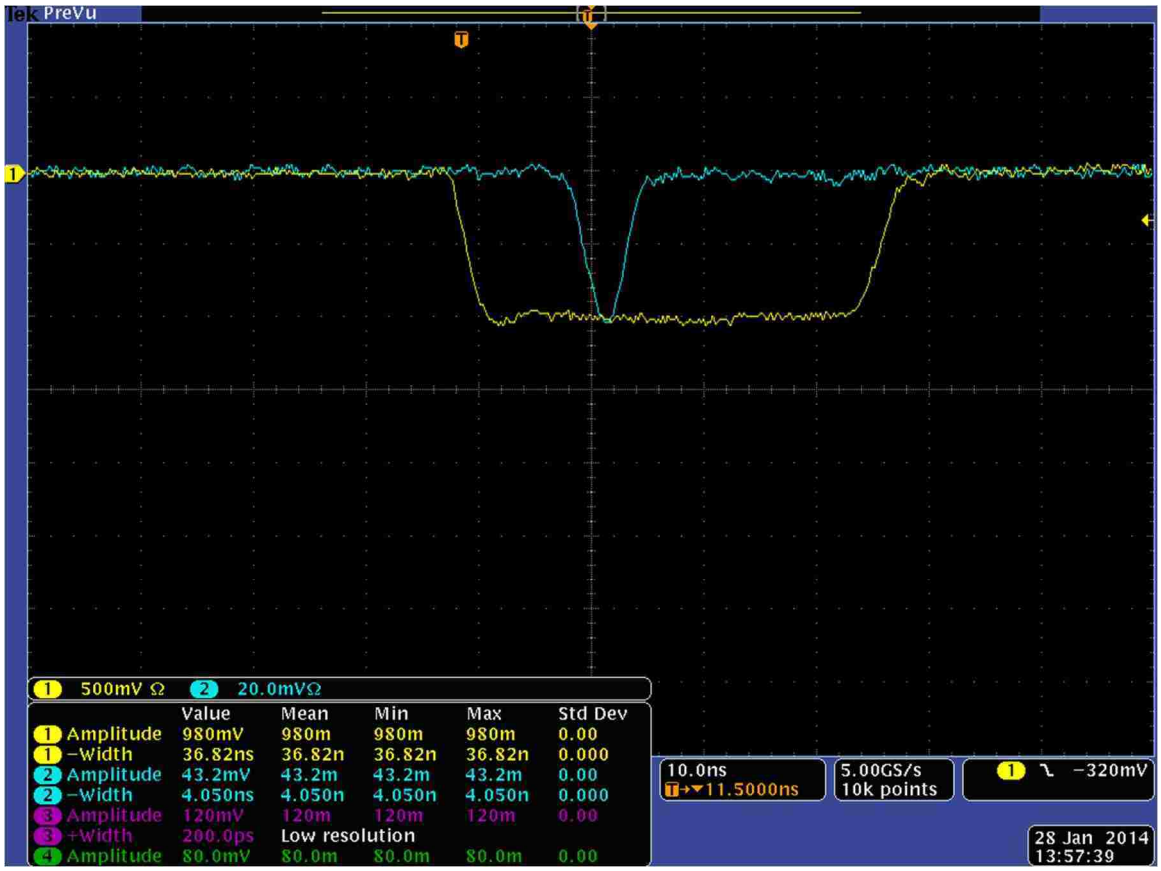

Figure 21: The Cosmic Ray Signal (Blue) from the Detector Under Test and the Coincident Trigger Signal (Yellow)

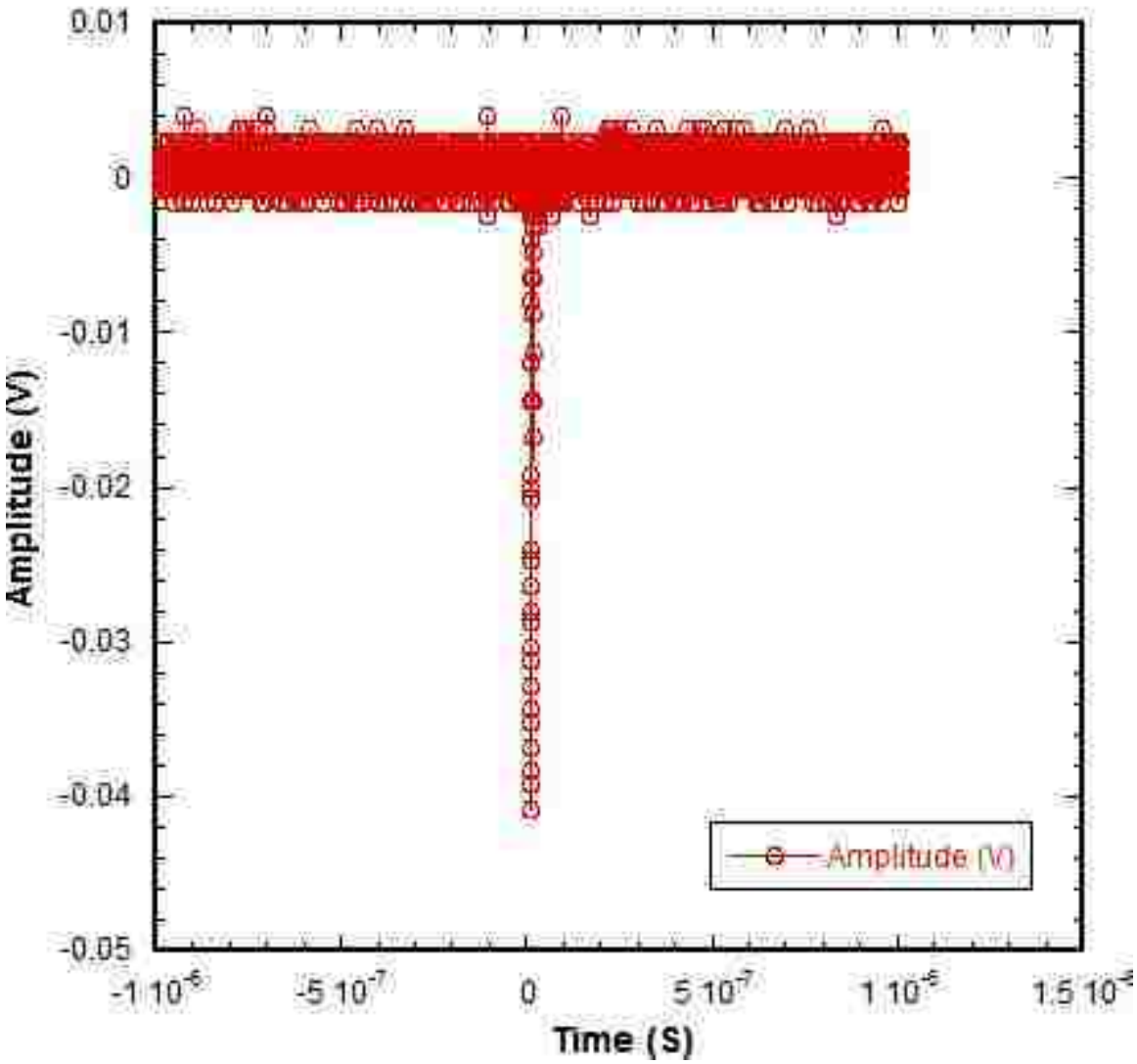

Figure 22: Raw nTOF Detector Output Waveform

This raw data was reduced to 107 data points (21 ns) beginning at the oscilloscope trigger and continuing until the entire waveform has returned to the normal noise level of the oscilloscope. The entire waveform was then inverted as the analytical software used to fit the curve accepts only positive wave forms. The resulting waveform was then normalized to an amplitude of one. Preparing the data in this way was designed to make fitting a curve to the data more efficient. An example of the resulting normalized waveform is plotted in Figure 23.

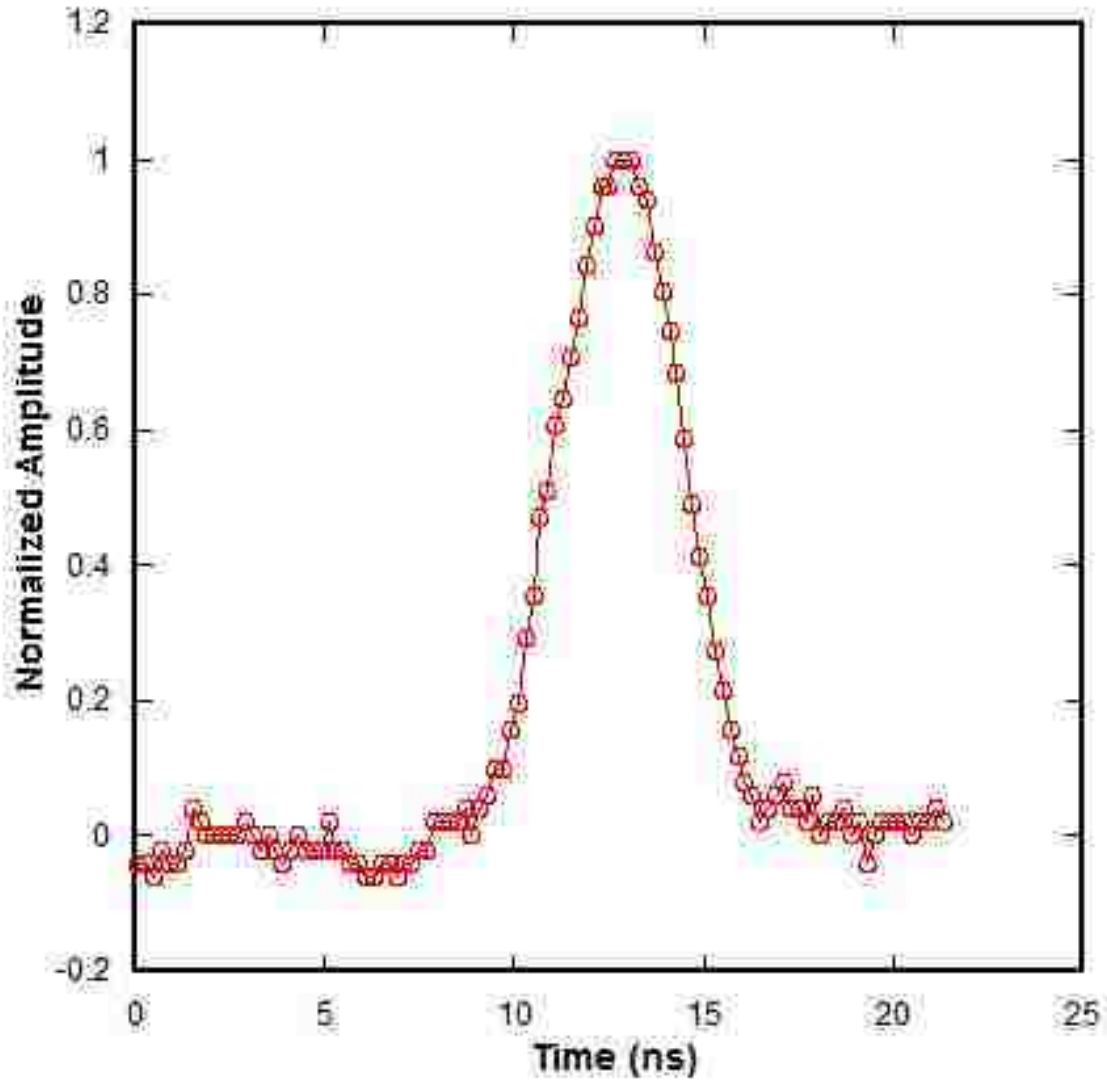

Figure 23: The Reduced and Modified Waveform

This waveform then became the input for the PeakFit analytical program. PeakFit is a peak separation and analysis software that uses residuals, second derivative, and deconvolution procedures to analyze peaks.[30] The PeakFit deconvolution procedure was designed to deconvolve the detector response from a signal to analyze the peaks of that signal. Because the detector response function is typically Gaussian in nature, PeakFit has a Gaussian deconvolution function, one of which is the fitting of an exponentially-

[30] SYSTAT Software Inc., *PeakFit: Peak Separation and Analysis Software,* 2002.

modified Gaussian function to a signal. The exponentially-modified Gaussian PeakFit function was applied to the data and the resulting curve fit is displayed in Figure 24. In Figure 24, the upper plot contains the individual data points as well as the exponentially modified Gaussian curve fit. The lower plot is a plot of the peaks PeakFit identified from the data points using the exponentially modified Gaussian model with their centroid location. This means that the central peak (12.841) is a plot of just the curve fit of the data, with its calculated centroid location. The additional smaller peaks are erroneously identified by PeakFit. The supporting data summary displays from the PeakFit program used in the analysis are located in Appendix K.

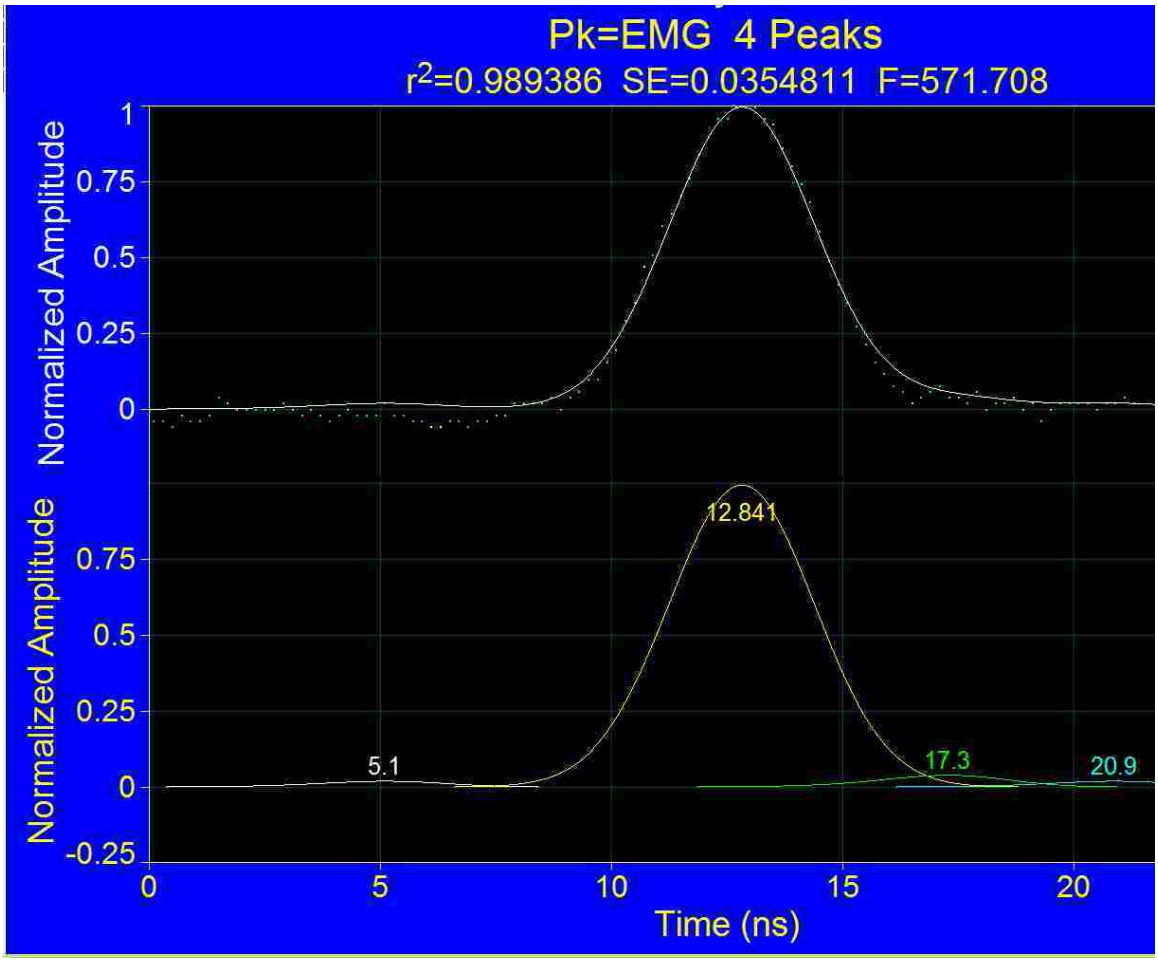

Figure 24: Exponentially Modified Gaussian Curve Fit

Statistical Analysis of the Curve Fit

PeakFit uses a least-square fit with Equation 5 to create the curve fit. As a result, the coefficient of determination, r^2, is calculated from the sum of squares based on error and the sum of squares about the mean. The sum of squares due to error is the sum of squared residuals and is the merit function in the least-squares fit. The sum of squares about the mean defines the lack of a fit. Thus, r^2 is calculated as 1 ï the sum of squares due to error divided by the sum of squares about the mean using the following equation:

$$r^2 = 1 - \frac{\sum_{i=1}^{n} w_i(\hat{y}_i - y_i)^2}{\sum_{i=1}^{n} w_i(y_i - \bar{y}_i)^2} \quad (9)$$

where n is the number of data points, w_i is the weight value, $\hat{R}_i$ is the estimated value, y-bar$_i$ is the mean value of all y data points, and the y_i is a single data point. The r^2 quantity is a statistical measure of how the curve fit corresponds to the real data points on a scale of zero to one, zero being the worst possible approximation and 1 being a perfect approximation.[31]

The SE is the fit standard error of the exponentially modified Gaussian curve fit. This is really the square root of the mean square error, which is the sum of squares due to error divided by the degree of freedom (DOF). The DOF is determined using Equation 10:

$$DOF = n - m \quad (10)$$

[31] John R. Taylor, *An Introduction to Error Analysis: The Study of Uncertainties in Physical Measurements,* 2nd ed. (Sausalito: University Science Books, 1997), 216-220.

where n is the number of data points and m is the total number of fitted parameters. For the case of the exponentially modified Gaussian, m = 4. The SE is thus calculated using Equation 11:

$$SE = \sqrt{\frac{\sum_{i=1}^{n} w_i(\hat{y}_i - y_i)^2}{DOF}} \qquad (11)$$

The mean square error combines together the variance and the squared bias of the curve fit which gives an indication of its precision and accuracy.[32] A mean square error of zero would mean the curve fit matches every single data point in the waveform. As the SE is the square root of the mean square error, it also gives an indication of precision and accuracy. Therefore, SEs close to zero give an indication of small variance between the curve fit and the experimental data.

The F statistic provided by the PeakFit analysis summary refers to the statistical test and regression analysis that determines variances between different populations. This value is not being used to determine the usefulness of the curve fit as it applies to the analysis of the time response data.

Determining the Through-Put Delay and the Time Response

Due to the variability in the experimental data, the through-put and the detector time response will be measured using the exponentially-modified Gaussian curve fit. This should result in more stable measurements of those quantities. The through-put delay will be measured at the point where the curve fit amplitude crosses the 10% point on the leading edge of the normalized waveform. To determine that point may require an interpolation of the curve fit data points around the 10% level. To determine the detector

[32]SAS/STAT® 9.2 User's Guide, Second Edition, "Mean Squared Error," accessed 11 March 2014, https://support.sas.com/documentation/cdl/en/statug/63033/HTML/default/viewer.htm#statug_intromod_sect005.htm .

time response from the curve fit data requires the calculation of the full width at half maximum. A depiction of the 10% level and FWHM of a waveform are displayed in Figure 25. This is done automatically and is displayed as part of PeakFitôs data summary function. Examples of the PeakFit data summary pages are given in Appendix K.

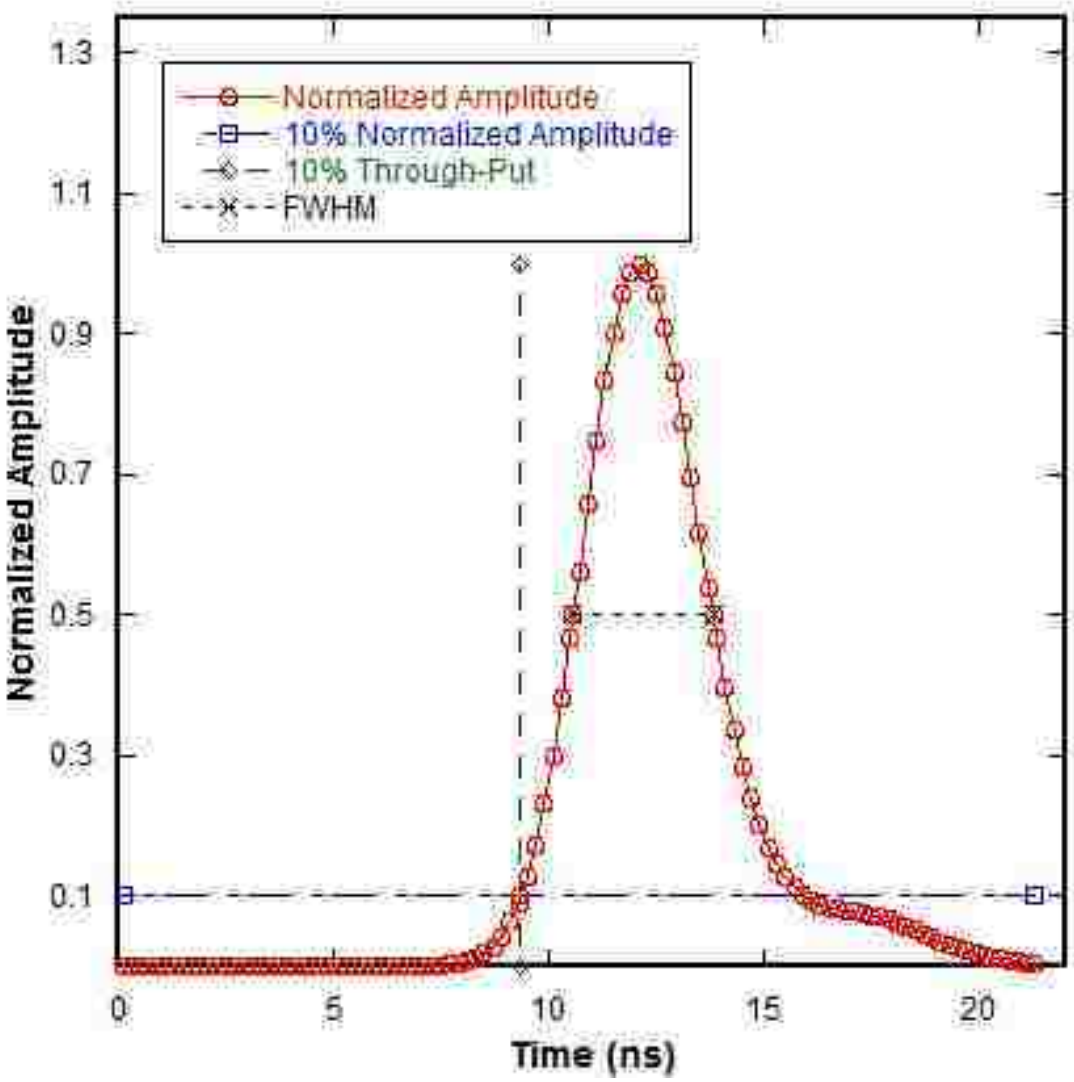

Figure 25: 10% Through-Put Level and FWHM

As there are twenty sets of data for every 100 V step in bias on detectors D1 and D2, the through-put and time responses will be averaged over twenty samples. This average will

be used to compare this data with the previously recorded through-put and time response measured at the Idaho facility in 2006.

Section 2: Data Analysis

Determining the Analytical Results for a Single bias Setting (D1 at -2500V)

As described above, to determine the through-put and time response of the nTOF detector under test at a specific bias setting required modifying the data into an input file that the PeakFit program could recognize, and then fitting an exponentially-modified Gaussian curve fit to the data. The data collected from detector D1 at the -2500 V bias setting will be used to describe the analytical process in detail. While only the major steps will be discussed in this section, a more detailed description of the program commands and file manipulations required by this process is provided in Appendix L.

There are several quantities produced after analyzing the experimentally measured waveforms using the PeakFit program. These include the r^2 and SE of the curve fit itself, the peak centroid, and the full width at half maximum (FWHM) in time units. The peak centroid will be useful in comparing the current data with the data from the earlier Idaho experiments. The FWHM is the width of the time response of the detector and requires no additional analysis. However, PeakFit does not produce a direct measurement of the detector through-put defined as the point in time when the waveform amplitude reaches ten percent of the peak amplitude. As the waveform is normalized, this would be the point at which the curve fit crosses an amplitude of 0.1. While PeakFit does not directly measure this, it does provide fitted data points from the fit, which can be linearly interpolated to provide a timing measurement for the through-put at ten percent of the normalized amplitude. These values for the twenty measurements of nTOF detector D1 at a bias setting of -2500 V are displayed in Table I.

TABLE I: Raw Data for Detector D1 at -2500 V

Run #	Centroid (ns)	FWHM (ns)	Through-Put (ns)	r^2	SE
1	12.2	3.24	9.35	0.998	0.014
2	12.8	3.73	8.9	0.984	0.045
3	11.7	5.0	11.7	0.99	0.035
4	10.9	3.1	7.96	0.99	0.03
5	10.5	3.75	7.7	0.98	0.044
6	11.3	3.3	8.3	0.99	0.03
7	10.45	2.85	8.16	0.99	0.03
8	10.5	3.05	8.1	0.998	0.014
9	12.96	3.2	10.5	0.987	0.035
10	10.37	3.2	7.83	0.98	0.04
11	9.9	3.0	7.6	0.995	0.02
12	10.98	3.14	8.36	0.99	0.03
13	11.0	3.1	8.36	0.989	0.033
14	11.3	2.8	8.8	0.99	0.03
15	11.6	2.8	9.5	0.98	0.04
16	12.0	3.0	9.55	0.99	0.027
17	10.8	2.9	8.6	0.986	0.035
18	11.09	3.3	8.64	0.98	0.04
19	11.1	3.4	8.6	0.987	0.036
20	11.0	4.5	7.9	0.99	0.03

Analytical Results from a Set of Data

Treating the measurements of the centroid, FWHM, through-put, r^2, and SE as single values allows for their analysis using counting statistics. For each of these quantities, the standard deviation, range, minimum value and maximum values are displayed in Table II. These values are also provided as part of the entire set of raw data for D1 located in Appendix M. In Table II, the range for the centroid, FWHM, through-put, r^2, and SE is the difference between the minimum value and the maximum value for those quantities.

TABLE II: Analyzed Data for Detector D1 at -2500 V

	Mean	Standard Deviation of Mean	Range	Minimum Value	Maximum Value
Centroid (ns)	11.2	0.8	3.06	9.9	12.96
r^2	0.989	0.005	0.016	0.981	0.998
SE	0.032	0.008	0.03	0.014	0.045
FWHM (ns)	3.3	0.6	2.23	2.78	5
Through-Put (ns)	8.7	1.0	4.1	7.6	11.7

The data analysis reveals that the curve fit of the exponentially-modified Gaussian function to the experimental data is a good fit. As an r^2 value of 1 is a theoretically perfect fit, the mean r^2 value of 0.989 implies an excellent fit of the experimental data. Additionally, a standard deviation of the r^2 mean value of only 0.005 and a range in the data of only 0.016 means that there was very little variance in the r^2 values. Additionally, the mean value of the standard error of the fit was only 0.032 with a standard deviation of 0.008 means that there was very little error in the curve fit of the raw data. This validates the use of the exponentially-modified Gaussian function to the data.

The centroid and through-put functionally represent the same elements of the waveform. The centroid is defined as the timing of the peak amplitude, and the through-put is the timing of the pulse at 10% of the peak amplitude. For -2500 V, both the centroid and the through-put had relatively large standard deviations at approximately 7% of the mean value for the centroid and 11 % for the through-put. This was a reflection of the wide range in measurements for both quantities as depicted by the histogram in Figure 26.

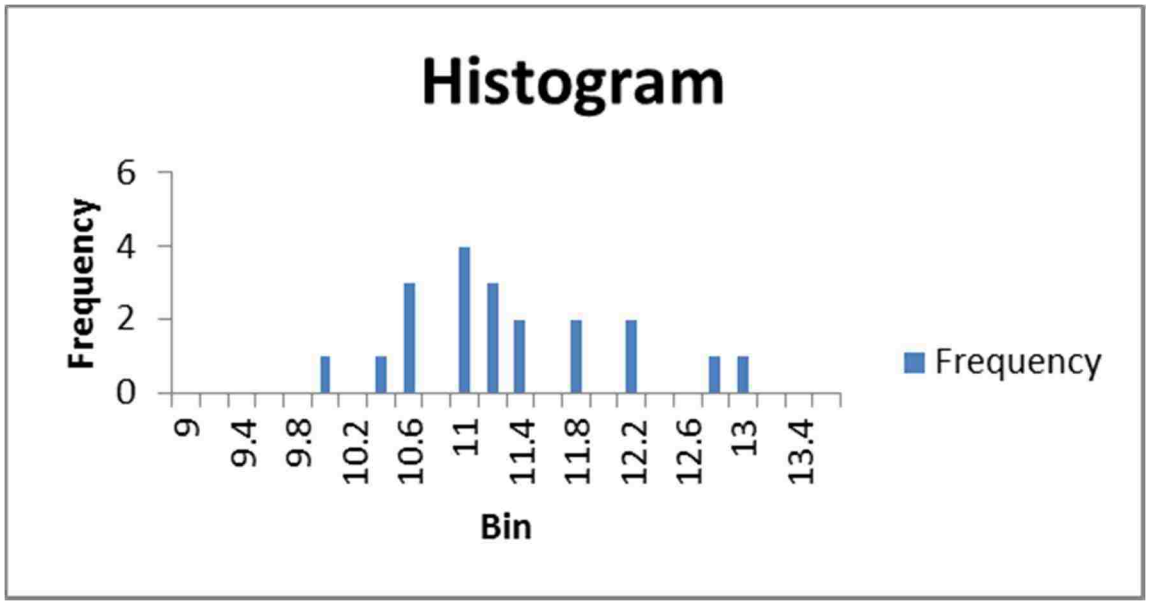

Figure 26: A Histogram of the Centroid Measurements of detector D1 at -2500 V

This histogram shows not only the wide spread in measured values, but the shape of the distribution of measurements. At 20 measurements, there is not a well-defined normal distribution. This has an impact on the statistics used to analyze the data.

The FWHM represents the time response width of the detector, which had more variation in the data than either the centroid or the through-put delay. The standard deviation of the FWHM was 17 % of the mean value. Like the centroid and the through-put, this was indicative of the large range of measured values of the FWHM. The range of 2.23 for a mean value of 3.31 reflected the wide variation in the measured data for the time response of the detector.

The raw data and analyzed results for each voltage step for detector D1 is located in Appendix M. The raw data and analyzed results for each voltage step for detector D2 is located in Appendix N.

Section 3: Results

The analysis described in the previous section was performed on data from detectors D1 and D2. The measurements were taken at 100 V steps for each detector from -2500 V to -1800 V. Measurements were limited to -1800 V and above because the output signals from the reference detector D1 at that bias setting were only 6 mV, which approached detector noise levels. Compared with the signal noise of 2-3 mV, there was doubt as to whether the measurements taken at -1800 V would result in good data. Part of this analysis will determine not only the comparison at that voltage to the previously measured experimental data from Idaho, but also whether these very low voltage measurements yield useful data.

The Results for Detector D1

The results for detector D1 at 100 V steps from -2500 V to -1800 V are displayed in Table III.

TABLE III: Results for Detector D1 from -2500 V to -1800 V

Bias (V)	Centroid (ns)	FWHM (ns)	Through-Put at 10% Amplitude (ns)	r^2	SE
-2500	11.2 ± 0.8	3.3 ± 0.6	8.7 ± 1.0	0.989 ± 0.005	0.03 ± 0.01
-2400	11.5 ± 1.0	3.5 ± 0.4	8.8 ± 0.9	0.999 ± 0.009	0.037 ± 0.011
-2300	11.6 ± 0.7	3.7 ± 0.4	8.8 ± 0.7	0.98 ± 0.01	0.045 ± 0.013
-2200	12.0 ± 0.8	3.7 ± 0.7	9.0 ± 0.7	0.965 ± 0.024	0.06 ± 0.02
-2100	11.8 ± 0.7	3.4 ± 0.4	9.0 ± 0.6	0.969 ± 0.023	0.054 ± 0.021
-2000	12.3 ± 0.8	3.5 ± 0.5	9.2 ± 0.7	0.91 ± 0.05	0.09 ± 0.04
-1900	12.5 ± 0.7	3.3 ± 0.7	9.6 ± 0.6	0.9 ± 0.1	0.104 ± 0.051
-1800	12.8 ± 1.1	3.5 ± 0.9	9.4 ± 1.7	0.85 ± 0.15	0.18 ± 0.21

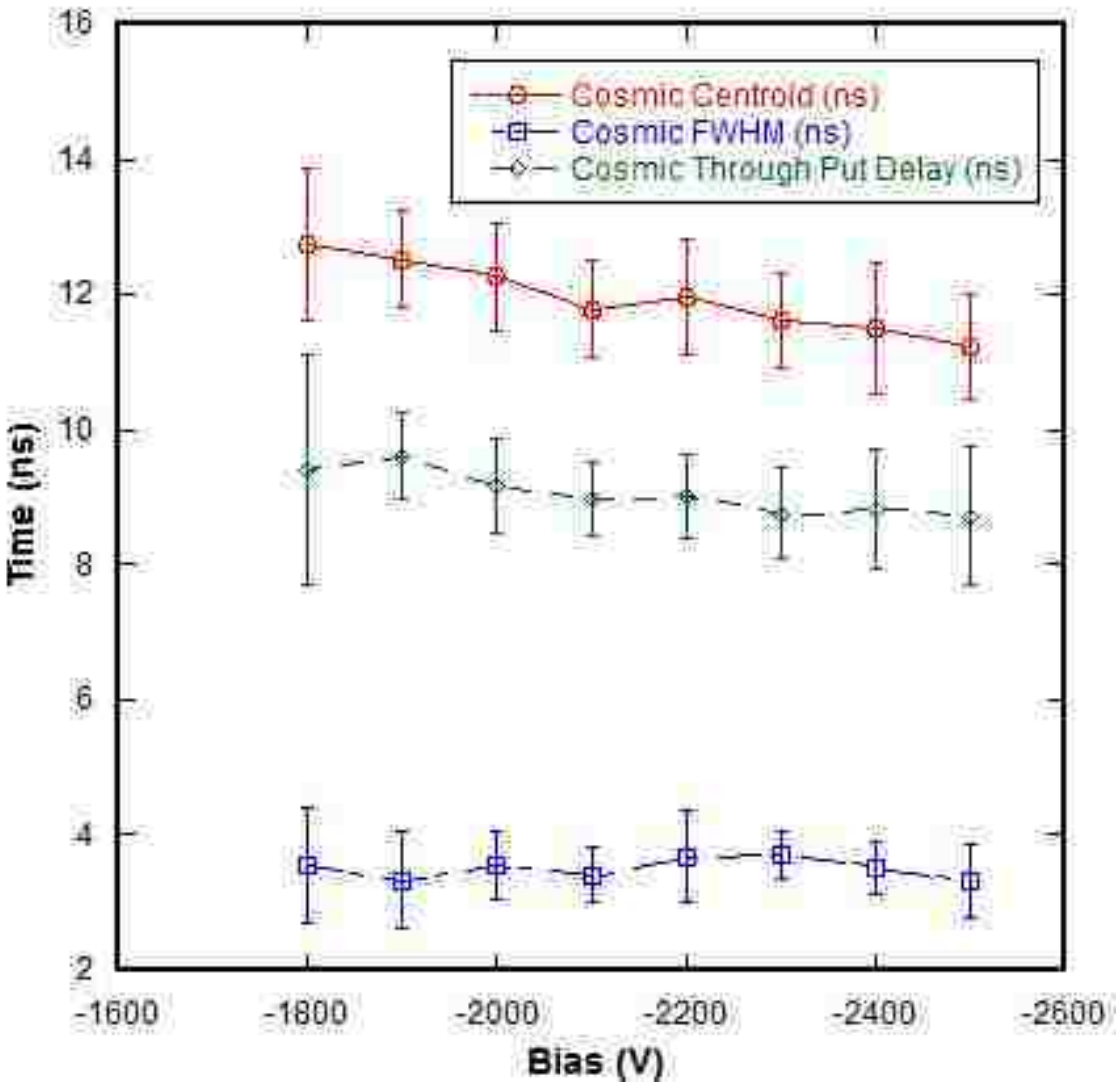

Figure 27: Detector D1 Results

The results for detector D1 display a number of trends in the experimental data, which are displayed in Figure 27. Note that the centroid and corresponding through-put increase as a function of decreasing detector bias. This is to be expected as decreasing the PMT bias reduces the voltage across the PMT dynodes, which slows the transit time of the signal. While the mean values for the FWHM displays a trend towards increasing width as the applied bias decreases, but the plot, Figure 27, indicates a relatively flat history within the uncertainties. In Figure 27, and for all of the subsequent figures, the experimental data

measured during this cosmic radiation time response and through-put experiment are identified as cosmic. Thus the centroid measured in this experiment is graphically displayed as the cosmic centroid. This is as opposed to the measurements taken at the Idaho Accelerator Centre which is graphically displayed as the Idaho centroid. The r^2 values decrease with decreasing bias and there is a corresponding increase in the standard error of the fit across the same bias settings. The appropriateness of the exponentially-modified Gaussian function to the experimental measurements decreases with decreasing bias setting. However, even at -1800 V, the r^2 of 0.847 shows that the exponentially-modified Gaussian fit is still applicable to the D1 data.

The Results for Detector D2

The results for detector D2 at 100 V steps from -2500 V to -1800 V are displayed in Table IV.

TABLE IV: Results for Detector D2 from -2500 V to -1800 V

Bias (V)	Centroid (ns)	FWHM (ns)	Through-Put at 10% Amplitude (ns)	r^2	SE
-2500	12.2 ± 0.5	3.5 ± 0.4	9.6 ± 0.5	0.98 ± 0.01	0.033 ± 0.013
-2400	12.4 ± 0.9	3.6 ± 0.6	9.6 ± 0.7	0.988 ± 0.008	0.033 ± 0.013
-2300	12.8 ± 0.7	3.6 ± 0.4	10.1 ± 0.9	0.99 ± 0.01	0.026 ± 0.009
-2200	12.6 ± 0.5	3.8 ± 0.4	9.8 ± 0.7	0.984 ± 0.014	0.03 ± 0.01
-2100	12.9 ± 0.5	3.7 ± 0.4	10.1 ± 0.4	0.989 ± 0.007	0.038 ± 0.03
-2000	13.2 ± 0.5	4.0 ± 0.4	10.2 ± 0.6	0.987 ± 0.009	0.036 ± 0.01
-1900	13.1 ± 0.6	3.8 ± 0.5	10.4 ± 0.6	0.98 ± 0.01	0.045 ± 0.009
-1800	13.6 ± 0.6	3.7 ± 0.4	11.0 ± 0.7	0.965 ± 0.024	0.053 ± 0.025

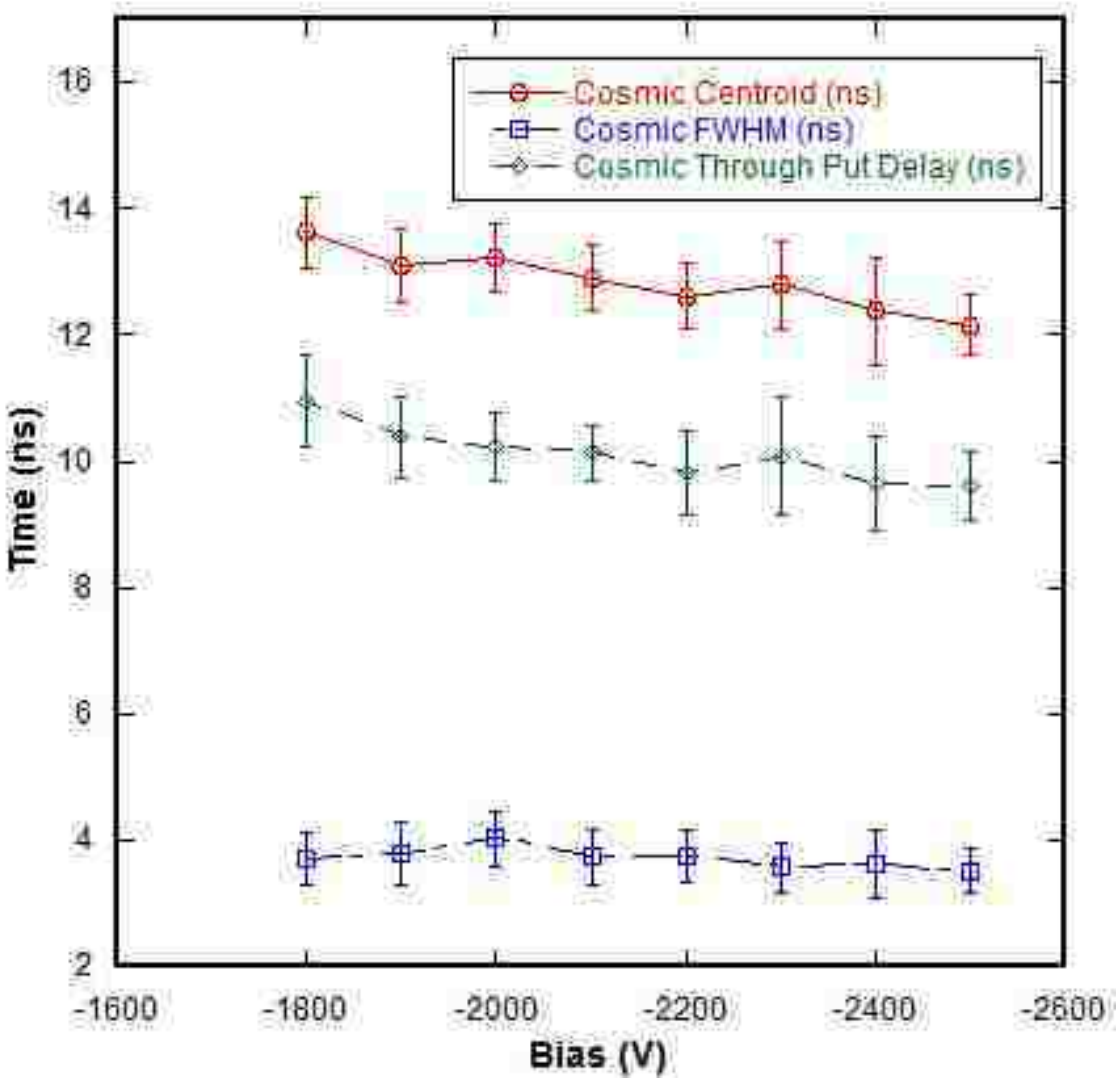

Figure 28: Detector D2 Results

The trends for the centroid, FWHM, and through-put are displayed in Figure 28. Similar to detector D1, the centroid and through-put for detector D2 increases with decreasing bias settings. Due to the uncertainties the FWHM was statistically flat. As far as the correctness of the curve fit to the experimental data from detector D2, there is a trend of decreasing the r^2 values with decreasing bias settings. However, the change from 0.981 at -2500 V to 0.965 at -1800 V is much less of a change than for detector D1. Additionally,

the standard error of the fit does not change significantly across the range of bias settings. For D2, the use of an exponentially-modified Gaussian fit is reasonable.

Section 4: Comparing the Cosmic Experimental Results with the Idaho Experimental Results

A Description of the Idaho Experiments

In July 2006, a series of measurements of the through-put delay and time response of nTOF detectors was taken at the Idaho State University Accelerator Center. These experiments were conducted using a 44 MeV Short-Pulse Electron LINAC.[33] The accelerator was used to produce a 50 ps pulse of 5 MeV electrons impinging onto a Tungsten target. The interaction of the electrons in the Tungsten produced a beam of photons with approximately the same characteristics as the electron beam (5 MeV peak energy, 50 ps pulse). The facility used a photo-Compton diode near the target (a few cm away) as a way to measure the initial time of the photon beam pulse.[34] The beam then progressed through a 0.635 cm shielded collimator five feet long into the detector under test (D1). The pulse from the Compton diode provided a trigger to a 20 GHz fast digitizer. This digitizer recorded the resulting waveform from detector D1, and was set to accumulate 300 individual measurements and an average waveform. The individual waveforms were not recorded during these experiments. The average values for the centroid, FWHM, and through-put was used as the reference data to compare with measurements from the cosmic radiations experiments. A summary of the Idaho experimental data is located in Appendix H. The Idaho measurements did not record uncertainties for centroid, through-put, or FWHM.

[33] Idaho State University Accelerator Center, "Facilities and Capabilities," accessed on 24 March 2014, http://iac.isu.edu/facilities.html.
[34] Private Communication, Brent Davis, NSTec, Las Vegas, Nevada.

Comparing the D1 Cosmic Experimental Data with the Idaho Experimental Data

Figure 29 and Table V show the comparison between the current cosmic experimental data and the Idaho data for nTOF detector D1. The uncertainties for the cosmic radiation experimental data from D1 represent one standard deviation.

TABLE V: Comparison of D1 Detector Results Between the Cosmic Radiation Experiments and the Idaho Experiments

Bias (V)	Centroid (ns)	Idaho Centroid (ns)	FWHM (ns)	Idaho FWHM (ns)	Through-Put at 10% Amplitude (ns)	Idaho Through-Put at 10% Amplitude (ns)
-2500	11.2 ± 0.8	11.57	3.3 ± 0.6	3.42	8.7 ± 1.0	9.34
-2400	11.5 ± 1.0	11.98	3.5 ± 0.4	3.36	8.8 ± 0.9	9.46
-2300	11.6 ± 0.7	11.89	3.7 ± 0.4	3.48	8.8 ± 0.7	9.47
-2200	12.0 ± 0.8	12.0	3.7 ± 0.7	3.48	9.0 ± 0.6	9.65
-2100	11.8 ± 0.7	12.34	3.4 ± 0.4	3.41	9.0 ± 0.6	9.87
-2000	12.3 ± 0.8	12.4	3.5 ± 0.5	3.55	9.2 ± 0.7	10.04
-1900	12.5 ± 0.7	12.74	3.3 ± 0.7	3.62	9.6 ± 0.6	10.17
-1800	12.8 ± 1.1	13.1	3.5 ± 0.9	3.59	9.4 ± 1.7	10.39

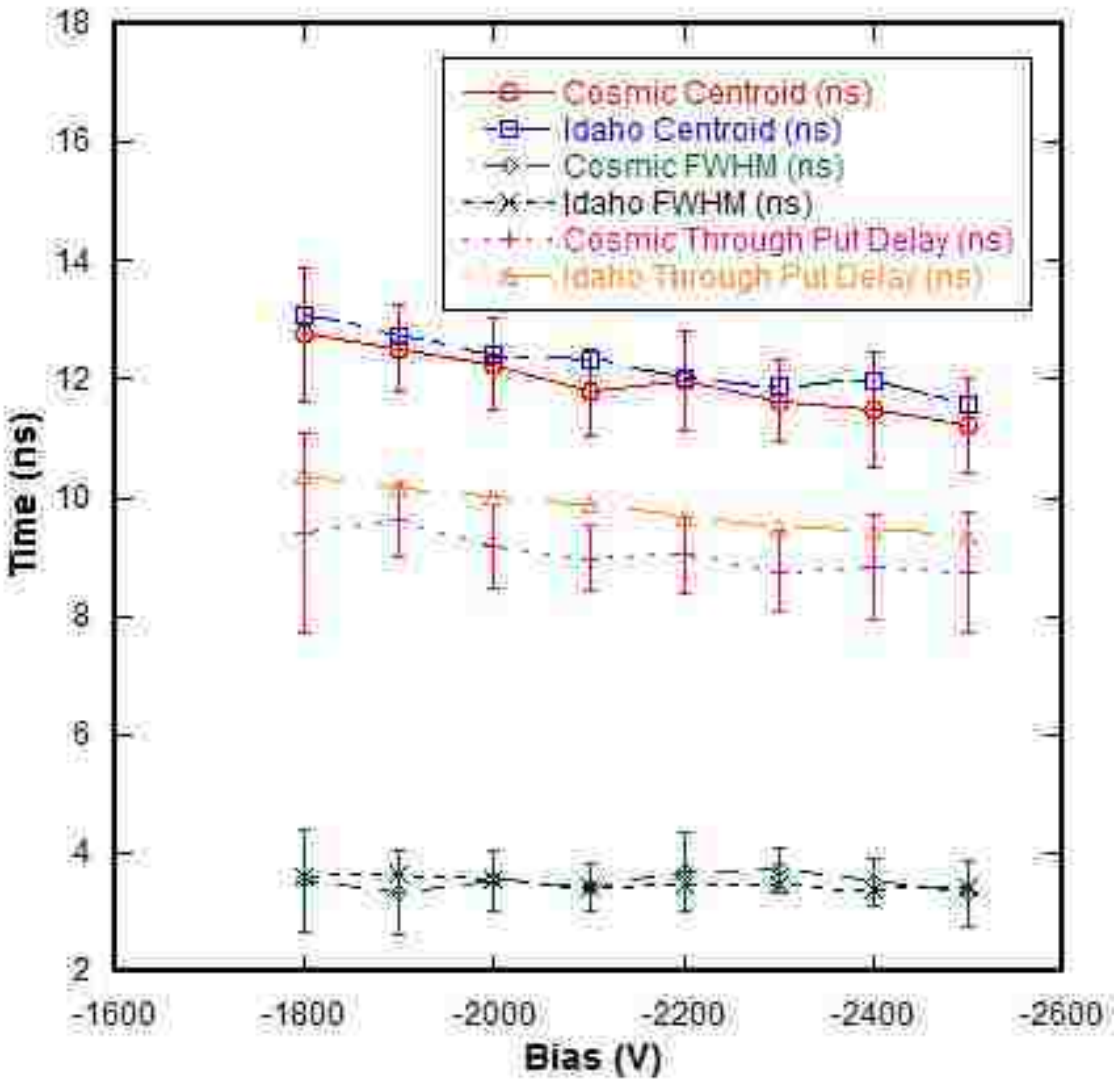

Figure 29: Detector D1 Cosmic Experiment Data versus Idaho Experiment Data

The Idaho experimental data results for the centroid and through-put all exhibit a decreasing trend with increasing bias, which matches the trends in the cosmic experimental data. The FWHM Idaho values indicate a relatively flat history and are in agreement with the cosmic measurements.

The cosmic data displayed in Figure 29 includes uncertainties that represent the standard deviations in the cosmic data derived from the 20 measurements at each 100 V bias setting. While the cosmic data does not perfectly match the Idaho data, there are

overlaps in the results when the error bars are taken into account. For the centroid value, the Idaho data falls within a standard deviation of all of the cosmic data points. For the through-put, seven of the eight Idaho data points fall within one standard deviation of the cosmic data, and the eighth data point is not very far outside the standard deviation. For the FWHM, all of the Idaho data points fall within one standard deviation of the cosmic data, and most of those data points match very closely with the cosmic data. Based on this comparison, the cosmic radiation experimental data match reasonably well with the Idaho experimental data.

Comparing the D2 Cosmic Experimental Data with the Idaho Experimental Data

The detector D2 cosmic radiation experimental data is compared with the detector D2 Idaho experimental data in Table VI and in Figure 30.

TABLE VI: Comparison of D2 Detector Results Between the Cosmic Radiation Experiments and the Idaho Experiments

Bias (V)	Centroid (ns)	Idaho Centroid (ns)	FWHM (ns)	Idaho FWHM (ns)	Through-Put at 10% Amplitude (ns)	Idaho Through-Put at 10% Amplitude (ns)
-2500	12.2 + 0.5	11.25	3.5 + 0.4	3.31	9.6 + 0.5	8.79
-2400	12.4 + 0.9	11.33	3.6 + 0.6	3.41	9.6 + 0.7	9.02
-2300	12.8 + 0.7	11.63	3.6 + 0.4	3.41	10.1 + 0.9	9.15
-2200	12.6 + 0.5	11.69	3.8 + 0.4	3.31	9.8 + 0.7	9.39
-2100	12.9 + 0.5	11.57	3.7 + 0.4	3.11	10.1 + 0.4	9.57
-2000	13.2 + 0.5	11.78	4.0 + 0.4	3.31	10.2 + 0.6	9.65
-1900	13.1 + 0.6	12.19	3.8 + 0.5	3.02	10.4 + 0.6	9.95
-1800	13.6 + 0.6	12.69	3.7 + 0.4	2.55	11.0 + 0.7	9.99

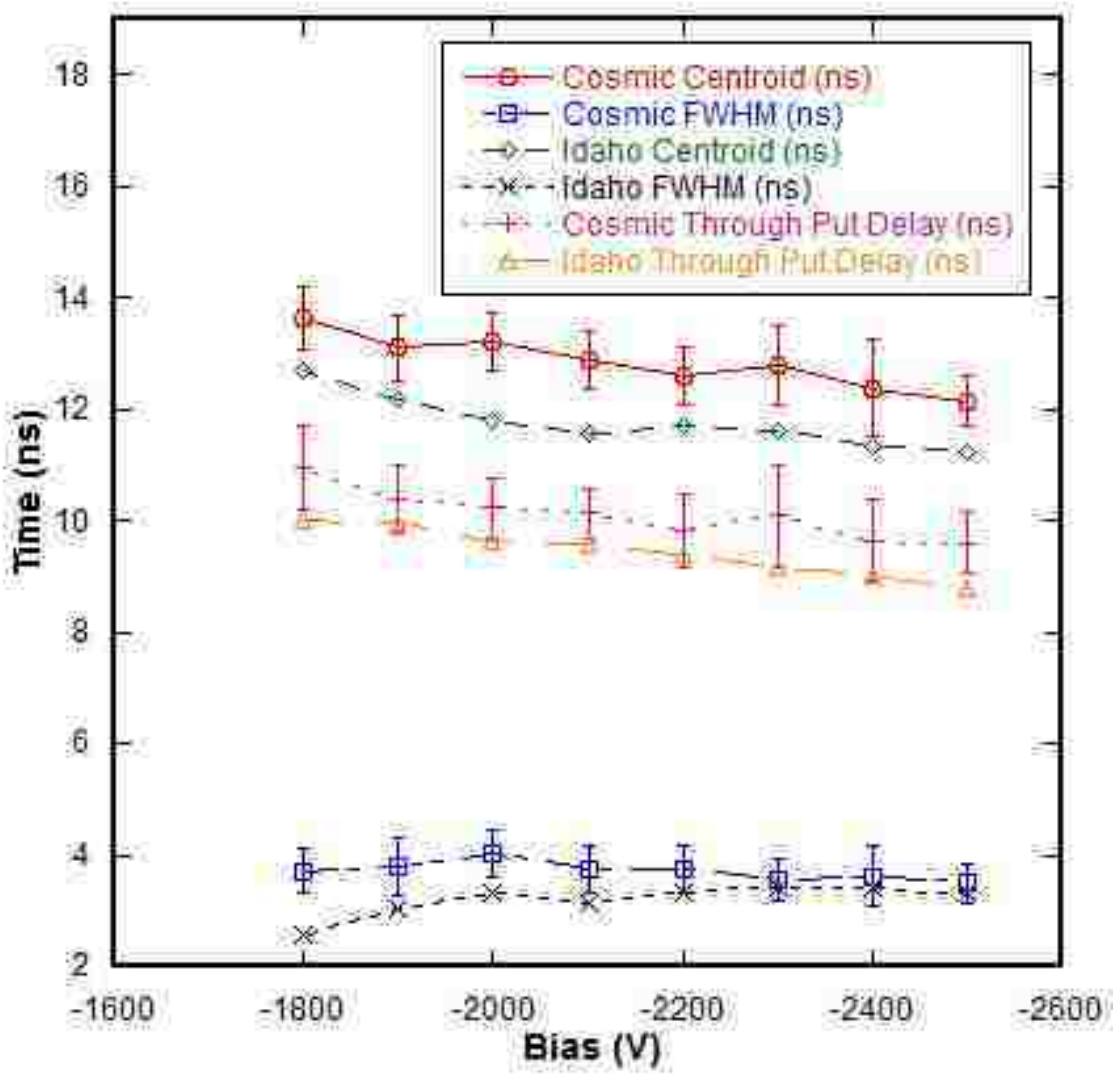

Figure 30: Detector D2 Cosmic Experiment Data versus Idaho Experiment Data

The Idaho experimental data results for the centroid and through-put for detector D2 exhibit a decreasing trend with increasing bias. This matches reasonably well with D2 cosmic data. However, the Idaho FWHM increases with increasing bias and is not consistent with the D2 FWHM , or with comparable D1 data. Although the cosmic experimental data ends at the lowest bias of -1800 V, the Idaho data continues down to -1000 V. When this additional data is analyzed, the -1800 V value of 2.55 ns appears to be an inflection point, and the data below -1800 V trends upward with decreasing bias

similar to the other measured data. Therefore, it appears that the cosmic and Idaho data are consistent when taking the entire trend into account disregarding the unusual -1800V data.

When the uncertainties representing the standard deviation of each cosmic data point are plotted alongside the Idaho data, there appears to be less agreement than there was with the D1 data. While this data seems to trend well with the Idaho centroid data, none of the Idaho centroid data points fall within one standard deviation of the cosmic data points. For the through-put delay, there is better agreement between the cosmic and the Idaho data. Five of eight Idaho data points fall within one standard deviation of the cosmic data, and all of these points seem to agree very close to the standard deviation value away from the cosmic through-put measurements. Additionally, only four of eight Idaho data points fall within one standard deviation of the cosmic data points. Taking all three quantities together, the cosmic radiation experimental data for D2 do not compare as well with the Idaho data exhibited by the D1 results.

The Results from Taking Additional Measurements

The D1 and D2 results were the product of a statistical analysis of twenty measurements per bias setting per detector. Only twenty measurements were taken due to the time required to collect the measurements. As demonstrated in the histogram in Figure 26, twenty measurements do not produce a normal distribution of data points. To demonstrate this is possible, eighty additional measurements were taken on detector D1 at -2500 V for a total of 100 measurements total at -2500 V. The results were analyzed in cumulative twenty-measurement intervals and are displayed in Figure 31 and Table VII.

TABLE VII: The Results of taking More Measurements at -2500 V on D1

Number of Measure-ments	Centroid (ns)	Idaho Centroid (ns)	FWHM (ns)	Idaho FWHM (ns)	Through Put at 10% Amplitude (ns)	Idaho Through Put at 10% Amplitude (ns)
20	11.2 ± 0.8	11.566	3.3 ± 0.6	3.42	8.7 ± 1.0	9.3375
40	12.1 ± 1.1	11.566	3.3 ± 0.5	3.42	9.4 ± 1.1	9.3375
60	12.1 ± 1.0	11.566	3.3 ± 0.5	3.42	9.5 ± 1.0	9.3375
80	12.2 ± 0.9	11.566	3.4 ± 0.5	3.42	9.6 ± 0.9	9.3375
100	12.25 ± 0.9	11.566	3.4 ± 0.5	3.42	9.6 ± 0.8	9.3375

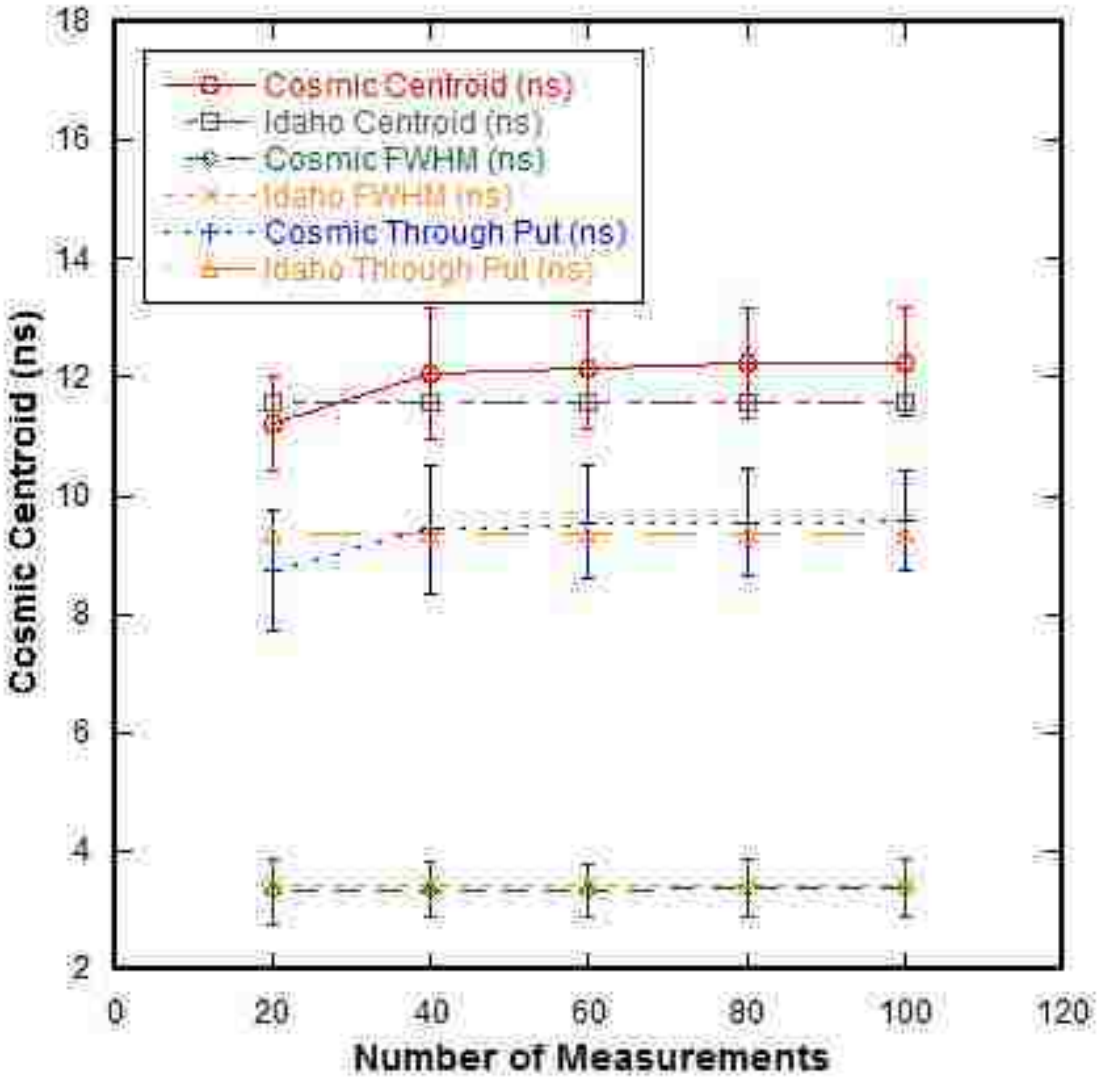

Figure 31: Analytical Results from Taking Additional Measurements on D1 at -2500V

As predicted, the statistics improved with the additional eighty measurements on D1 at -2500V. The mean values for the centroid, FWHM, and through-put changed from the mean values of only twenty measurements. However, all three measurements seem to be converging on a single value as the measurements increased. The values for the centroid changed the most from the twenty-measurement value and the standard deviation increased. This leads to a conclusion that the additional measurements did produce better statistics.

At twenty measurements, the cosmic FWHM was 110 ps less than the Idaho value. After 100 measurements, the cosmic FWHM was 42 ps less than the Idaho value. At twenty measurements, the cosmic through-put was 608 ps less than the Idaho value. After 100 measurements, the cosmic through-put was 243 ps more than the Idaho value. For both the FWHM and the through-put, the standard deviation was progressively less as the number of measurements increased. As the timing bin size on the digitizer is 200 ps, the FWHM was within this uncertainty. However, the difference between the cosmic through-put delay and the Idaho through-put reduced to just slightly more than 200 ps. Analyzing both of these quantities, taking more measurements clearly resulted in better results for the mean FWHM and through-put.

CHAPTER 5: CONCLUSION AND FUTURE WORK

Section 1: Conclusion

The analysis of the results from the cosmic radiation experiments with detectors D1 and D2 to determine the detector time responses and through-put delays demonstrate that this technique yields results consistent with earlier Idaho-based experimental data. The only limitation of the technique is a function of the gain of the PMT of the detector under test. The R329 tube has high gain affording coincidence detection of cosmic radiation down to -1000V. But, the gain of the R5946 mesh PMT is a factor of ten less than that of the R329, and could only detect cosmic radiation from -2500V to -1800V. Thus the cosmic radiation technique could only characterize the FWHM and through-put for a limited range of detector bias settings.

The cosmic data matched the Idaho data for D1 very well. The D1 results were within one standard deviation of the Idaho data for the centroid, FWHM, and the through-put. However, this may have been a function of using Idaho D1 data as a reference for calibrating the through-put delay of the coincidence detectors and electronics. For D2, the cosmic experiment results did not match the Idaho results as well as the D1 results. The cosmic D2 FWHM results were outside of one standard deviation for bias settings below -2100V. However, the Idaho data for the FWHM of D2 trends in an opposite way from the D1 detector data (see Appendix H). While the Idaho D1 FWHM increases with decreasing bias, the Idaho D2 data decreases with decreasing bias to -1800V and then begins increasing from -1700V to -1000V. If you drew a line between the Idaho D2 FWHM values from -1000V to -2500V, then the cosmic data for D2 matches that overall

trend in the Idaho D2 data. This plot is displayed in Figure 32. There is no explanation for this discrepancy at -1800V. The validity of the Idaho D2 FWHM data is in question.[35]

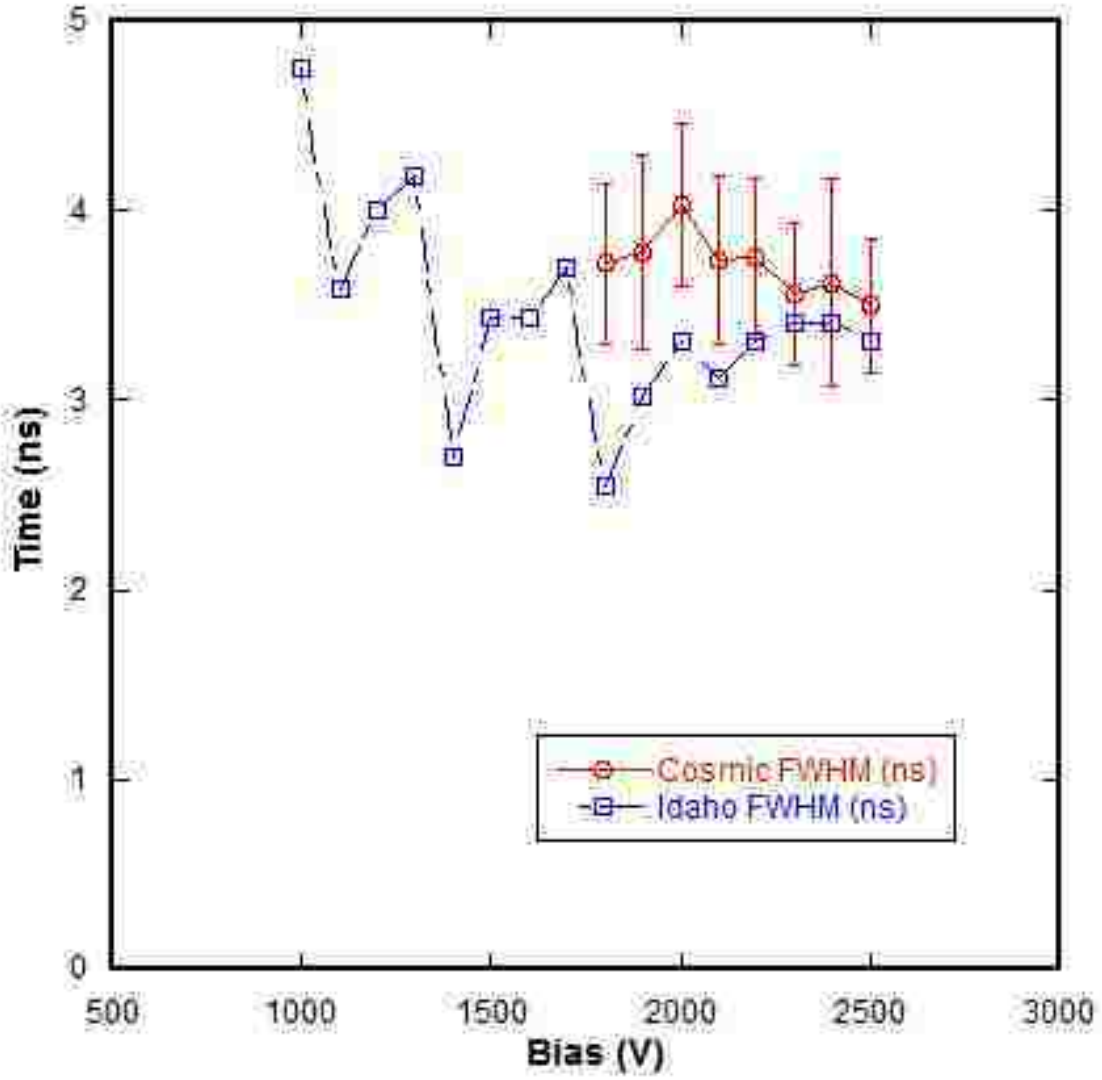

Figure 32: Complete Idaho D2 FWHM and Cosmic D2 FWHM data

Both the cosmic D2 centroid and the through-put results were within one standard deviation of the Idaho results. However, both of these results were greater than the Idaho results. As the difference between the cosmic results and the Idaho results appears to be constant, this may also be a function of using the Idaho D1 results to calibrate the

[35] Private Communication, C.L. Ruiz, Sandia National Laboratories, 2013.

coincidence detectors. Calibrating the coincidence detectors with the Idaho D2 results could eliminate this increase in values and bring the FWHM and through-put values closer to the Idaho D2 results.

The additional eighty measurements taken with D1 at -2500V resulted in a significant increase in the centroid and through-put values. This occurred when combining the original twenty measurements with the second twenty measurements, and then continued to make a slight increase with the additional sixty measurements. Thus it appears that the measurements taken on different days returned different results. While the results at 100 measurements were closer to the Idaho data, they were different than the original data taken approximately one month before the second experiment. Even though both the first twenty and the additional eighty measurements were within one standard deviation of the Idaho D2 results, the difference calls into question the repeatability of the cosmic measurement technique.

Additionally, the experimental data reveals an important characteristic of plastic scintillator-PMT detectors in general. The experimental electronics were calibrated using the Idaho D1 centroid data at -2500V. This provided for the through-put delay of the coincidence detectors and the corresponding coincidence electronics. However, this calibration had no effect on the time response of the detector. The cosmic FWHM results for D1 were remarkably consistent with the FWHM from the Idaho experiments conducted eight years earlier. This means that although age reduces the amplitude of the signals from scintillation detectors, it does not seem to have a statistically significant effect on the time resolution of these systems.

Section 2: Future Work

While the results from the cosmic radiation experiments demonstrated that the technique of using cosmic rays in a coincidence system to measure the through-put delay and time response of a plastic scintillator detector is valid, there were several things that appeared throughout the experiment that indicated ways to improve the technique. The first of these is the requirement for an accurate independent measurement of the through-put of the coincidence detectors. As the accuracy of the through-put delay measurement requires an accurate knowledge of the time that the incident radiation interacted in the scintillator, using the D1 reference data to manually adjust the delay in the system to account for the through-put delay of the coincidence detectors and associated electronics introduced uncertainty in the measurement. Taking the coincidence detectors to an accelerator facility to measure the through-put delay would make the determination of the initial incident cosmic radiation timing more accurate, resulting in a more accurate determination of the through-put delay of the nTOF detector under test.

If taking the coincidence detector to an accelerator is not feasible, there may be better ways to calibrate the coincidence system than using the Idaho centroid data. Using the additional D1 measurements taken at -2500V to evaluate the coincidence calibration leads to the conclusion that the calibration was off approximately 700 ps at 12.25 ns. The centroid calibration should have been at 11.5 ns, thus after taking 100 measurements the delay in the signal from the detector under test should be increased by 500 ps and the study repeated until the calibration is within 200 ps of the 11.5 ns Idaho D1 centroid value. However, even with the centroid calibration off approximately 700 ps, the through-put delay from the cosmic D1 data was only 243 ps more than the Idaho D1 data. With a digitizer bin size of 200 ps, this is almost within the error in the experimental set-

up. As there seems to be no linear relationship between the centroid value and the through-put value, the calibration of the coincidence detectors should use the Idaho through-put delay value at -2500V and not the centroid value.

The inconsistent results for nTOF detector D2 should be examined in greater detail. One way to do this is to calibrate the coincidence detectors to the Idaho results for D2. The results from these experiments would determine if the increased values for the centroid and through-put for D2 were a function of the detector itself, or the calibration process. Then, with the D2 calibration, detector D1 should also be evaluated to see if there is an impact on the centroid and through put values. This would also validate the use of a reference detector in calibrating the coincidence detectors.

As the measurements taken on different days produced different results for D1, additional studies should be done to assess the reliability of the cosmic radiation experimental methodology. These studies should be separated by at least a week to determine if time has an effect on the results. They should be conducted on both detectors and at the bias settings from -1800V to -2500V. Such studies would establish the reliability of the cosmic radiation technique. It would also determine whether the variability in the cosmic radiation makes it a reliable source for these experiments.

To get more accurate results, more than twenty measurements need to be taken per bias setting. While the results after 100 measurements demonstrated that the values began to converge, it appeared that the values had not fully converged. Therefore, to get the most accurate values for the FWHM and through-put at a given bias setting, more than 100 analyzable measurements need to be taken.

APPENDICIES

APPENDIX A: BC-404 PLASTIC SCINTILLATOR SPECIFICATIONS

BC-400/BC-404/BC-408/BC-412/BC-416
Premium Plastic Scintillators

General Description The premium plastic scintillators described in this data sheet include the most economical (BC-416) as well as those with the highest light output.

General Technical Data

Base ..... Polyvinyltoluene
Density ..... 1.032 g/cc
Refractive Index 1.58
Coefficient of Linear Expansion ..... 7.8×10^{-5}, below 67°C
Atomic Ratio, H/C ..... ~1.1
Light Output Temperature Dependence ..... At +60°C = 95% of that at +20°C; independent of temperature from -60°C to +20°C
Vapor Pressure ..... May be used in a vacuum
Solubility ..... Soluble in aromatic solvents, chlorine, acetone, etc. Insoluble in water, dilute acids, lower alcohols, silicone fluid, grease and alkalis.

Radiation Detected	Scintillator
< 100 keV X-rays	BC-404
100 keV to 5 MeV gamma rays	BC-408
>5 MeV gamma rays	BC-400 BC-416
Fast neutrons	BC-408 BC-412
Alphas, betas	BC-400 BC-404
Charged particles, cosmic rays, muons, protons, etc.	BC-408 BC-412 BC-416

Properties	BC-400	BC-404	BC-408	BC-412	BC-416
Light Output, % Anthracene	65	68	64	60	38
Rise Time, ns	0.9	0.7	0.9	1.0	—
Decay Time, ns	2.4	1.8	2.1	3.3	4.0
Pulse Width, FWHM, ns	2.7	2.2	~2.5	4.2	5.3
Light Attenuation Length, cm*	160	140	210	210	210
Wavelength of Max. Emission, nm	423	408	425	434	434
No. of H Atoms per cm^3, ($x10^{22}$)	5.23	5.21	5.23	5.23	5.25
No. of C Atoms per cm^3, ($x10^{22}$)	4.74	4.74	4.74	4.74	4.73
Ratio H:C Atoms	1.103	1.100	1.104	1.104	1.110
No. of Electrons per cm^3, ($x10^{23}$)	3.37	3.37	3.37	3.37	3.37
Principal uses/applications	general purpose	fast counting	TOF counters, large area	large area	large area economy

*The typical 1/e attenuation length of a 1 x 20 x 200 cm cast sheet with edges polished as measured with a bialkali photomultiplier tube coupled to one end

(continued over)

BICRON®
Saint-Gobain Industrial Ceramics, Inc.

BICRON • 12345 Kinsman Road • Newbury, Ohio 44065 USA
Phone: (440) 564-2251 • Fax: (440) 564-8047 • Internet: http://www.bicron.com
Bicron FaxBack Information Access System: (800) 892-8708
European Office • P.O. Box 3093, 3760 DB Soest, The Netherlands
Phone: (31) 35 60 29 700 • Fax: (31) 35 60 29 214
Nippon Bicron • 8F Shinyokohama Station Building, 2-6-13 Shinyokohama
Kohoku-ku, Yokohama 222 Japan • Phone: (81) 45.474.5786 • Fax: (81) 45.474.5787

BC-400/BC-404/BC-408/BC-412/BC-416
Premium Plastic Scintillators

(continued from first page)

Emission Spectra

BC-400

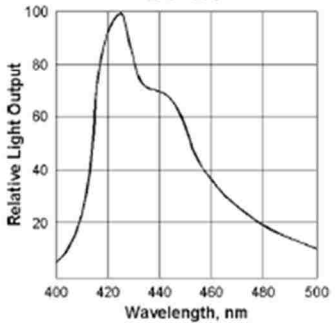

BC-408

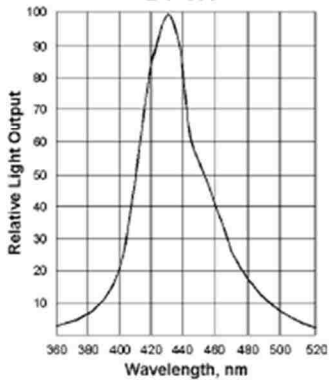

BC-404

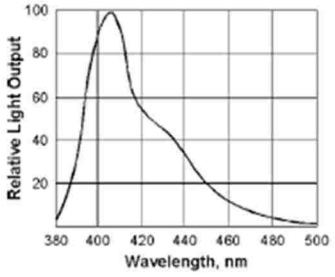

BC-412 & BC-416

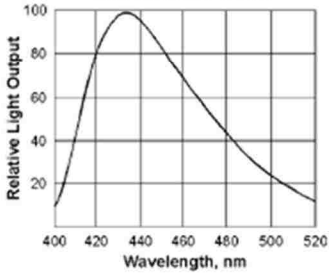

Premium Plastic Scintillators
Response to Atomic Particles

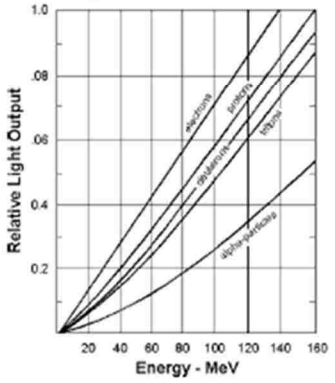

Range of Atomic Parlicles in
Premium Plastic Scintillators

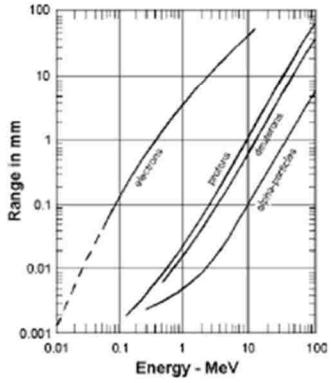

3/4/98

APPENDIX B: HAMAMATSU R329 PMT SPECIFICATIONS

HAMAMATSU

TECHNICAL DATA SHEET

R329

PHOTOMULTIPLIER TUBE
June 82

FOR SCINTILLATION COUNTING AND HIGH ENERGY PHYSICS
2 INCH DIAMETER, FAST TIME RESPONSE, BIALKALI PHOTOCATHODE
12-STAGE, HEAD-ON, DIRECT REPLACEMENT FOR RCA 8575

GENERAL:

Spectral Response	300 to 650 nm
Wavelength of Maximum Response	420 nm
Photocathode	
Material	Bialkali
Minimum Useful Size	46 mm dia.
Window Material	Borosilicate glass
Dynode	
Structure	Linear focused
Number of Stages	12
Direct Interelectrode Capacitances	
Anode to Last Dynode	2 pF
Anode to All Other Electrodes	2.5 pF
Base	21-pin glass base
Suitable Socket	E678-21A (supplied)

MAXIMUM RATINGS (Absolute Maximum Values):

Supply Voltage	
Between Anode and Cathode	2700 Vdc
Between Anode and Last Dynode	500 Vdc
Average Anode Current	0.2 mA
Ambient Temperature	-80 to +50°C

CHARACTERISTICS (at 25°C):	Min.	Typ.	Max.	Units
Anode Sensitivity				
Luminous (2856K)	15	50	-	A/lm
Radiant at 420 nm	-	3.5×10^4	-	A/W
Cathode Sensitivity				
Luminous (2856K)	60	80	-	μA/lm
Radiant at 420 nm	-	80	-	mA/W
Blue (with CS No.5-58 filter)	9.0	10.5	-	μA/lm-b
Quantum Efficiency at 390 nm	-	25	-	%
Current Amplification	-	6.3×10^5	-	
Anode Dark Current (after 3 hrs)	-	1	2	nA
Time Response				
Anode Pulse Rise Time	-	2.6	-	ns
Electron Transit Time	-	48	-	ns
Transit Time Spread	-	0.9	-	ns
Pulse Height Resolution with ^{137}Cs	-	7.3	-	%
Pulse Height Stability				
Long Term (For 16 h at 1000 cps)	-	1	-	%
Short Term (10000 to 1000 cps)	-	1	-	%
Pulse Linearity				
At 2 % Deviation	-	80	-	mA
At 5 % Deviation	-	110	-	mA

VOLTAGE DISTRIBUTION RATIO AND SUPPLY VOLTAGE:

Electrodes:	K	G	DY1	DY2	DY3	DY4	DY5	DY6	DY7	DY8	DY9	DY10	DY11	DY12	P
Ratio:	4	0	1	1.4	1	1	1	1	1	1	1	1	1	1	

Supply Voltage:1500 Vdc, K:Cathode, DY:Dynode, P:Anode, G:Grid

* Shield is connected to DY5.

Fig.1 Typical Spectral Response

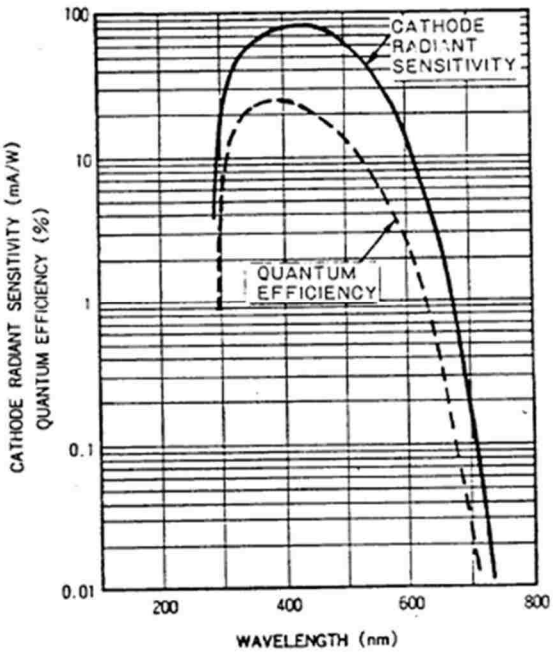

Fig.2 Dimensional Outline and Basing Diagram (Unit:mm)

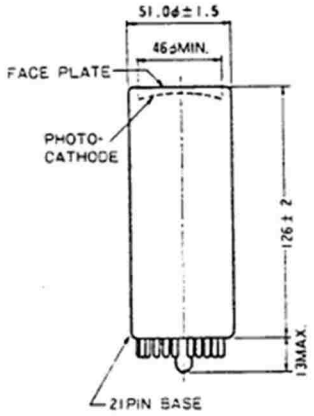

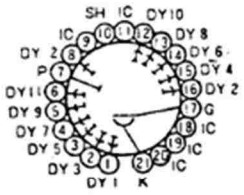

HAMAMATSU

Phone: 0534/34-3311 Telex: 4225-185

APPENDIX C: CONSTANT FRACTION DISCRIMINATION AND LOGIC UNIT OPERATIONS

Fast Timing and Constant Fraction Discrimination

In constructing a coincidence system, it is imperative to have electronics that mark the arrival of incident radiation with consistency and precision. There are three major phenomena that constrain timing resolution. These are jitter, walk, and drift. Jitter is a function of electrical noise that causes an uncertainty in the timing of the signal to be introduced into the output pulse. Walk is the dependence of the output signal on the amplitude of the incoming pulse, thus the larger the amplitude the smaller the walk. An example of Jitter and walk is displayed in the figure below. Drift is long-term systemic error from the aging of electronics and variations in the temperature effects on the discriminator.[36] Optimal timing resolution requires the use of a timing discriminator which suppresses these phenomena.

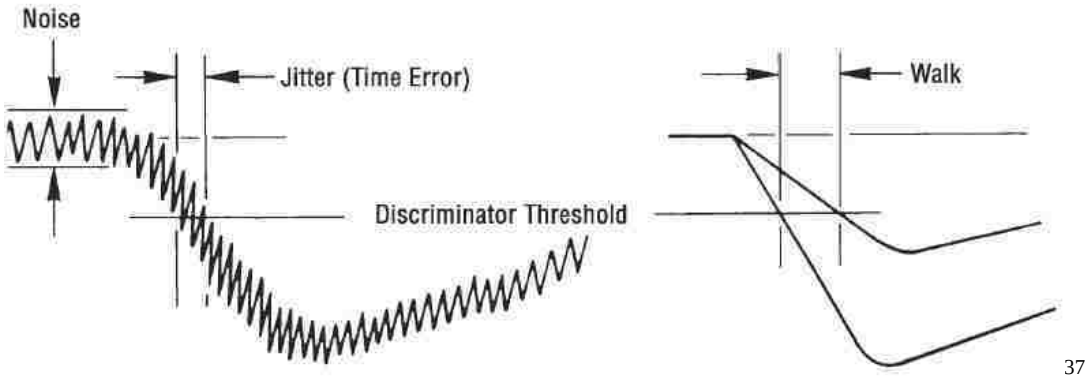

[37]

[36] Ortec, *Fast-Timing Discriminator Introduction* (Oak Ridge: Ametek Advanced Measurement Technology), 3.
[37] Ibid., 3.

To solve the problem of precise and consistent timing resolution, constant fraction discrimination, CFD, was developed.[38] The goal of CFD is to trigger at some constant optimum fraction of the pulse over a broad spectrum of input pulse shapes of varying amplitude. To do this, the incoming pulse is split into two parts. The first part is attenuated to some constant fraction of the initial amplitude while the second part is delayed and inverted. Both parts are then added together to form the timing signal. A visual description of this process is displayed in the figure below.

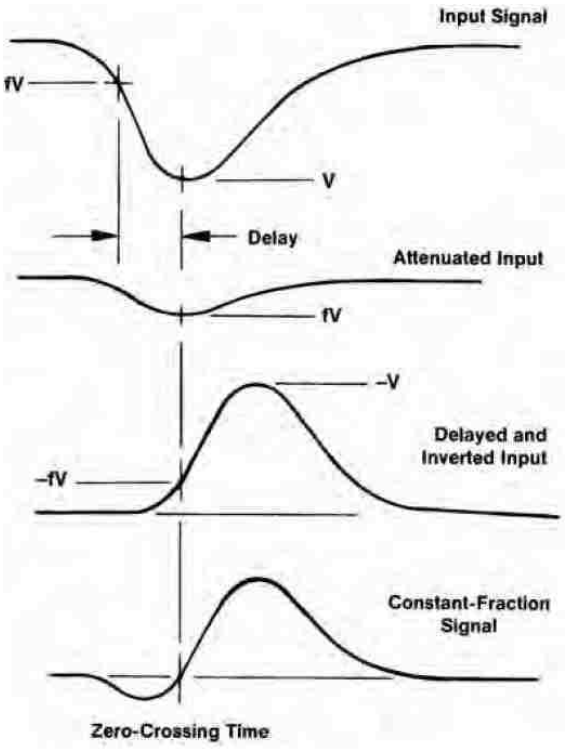

[39]

The timing signal produced by CFD provides a precise and consistent marking of the time an incident radiation interacts in a scintillator and produces an output signal. When the proper constant fraction is chosen the walk and jitter of the signal are minimized. This optimum constant fraction has been experimentally determined to be

[38] D.A. Gedcke, and W.J. McDonald, "A Constant Fraction of Pulse Height Trigger For Optimum Time Resolution," *Nuclear Instruments and Methods* 55 (1967): 377-380.
[39] Ortec, *Fast-Timing Discriminator Introduction*, 4.

roughly 20%. This makes constant fraction discrimination the optimal technique for timing resolution in scintillator-PMT detectors. CFD has also been experimentally proven to be a successful technique in fast scintillator-PMT systems for providing optimal time resolution.[40] For this reason, a CFD unit was used as part of the coincidence system.

The CFD unit used in this experiment was the Ortec 935 Quad 200-MHz CFD. The specifications for the Ortec Model 935 are located in Appendix D. The Model 935 reduces the walk of any given signal to within $\pm$ 50 ps. The timing signals have a FWHM of 1 ns and a pulse-pair resolving time of <5 ns. The output signal is a negative-NIM signal with an adjustable width from 4 ns to 200 ns.

Logic Unit

A logic unit compares input signals and determines if those logic signals are coincident or not. When the input signals overlap then the unit generates a logic output signal, and when the input signals do not overlap no signal is produced. The overlap that determines a coincident event is determined by the electronics of the logic unit. While the logic unit has a variety of different functions, the coincidence unit portion of the logic system performs the ñANDò operations.[41] Thus, when two inputs overlap, the unit determines that signal 1 AND signal 2 are in coincidence and produces an output signal.

The logic unit used in this experiment was the Ortec Model CO4020 Quad 4-input Logic Unit. The specification of the CO4020 is located in Appendix E. This unit accepts fast negative-NIM logic pulses. The minimum pulse overlap is 3 ns. The Y outputs have an adjustable width from 40 ns to 40 μs, and have both a fast negative-NIM output signal

[40] D.A. Gedcke, and W.J. McDonald, "A Constant Fraction of Pulse Height Trigger For Optimum Time Resolution," *Nuclear Instruments and Methods* 55 (1967): 380.
[41] Leo, *Techniques for Nuclear and Particle Physics Experiments,* 295-96.

and a positive TTL output signal. For the purposes of this experiment, only the fast negative-MIN output signal was used.

APPENDIX D: Ortec Model 935 Quad 200-MHz CFD

ORTEC®

935

Quad 200-MHz Constant-Fraction Discriminator

- **Constant-fraction timing on signals as narrow as 1 ns FWHM — ideal for microchannel plates, fast photomultiplier tubes, fast scintillators, and fast silicon detectors**
- **Ultra-low walk, guaranteed <±50 ps (typically <±25 ps) over a 100:1 dynamic range**
- **Pulse-pair resolving time <5 ns**
- **Quick and accurate walk adjustment with a zero-crossing signal monitor that displays the full amplitude range**
- **Blocking or updating outputs with adjustable widths**
- **Selectable functions for each of the four channels include a fast veto input, individual gates with coincidence/anticoincidence options, and a bin gate**

The Model 935 Quad 200-MHz Constant-Fraction Discriminator incorporates four separate and independently adjustable timing discriminators in a single-width NIM module. Except where indicated otherwise, the descriptions and specifications apply to each of the four channels in the module.

The ability of the Model 935 to provide constant-fraction timing on fast, negative-polarity signals as narrow as 1 ns (FWHM) makes it ideal for use with microchannel plates, fast photomultiplier tubes, fast scintillators, and fast silicon detectors. The exceptionally low walk delivered by the Model 935 is vital in achieving the excellent time resolution inherent in these fast detectors over a wide dynamic range of pulse amplitudes. The Model 935 can also be used with scintillators such as NaI(Tl) which have long decay times. To prevent multiple triggering on the long decay times, the width of the blocking output can be adjusted up to 1 µs in duration.

The Model 935 uses the constant-fraction timing technique to select a timing point on each input pulse that is independent of pulse amplitude. When properly adjusted, the generation of the output logic pulse corresponds to the point on the leading edge of the input pulse where the input pulse has risen to 20% of its maximum amplitude. To achieve this constant-fraction triggering, the input pulse is inverted and delayed. The delay time is selected by an external delay cable (DLY) to be equal to the time taken for the input pulse to rise from 20% of maximum amplitude to maximum amplitude. Simultaneously, the prompt input signal is attenuated to 20% of its original amplitude. This attenuated signal is added to the delayed and inverted signal to form a bipolar signal with a zero crossing. The zero crossing occurs at the time when the inverted and delayed input signal has risen to 20% of its maximum amplitude. The zero-crossing discriminator in the Model 935 detects this point and generates the corresponding timing output pulse.

"Walk" is the systematic error in detecting the time for the 20% fraction as a function of input pulse amplitude. Minimizing walk is important when a wide range of pulse amplitudes must be used, because walk contributes to the time resolution. The Model 935 uses a transformer technique for constant-fraction shaping to achieve the exceptionally wide bandwidth essential for processing input signals with subnanosecond rise times. As shown in Fig. 1, this results in a walk guaranteed <±50 ps and typically <±25 ps over a 100:1 dynamic range of input pulse amplitudes. The patented shaping technique also provides a zero-crossing monitor output that facilitates quick and accurate walk adjustment, because it displays the full input signal amplitude range.

The extremely short pulses from microchannel plate multipliers and ultra-fast photomultiplier tubes require very short constant-fraction shaping delays. To accommodate

these detectors, the Model 935 incorporates a selectable compensation for the inherent internal delay.

The Model 935 includes a number of controls that considerably broaden its utility. The threshold discriminator is useful for rejecting low-level noise. A front-panel test point permits precise measurement of its setting in the range from –20 to –1000 mV. Each channel provides three bridged timing outputs. These are standard, fast negative NIM outputs. The outputs can be selected to have either updating or blocking characteristics. The updating mode is useful for reducing dead time in overlap coincidence experiments. The blocking mode simultaneously minimizes multiple triggering and dead time on scintillators with long decay times. The output pulse width is adjustable from <4 ns to >200 ns in the updating mode, and from <5 ns to >1 µs in the blocking mode. The pulse-pair resolution is <5 ns at minimum pulse width in the updating mode.

Switches on the printed circuit board allow selection of which channels will respond to the front-panel fast-veto input. Additional fast gating capability is provided by individual gate inputs for each channel on the rear panel. The mode of these separate gate inputs can be individually selected to be either coincidence or anticoincidence via DIP switches on the printed circuit board. Each channel can also be programmed to ignore or respond to the slow bin gate signal on pin 36 of the power connector for NIM bins incorporating that signal.

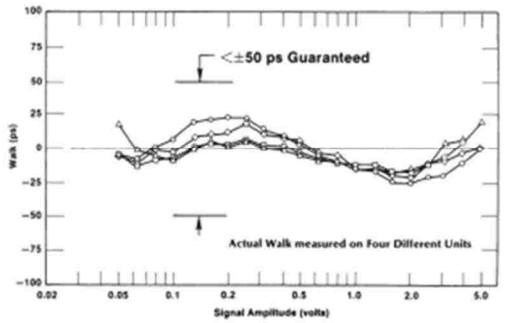

Fig. 1. Actual Walk Measured on Four Different Units.
See Walk Specification for Measurement Conditions.

Specifications

The Model 935 contains four independent and identical constant-fraction discriminators. Except where stated otherwise, the descriptions and specifications are given for an individual channel, and apply to each of the four channels.

PERFORMANCE

WALK Guaranteed <±50 ps (typically <±25ps) over a 100:1 dynamic range. Measured under the following conditions: input pulse amplitude range from 50 mV to 5 V, rise time <1 ns, pulse width 10 ns, external shaping delay approximately 1.6 ns (33 cm or 13 in.), internal offset delay enabled, threshold approximately 20 mV.

CONSTANT FRACTION 20%.

PULSE-PAIR RESOLUTION <5 ns in the updating mode, <7 ns in the blocking mode.

INPUT/OUTPUT RATE Operates at burst rates >200 MHz in the updating mode, and >150 MHz in the blocking mode.

TRANSMISSION DELAY Typically <13 ns with 1.6-ns external delay.

OPERATING TEMPERATURE RANGE 0 to 50°C.

THRESHOLD TEMPERATURE SENSITIVITY <0.01%/°C, from 0 to 50°C. Threshold referenced to the –12 V supply level supplied by the NIM bin.

TRANSMISSION DELAY TEMPERATURE SENSITIVITY <±10 ps/°C from 0 to 50°C.

CONTROLS

THRESHOLD (T) A front-panel, 20-turn screwdriver adjustment for each discriminator channel sets the minimum pulse amplitude that will produce a timing output. Variable from –20 to –1000 mV. A front-panel test point located to the left of the threshold adjustment monitors the discriminator threshold setting. The test point voltage is 10X the actual threshold setting. Output impedance: ≤2 kΩ.

WALK ADJUSTMENT (Z) A front-panel, 20-turn screwdriver adjustment for fine-tuning the zero-crossing discriminator threshold to achieve minimum walk. Adjustable over a ±15 mV range. A front-panel test point located to the left of the walk adjustment monitors the actual setting of the zero-crossing discriminator. Output impedance, 1 kΩ.

OUTPUT WIDTH (W) A front-panel, 20-turn screwdriver adjustment for each discriminator channel sets the width of the three output logic pulses. The range of width adjustment depends on the positions of jumpers W2 and W3.

B GATE ON/OFF Rear-panel switch turns the Bin Gate on or off for all channels programmed to accept the Bin Gate.

GATE COIN/ANTI A printed wiring board DIP switch selects either the coincidence or anticoincidence mode for the individual channel's response to the rear-panel gate input.

VETO YES/NO A printed wiring board DIP switch selects whether or not an individual channel will respond to the front-panel VETO input.

BIN GATE YES/NO A printed wiring board DIP switch selects whether or not an individual channel will respond to the bin gate signal.

INTERNAL OFFSET DELAY (W1) Printed wiring board jumper W1 is normally omitted to enable the 1.7-ns internal offset delay. This delay compensates for internal delays and makes it possible to implement the very short shaping delays required with 1-ns input pulse widths. With jumper W1 installed, the minimum shaping delay is limited by a +0.7-ns internal contribution. With W1 omitted, the internal delay contribution is effectively –1.0 ns. The Model 935 is shipped from the factory with the W1 jumper omitted. Spare jumpers for this position are located in the storage area towards the rear of the module.

UPDATING/BLOCKING MODE (W2) The printed wiring board jumper W2 selects either the updating mode (U), or the blocking mode (B) for the output pulse widths. In the blocking mode, a second input pulse will generate no output pulse if it arrives within the output pulse width W caused by a previous input pulse. In the updating mode, a second input pulse arriving within the output pulse width W from a previous pulse will extend the output pulse, from the time of arrival, by a length W. The Model 935 is shipped from the factory in the updating mode.

OUTPUT PULSE WIDTH RANGE (W3) The printed wiring board jumper W3 selects the range of output width adjustment as listed in Table 1. The Model 935 is shipped from the factory with the W3 jumper omitted. Spare jumpers for this position are located in the storage area towards the rear of the module.

INPUTS

IN1, IN2, IN3, or IN4 A front-panel LEMO connector input on each channel accepts the fast linear signal from a detector for constant-fraction timing. Linear range from 0 to –10 V. Signal input impedance, 50 Ω, dc-coupled; input protected with diode clamps at ±10 V. Input reflections <10% for input rise times >2 ns.

GATE INPUTS 1, 2, 3, or 4 A rear-panel BNC connector for each channel accepts a negative, fast NIM logic signal to gate the respective constant-fraction timing output. Coincidence or anticoincidence gating is selected by a printed wiring

board DIP switch (See GATE COIN/ANTI). Input impedance, 50 Ω. For proper gating operation, the leading edge of the GATE INPUT should precede the IN1 (IN2, IN3, or IN4) signal by 1 ns and have a width equal to the CF Shaping Delay plus 5 ns.

VETO A single, front-panel LEMO connector accepts NIM negative fast logic pulses to inhibit the timing outputs on all the channels chosen with the VETO YES/NO switch. Input impedance, 50 Ω. For proper FAST VETO operation, the leading edge of the VETO signal must precede the IN1 (IN2, IN3, or IN4) signal by 3 ns and have a width equal to the CF Shaping Delay plus 5 ns.

BIN GATE A slow master gate signal enabled by the rear-panel B GATE ON/OFF switch permits gating of the timing outputs when the Model 935 is installed in a bin that provides a bin gate signal on pin 36 of the NIM power connector. Clamping pin 36 to ground from +5 V inhibits operation of all channels selected by the BIN GATE YES/NO switch.

OUTPUTS

CF SHAPING DELAY (DLY) A front-panel pair of LEMO connectors for selecting the required constant-fraction shaping delay. A 50-Ω cable is required. For triggering at a 20% fraction, the length of the shaping delay is approximately equal to the time taken for the input pulse to rise from 20% of its full amplitude to full amplitude.

CF MONITOR (M) Permits observation of the constant-fraction shaped signal through a LEMO connector on the front panel. Output impedance, 50 Ω, ac-coupled. The monitor output is attenuated by a factor of approximately 5 with respect to the input when driving a terminated 50-Ω cable.

OUT Three bridged, updating or blocking, fast negative NIM output signals, furnished through front-panel LEMO connectors, mark the CF zero-crossing time. Amplitude –800 mV on 50-Ω load. Each output connector has its own 51-Ω resistor in series with the common output driver.

GND Front-panel test point provides a convenient ground connection for test probes.

EVENT-OCCURRED LED Front-panel LED for each channel indicates that an output signal has occurred.

ELECTRICAL AND MECHANICAL

POWER REQUIREMENTS The Model 935 derives its power from a NIM bin/power supply. Required dc voltages and currents are: +24 V at 0 mA; +12 V at 33 mA; +6 V at 225 mA; –6 V at 1400 mA; –12 V at 169 mA; –24 V at 55 mA.

WEIGHT
Net 1.1 kg (2.6 lb).
Shipping 2.0 kg (4.4 lb).

DIMENSIONS NIM-standard single-width module, 3.43 X 22.13 cm (1.35 X 8.714 in.) per DOE/ER-0457T.

Ordering Information

To order, specify:

Model	Description
935	Quad 200-MHz Constant-Fraction Discriminator

ORTEC®
www.ortec-online.com
Tel. (865) 482-4411 • Fax (865) 483-0396 • ortec.info@ametek.com
801 South Illinois Ave., Oak Ridge, TN 37831-0895 U.S.A.
For International Office Locations, Visit Our Website

AMETEK®
ADVANCED MEASUREMENT TECHNOLOGY

APPENDIX E: Ortec NIM Model 772 Counter

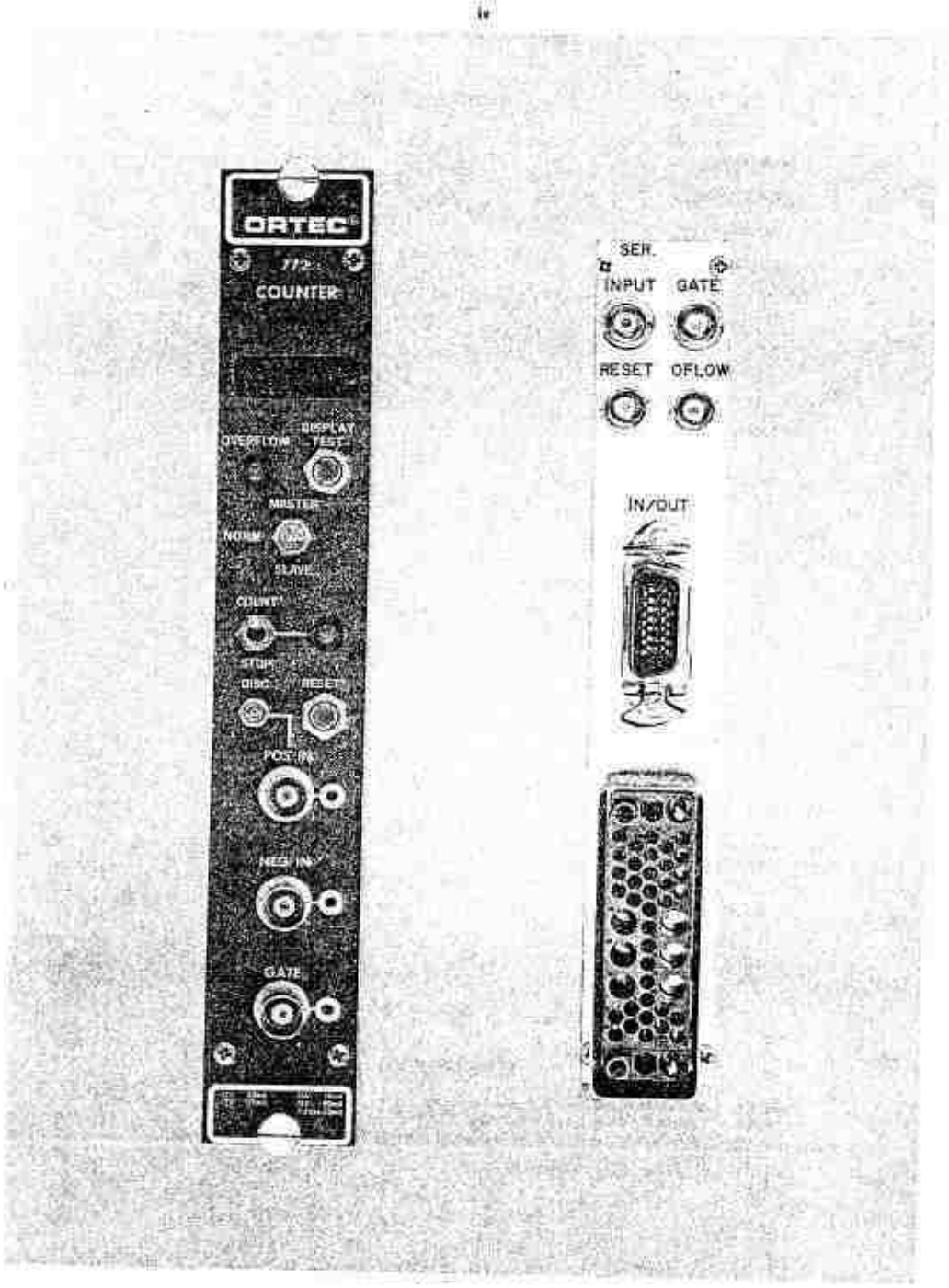

2. SPECIFICATIONS

2.1. PERFORMANCE

Count Capacity 6 decades, for 000 000 through 999 999.

Counting Rates Negative input, 100 MHz; positive input, 20 MHz.

Discriminators Negative input trigger level fixed at −250 mV; positive input trigger level adjustment range 100 mV to 10 V; drift is <10 mV/°C from 0°C to 50°C.

Pulse Pair Resolution Positive input, 50 nsec; negative input, 10 nsec; minimum duty cycle, 40% at either input at maximum counting rate.

Automatic Clear Generated when power is turned on initially or after a power failure.

2.2. INDICATORS

Display 6 direct-reading 7-segment LED digits with automatic blanking of insignificant zeros.

Overflow LED, illuminated from the first overflow until reset.

Gate LED, illuminated while unit is in the counting condition.

2.3. CONTROLS

Display Test Push-button switch illuminates all segments of each digit in the display when depressed; display reads 888 888.

Master/Norm/Slave 3-position locking toggle switch selects the counter's function when the module is connected in a data acquisition system. Master selects control over all slaves in the system by furnishing control signals through the common gate and reset lines. Norm isolates this module from system control through gate and reset lines. Slave accepts control from another module in the system, operating as a Master, that furnishes the system gate and reset signals.

Disc Single-turn screwdriver potentiometer sets the discrimination level for positive input signals; range 100 mV to 10 V.

Reset Push-button switch resets display and internal logic to an initial zero condition when pressed.

Count/Stop Toggle switch selects counting or noncounting condition of the unit manually.

2.4. CONNECTORS

Pos In Front and rear panel type BNC connectors accept positive unipolar or positive-leading bipolar signals to ±25 V maximum. Input amplitude must exceed the adjusted discriminator level for a minimum of 20 nsec to be counted. Z_{in} = 1 kΩ to ground, dc-coupled.

Neg In Front panel type BNC connector accepts NIM-standard fast negative signals, 14 mA into 50Ω, with 4-nsec minimum width. Input is protected to ±25 V at 10% duty cycle and has a fixed −250-mV discriminator level.

Gate Front and rear panel type BNC connectors accept NIM-standard slow positive logic signals to control the counter gate and the gate indicator. An open circuit or the application of a signal with ≥+3-V amplitude enables the counting. ≤+1.5 V inhibits counting. Input protected for 25 V maximum, 100-nsec minimum pulse width; driving source must be capable of sinking 0.5 mA of positive current.

Reset Rear panel type BNC connector accepts NIM-standard slow positive logic signal to reset the unit to an initial condition. A signal ≥+3 V resets; ≤+1.5 V does not reset; 25 V maximum, 100-nsec minimum pulse width. Z_{in} = 2 kΩ to ground, dc-coupled.

Oflow Rear panel type BNC connector furnishes NIM-standard positive logic output, +5 V for 2 μsec, whenever the counter overflows from 999 999 to zero. Driving source impedance ≤10Ω, dc-coupled.

In/Out Rear panel Amphenol type 57-40140 connector includes four common data lines and all system logic for the standard ORTEC printing and/or counting system interconnections.

2.5. OPTION

772H Counter The 772H Counter is a complete unit, equal in performance to the 772; requires +6 V from Bin and Power Supply.

2.6. ELECTRICAL AND MECHANICAL

Power Required For the 772 Counter, +12 V, 80 mA; −12 V, 165 mA; +24 V, 75 mA; −24 V, 80 mA; 115 V ac (50 or 60 Hz), 50 mA. An internal power supply generates the +5-V source that is required by the integrated circuits; protected by a chassis-mounted 1-A 3AG fuse.

APPENDIX F: TEKTRONIX DPO 4104 SPECIFICATIONS

Mixed Signal Oscilloscopes

MSO4000B, DPO4000B Series Datasheet

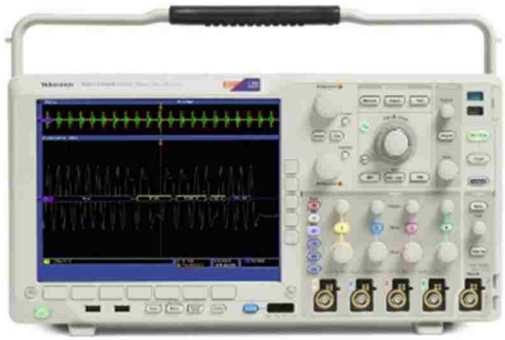

With the MSO/DPO4000B Mixed Signal Oscilloscope Series, you can analyze up to 20 analog and digital signals with a single instrument to quickly find and diagnose problems in complex designs. Bandwidths up to 1 GHz and up to 5X oversampling on all channels ensure you have the performance you need to see fast-changing signal details. To capture long windows of signal activity while maintaining fine timing resolution, the MSO/DPO4000B Series offers deep record length of up to 20M points standard on all channels. And with Wave Inspector® controls for rapid waveform navigation, automated serial and parallel bus analysis, limit and mask testing, and automated power analysis – your Tektronix oscilloscope provides the feature-rich tools you need to simplify and speed debug of your complex design.

Key performance specifications

- 1 GHz, 500 MHz, 350 MHz, and 100 MHz bandwidth models
- 2 and 4 analog channel models
- Up to 5 GS/s sample rate on all channels
- Up to 20 mega-point record length on all channels
- >50,000 wfm/s maximum waveform capture rate
- Standard passive voltage probes with less than 4 pF capacitive loading and 500 MHz or 1 GHz analog bandwidth
- Suite of advanced triggers

Key features

- Wave Inspector® controls provide easy navigation and automated search of waveform data
- 41 automated measurements, and FFT analysis for simplified waveform analysis
- 16 digital channels (MSO series)
- Mixed signal design and analysis (MSO series)
  - Automated triggering, decode, and search on parallel buses
  - Per-channel threshold settings
  - Multichannel setup and hold triggering
  - MagniVu™ High-speed acquisition provides 60.6 ps fine timing resolution on digital channels
- Optional serial triggering and analysis - automated serial triggering, decode, and search options for I^2C, SPI, USB, Ethernet, CAN, LIN, FlexRay, RS-232/422/485/UART, MIL-STD-1553, and I^2S/LJ/RJ/TDM
- TekVPI® probe interface supports active, differential, and current probes for automatic scaling and units
- 10.4 in. (264 mm) bright XGA color display
- Small footprint and lightweight – Only 5.8 in. (147 mm) deep and 11 lb. (5 kg)

Connectivity

- Two USB 2.0 host ports on the front panel and two on the rear panel for quick and easy data storage, printing, and connecting a USB keyboard
- USB 2.0 device port on the rear panel for easy connection to a PC or direct printing to a PictBridge®-compatible printer
- Integrated 10/100/1000BASE-T Ethernet port for network connection and video out port to export the oscilloscope display to a monitor or projector

Optional application support

- Power analysis
- Limit and mask testing
- HDTV and custom video analysis

Datasheet

Specifications

All specifications apply to all models unless noted otherwise.

Model overview

	DPO4014B [1]	DPO4034B [1]	DPO4054B [1]	DPO4102B-L, MSO4102B-L	DPO4102B, MSO4102B	DPO4104B-L, MSO4104B-L	DPO4104B, MSO4104B [1]
Analog channels	4	4	4	2	2	4	4
Bandwidth	100 MHz	350 MHz	500 MHz	1 GHz	1 GHz	1 GHz	1 GHz
Rise time	3.5 ns	1 ns	700 ps	350 ps	350 ps	350 ps	350 ps
Sample rate (1 ch)	2.5 GS/s	2.5 GS/s	2.5 GS/s	5 GS/s	5 GS/s	5 GS/s	5 GS/s
Sample rate (2 ch)	2.5 GS/s	2.5 GS/s	2.5 GS/s	2.5 GS/s	5 GS/s	5 GS/s	5 GS/s
Sample rate (4 ch)	2.5 GS/s	2.5 GS/s	2.5 GS/s	—	—	2.5 GS/s	5 GS/s
Record length (1 ch)	20M	20M	20M	5M	20M	5M	20M
Record length (2 ch)	20M	20M	20M	5M	20M	5M	20M
Record length (4 ch)	20M	20M	20M	—	—	5M	20M
Duration at highest sample rate	8 ms	8 ms	8 ms	1 ms	4 ms	1 ms	4 ms
Digital channels	MSO models add 16 digital channels to the corresponding DPO model						

Vertical system analog channels

Hardware bandwidth limits	
≥350 MHz models	20 MHz or 250 MHz
100 MHz models	20 MHz
Input coupling	AC, DC
Input impedance	1 MΩ ±1%, 50 Ω ±1%
Input sensitivity range	
1 MΩ	1 mV/div to 10 V/div
50 Ω	1 mV/div to 1 V/div
Vertical resolution	8 bits (11 bits with Hi Res)
Maximum input voltage	
1 MΩ	300 V_{RMS} CAT II with peaks ≤ ±425 V
50 Ω	5 V_{RMS} with peaks ≤ ±20 V (DF ≤ 6.25%)
DC gain accuracy	±1.5%, derated at 0.10%/°C above 30 °C
Channel-to-channel isolation	Any two channels at equal vertical scale ≥100:1 at ≤100 MHz and ≥30:1 at >100 MHz up to the rated bandwidth

Vertical system analog channels

Offset range

Volts/div setting	Offset range	
	1 MΩ input	50 Ω
1 mV/div to 50 mV/div	±1 V	±1 V
50.5 mV/div to 99.5 mV/div	±0.5 V	±0.5 V
100 mV/div to 500 mV/div	±10 V	±10V
505 mV/div to 995 mV/div	±5 V	±5 V
1 V/div to 5 V/div	±100 V	±5 V
5.05 V/div to 10 V/div	±50 V	NA

Vertical system digital channels

Input channels	16 digital (D15 to D0)
Thresholds	Per-channel thresholds
Threshold selections	TTL, CMOS, ECL, PECL, User-defined
User-defined threshold range	±40 V
Threshold accuracy	±[100 mV + 3% of threshold setting]
Maximum input voltage	±42 V_{peak}
Input dynamic range	30 V_{p-p} ≤200 MHz 10 V_{p-p} >200 MHz
Minimum voltage swing	400 mV
Probe loading	100 kΩ in parallel with 3 pF
Vertical resolution	1 bit

Horizontal system analog channels

Time base range	
1 GHz models	400 ps to 1000 s
≤ 500 MHz models	1 ns to 1000 s
Time-base delay time range	-10 divisions to 5000 s
Channel-to-channel deskew range	±125 ns
Time base accuracy	±5 ppm over any ≥1 ms interval

Horizontal system digital channels

Maximum sample rate (Main)	500 MS/s (2 ns resolution)
Maximum record length (Main)	20M points (5M points on -L models)
Maximum sample rate (MagniVu)	16.5 GS/s (60.6 ps resolution)
Maximum record length (MagniVu)	10k points centered around the trigger
Minimum detectable pulse width (typical)	1 ns
Channel-to-channel skew (typical)	200 ps
Maximum input toggle rate	500 MHz (Maximum frequency sine wave that can accurately be reproduced as a logic square wave. Requires the use of a short ground extender on each channel. This is the maximum frequency at the minimum swing amplitude. Higher toggle rates can be achieved with higher amplitudes.)

Trigger system

Trigger modes	Auto, Normal, and Single
Trigger coupling	DC, AC, HF reject (attenuates >50 kHz), LF reject (attenuates <50 kHz), noise reject (reduces sensitivity)
Trigger holdoff range	20 ns to 8 s

Trigger sensitivity

Internal DC coupled

Trigger source	Sensitivity
1 MΩ path (all models)	For 1 mV/div to 4.98 mV/div; 0.75 div from DC to 50 MHz, increasing to 1.3 div at rated bandwidth
50 Ω path (≤500 MHz models)	For ≥5 mV/div; 0.4 div from DC to 50 MHz, increasing to 1 div at rated bandwidth
50 Ω path (1 GHz models)	0.4 div from DC to 50 MHz, increasing to 1 div at rated bandwidth

External

Trigger source	Sensitivity
Auxiliary Input	200 mV from DC to 50 MHz, increasing to 500 mV at rated bandwidth

Trigger level ranges

Any input channel	±8 divisions from center of screen, ±8 divisions from 0 V when vertical LF reject trigger coupling is selected
Aux Input (external trigger)	±8 V
Line	The line trigger level is fixed at about 50% of the line voltage.
Trigger frequency readout	Provides 6-digit frequency readout of triggerable events.

Trigger types

Edge	Positive or negative slope on any channel or front-panel auxiliary input. Coupling includes DC, AC, HF reject, LF reject, and noise reject.
Sequence (B-trigger)	Trigger Delay by Time: 4 ns to 8 s. Or Trigger Delay by Events: 1 to 4,000,000 events.
Pulse Width	Trigger on width of positive or negative pulses that are >, <, =, ≠, or inside/outside a specified period of time.
Timeout	Trigger on an event which remains high, low, or either, for a specified time period (4 ns to 8 s).
Runt	Trigger on a pulse that crosses one threshold but fails to cross a second threshold before crossing the first again.

APPENDIX G: Ortec Model CO4020 Quad 4-Input Logic Unit

ORTEC®

CO4020
Quad 4-Input Logic Unit

- **General-purpose logic module for AND, OR, Veto, Fan-Out, and Gating functions**
- **Four independent channels**
- **Overlap outputs and adjustable-width outputs**
- **3-ns overlap resolution**
- **TTL and fast negative NIM outputs**

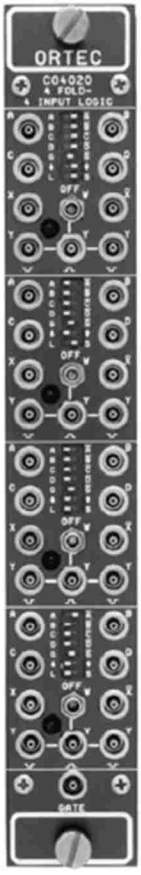

The ORTEC Model CO4020 Quad 4-Input Logic Unit has the flexibility to satisfy the logic requirements of most coincidence experiments without additional logic modules. The logic functions it can perform are: coincidence (AND), anticoincidence (veto), fan-in (OR), fan-out, fast negative NIM-to-TTL conversion, and pulse lengthening. The Model CO4020 contains four identical, independent channels of 4-input logic in a single-width NIM module.

Each of the four inputs (A, B, C, and D) accepts NIM fast negative logic pulses. Front-panel, three-position slide switches select the logic requirements separately for each input. The various combinations of logic functions that can be implemented are illustrated in Fig. 1 and in the specifications for the control switches.

The X output is a NIM fast negative logic pulse whose width is determined by the width and overlap of the active input pulses. The complement of the X output is available at the $\overline{X}$ output. The updating Y outputs can be set to trigger on either the leading edge or the trailing edge of the X output pulse. The width of the Y outputs can be adjusted from 40 ns to 40 µs in two selectable ranges. Two of the Y outputs provide NIM fast negative logic pulses. The third Y output delivers a positive TTL logic pulse that is suitable for gating ADCs and multichannel analyzers. Front-panel LEDs indicate which channel is generating an output.

Specifications

The Model CO4020 incorporates four separate channels with indentical functions. The specifications apply to each of the four channels unless stated otherwise.

PERFORMANCE

NUMBER OF IDENTICAL CHANNELS 4.

MAXIMUM COUNT RATE
X and $\overline{X}$ Outputs 100 MHz.
Y Outputs 1/(1.1 X width).

MINIMUM PULSE OVERLAP 3 ns.

PROPAGATION DELAY
Input to X, $\overline{X}$ <8 ns.
Input to Y (Neg) <13 ns.
Input to Y (Pos) <20 ns.

DEAD TIME OF Y OUTPUTS 110% of width setting.

CONTROLS AND INDICATORS

WIDTH ADJUST (W) Front-panel screwdriver adjustment allows width adjustment of Y outputs. Two ranges can be selected by the front-panel slide switch:

S (40–1200 ns) or L (1–40 µs).

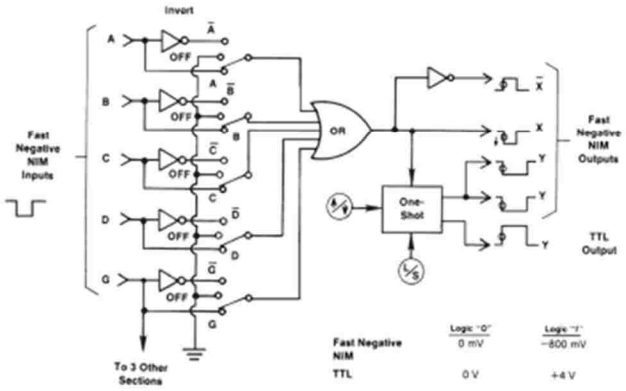

Fig. 1. Block Diagram of the Model CO4020 Logic Unit.

CO4020
Quad 4-Input Logic Unit

LED INDICATOR Front-panel, red LED lights when output has been activated.

CONTROL SWITCHES Front-panel 7- by 3-position slide switch selects logic function definition, gate operation, Y output trigger point, and Y output width adjustment range as follows:

Input Logic Switches (A/OFF/$\overline{A}$, B/OFF/$\overline{B}$, C/OFF/$\overline{C}$, D/OFF/$\overline{D}$, AND G/OFF/$\overline{G}$) As defined in Fig. 1, these switches select variations of the following basic logic functions. In the OFF position, the state of that input is ignored. With switches set to the A, B, C, D, and G positions, the module performs the OR function at the $\overline{X}$ output.

$X = A + B + C + D + G$

Setting the switches to the $\overline{A}$, $\overline{B}$, $\overline{C}$, $\overline{D}$, and $\overline{G}$ positions provide the AND (coincidence) function at the $\overline{X}$ output.

$\overline{X} = A \cdot B \cdot C \cdot D \cdot G$

Changing the $\overline{G}$ switch to G implements the common-gate veto (anticoincidence).

$\overline{X} = A \cdot B \cdot C \cdot D \cdot \overline{G}$

See Fig. 1 to determine other possible logic combinations.

Trigger Switch for Y Outputs (↓ or ↑) Allows either the negative transition (↓) or the positive transition (↑) of the X output to trigger the constant-width Y outputs.

Y Output Width Range Switch Sets either to S (40–1200 ns) or L (1–40 µs).

INPUTS

A, B, C, AND D INPUTS Front-panel LEMO connectors accept negative fast-NIM logic signals.
Minimum Amplitude –600 mV.
Minimum Width 3 ns.
Input Impedance 50 Ω.

GATE INPUT (G) Front-panel LEMO connector accepts negative Fast-NIM logic signals. The GATE input is delivered to all four sections.
Minimum Amplitude –600 mV.
Minimum Width 3 ns.
Input Impedance 50 Ω.

OUTPUTS

X AND $\overline{X}$ OUTPUTS Front-panel LEMO connectors provide the noninverted (X) and the inverted ($\overline{X}$) result of the logic satisfied by the input signals. Logic requirements are set by the front-panel slide switches A/OFF/$\overline{A}$, B/OFF/$\overline{B}$, C/OFF/$\overline{C}$, D/OFF/$\overline{D}$, and G/OFF/$\overline{G}$. X and $\overline{X}$ are Fast-NIM logic signals.
Amplitude –20 mA.
Rise Time <4 ns.
Output Width Determined by duration of input signals and logic selection.

Y OUTPUTS (⊐⊔ and ⊔⊏) Front-panel LEMO connectors provide two updating Fast-NIM logic outputs (⊔⊏) and one updating positive TTL logic output (⊐⊔) per channel. Output width of all three Y outputs is set by WIDTH adjustment. Y outputs are triggered by either the negative transition (↓) or positive transition (↑) of the X overlap output as selected by the front-panel slide switch.

ELECTRICAL AND MECHANICAL

POWER REQUIRED The Model CO4020 derives its power from a standard NIM bin and power supply. The required power is +6 V, 200 mA; –6 V, 1000 mA.

WEIGHT
Net 1.3 kg (2.3 lb).
Shipping 2.2 kg (4.8 lb).

DIMENSIONS NIM-standard single-width module 3.43 X 22.13 cm (1.35 X 8.714 in.) per DOE/ER-0457T.

Ordering Information

To order, specify:

Model	Description
CO4020	Quad 4-Input Logic Unit

Specifications subject to change
092707

ORTEC®
www.ortec-online.com
Tel. (865) 482-4411 • Fax (865) 483-0396 • ortec.info@ametek.com
801 South Illinois Ave., Oak Ridge, TN 37831-0895 U.S.A.
For International Office Locations, Visit Our Website

AMETEK®
ADVANCED MEASUREMENT TECHNOLOGY

APPENDIX H: Idaho Experimental Data

D1	Signal FWHM			D1 Thuput Delays					
				10%		Half Height		Peak	
Bias		Average			Average		Average		Average
2500	3.58	3.26	3.42	9.341	9.334	9.3375	10.284	10.288	10.286	11.598	11.533	11.5655
2400	3.30	3.43	3.36	9.529	9.382	9.4555	10.432	10.419	10.4255	11.861	12.089	11.975
2300	3.50	3.45	3.48	9.51	9.437	9.4735	10.51	10.538	10.524	11.904	11.877	11.8905
2200	3.58	3.39	3.48	9.625	9.668	9.6465	10.676	10.727	10.7015	12.138	11.903	12.0205
2100	3.54	3.29	3.41	9.872	9.875	9.8735	10.875	10.867	10.871	12.388	12.287	12.3375
2000	3.56	3.54	3.55	10.063	10.013	10.038	11.013	11.032	11.0225	12.461	12.378	12.4195
1900	3.53	3.70	3.62	10.172	10.171	10.1715	11.219	11.218	11.2185	12.719	12.756	12.7375
1800	3.70	3.47	3.59	10.32	10.454	10.387	11.363	11.488	11.4255	12.895	13.303	13.099
1700	2.76	2.95	2.85	10.811	10.83	10.8205	12.003	11.833	11.918	12.942	12.846	12.894
1600	3.72	3.60	3.66	10.82	10.811	10.8155	11.863	11.969	11.916	13.658	13.269	13.4635
1500	3.54	3.55	3.55	11.035	11.009	11.022	12.17	12.229	12.1995	13.678	13.725	13.7015
1400	4.11	4.12	4.12	11.025	11.04	11.0325	12.452	12.463	12.4575	14.078	14.332	14.205
1300	4.12	4.20	4.16	11.554	11.481	11.5175	12.711	12.709	12.71	14.114	14.334	14.224
1200	3.71	3.71	3.71	11.804	11.814	11.809	13.224	13.223	13.2235	15.153	14.706	14.9295
1100	4.73	4.71	4.72	12.064	11.899	11.9815	13.339	13.323	13.331	15.403	15.419	15.411
1000	4.88	4.89	4.89	12.203	12.271	12.237	13.809	13.81	13.8095	15.595	15.75	15.6725

D2	Signal FWHM			D2 Thuput Delays					
				10%		Half Height		Peak	
Bias		Average			Average		Average		Average
2500	3.26	3.35	3.31	8.77	8.81	8.79	9.81	9.77	9.79	11.39	11.11	11.25
2400	3.51	3.31	3.41	9.04	9.00	9.02	9.89	9.92	9.90	11.28	11.38	11.33
2300	3.40	3.42	3.41	9.25	9.05	9.15	10.17	10.06	10.11	11.78	11.49	11.63
2200	3.35	3.26	3.31	9.42	9.36	9.39	10.33	10.32	10.32	11.79	11.59	11.69
2100	3.11	3.12	3.11	9.55	9.59	9.57	10.35	10.51	10.43	11.48	11.65	11.57
2000	3.36	3.26	3.31	9.68	9.61	9.65	10.65	10.61	10.63	11.78	11.79	11.78
1900	3.06	2.99	3.02	10.00	9.89	9.95	10.85	11.01	10.93	12.28	12.09	12.19
1900	3.07	3.14	3.11	10.00	9.98	9.99	10.84	10.87	10.86	12.08	12.08	12.08
1800	2.41	2.69	2.55	10.31	10.17	10.24	11.35	11.33	11.34	12.84	12.54	12.69
1800	3.68	3.71	3.70	9.80	9.83	9.81	10.80	10.84	10.82	12.31	12.31	12.31
1700	3.49	3.38	3.43	10.02	10.03	10.03	11.22	11.21	11.22	12.66	12.93	12.79
1600	3.30	3.56	3.43	10.32	10.30	10.31	11.46	11.36	11.41	12.95	12.70	12.83
1500	2.59	2.81	2.70	10.61	10.82	10.71	11.99	11.97	11.98	13.05	12.99	13.02
1400	4.07	4.30	4.19	10.49	10.58	10.54	11.79	11.69	11.74	13.61	13.42	13.51
1300	3.99	4.04	4.01	10.96	10.80	10.88	12.18	12.00	12.09	14.07	14.09	14.08
1200	3.59	3.59	3.59	11.20	11.46	11.33	12.59	12.59	12.59	14.08	14.07	14.08
1100	4.83	4.67	4.75	11.30	11.29	11.29	12.64	12.66	12.65	14.49	14.49	14.49
1000	4.72	4.26	4.49	11.77	11.63	11.70	13.25	13.23	13.24	15.36	15.36	15.36

APPENDIX I: Cosmic Radiation Experimental Set-up Pictures

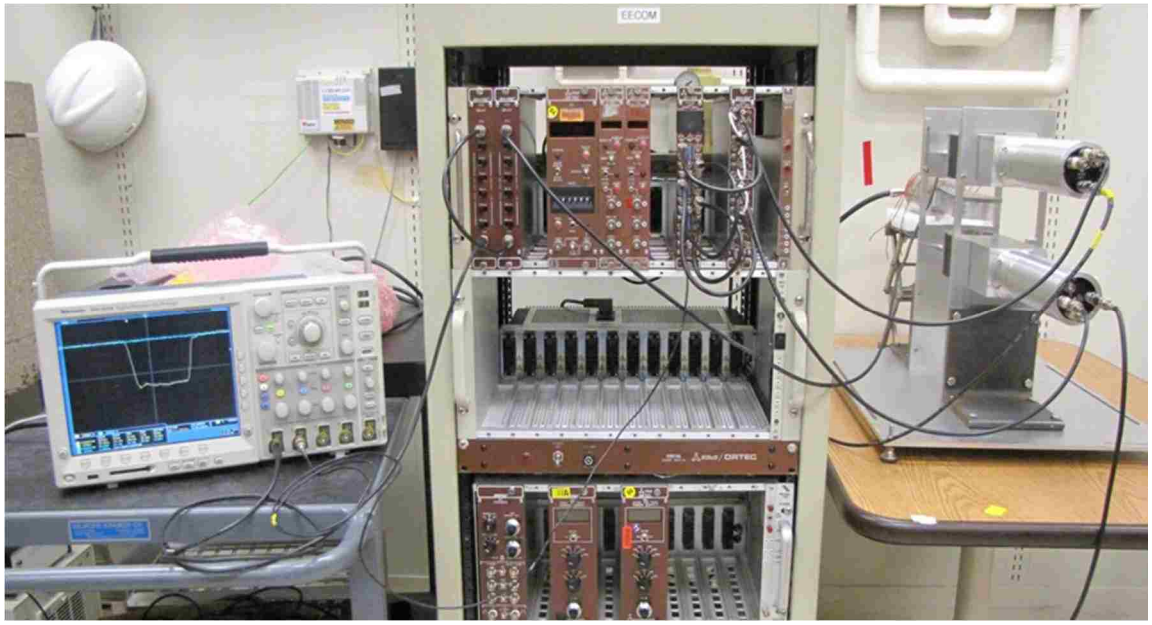

The Cosmic Ray Time Response Measurement System Experimental Set-up

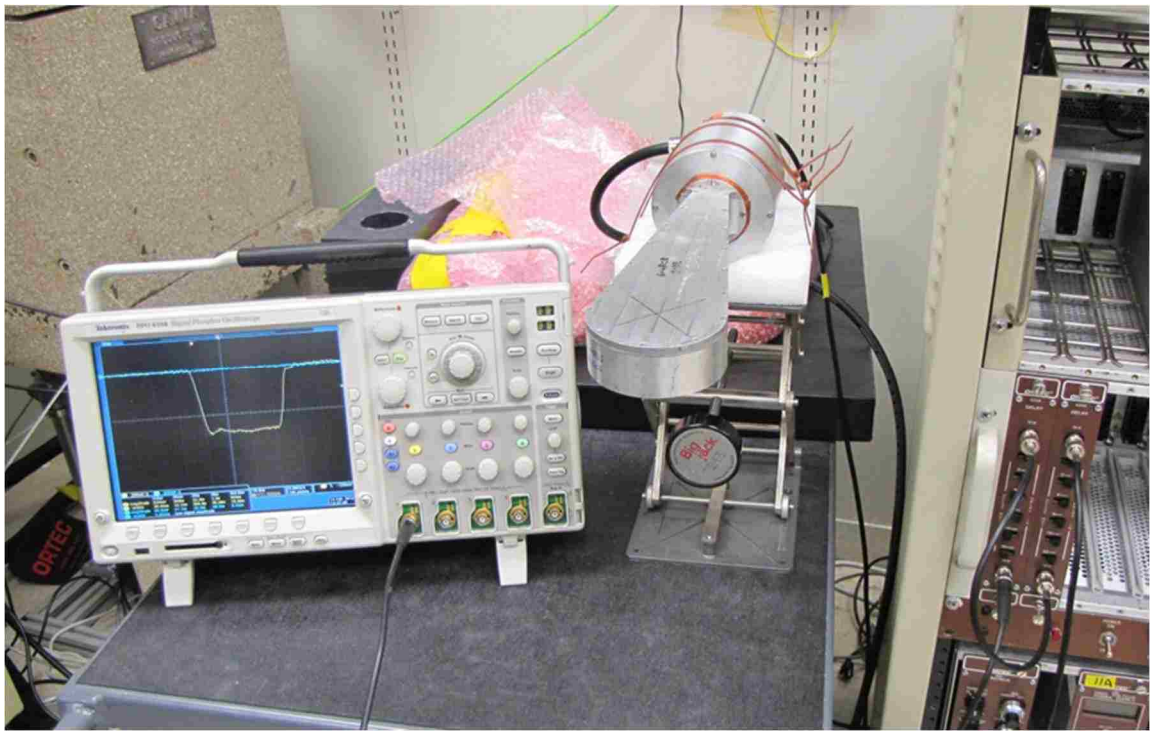

The Detector Under Test Experimental Set-up

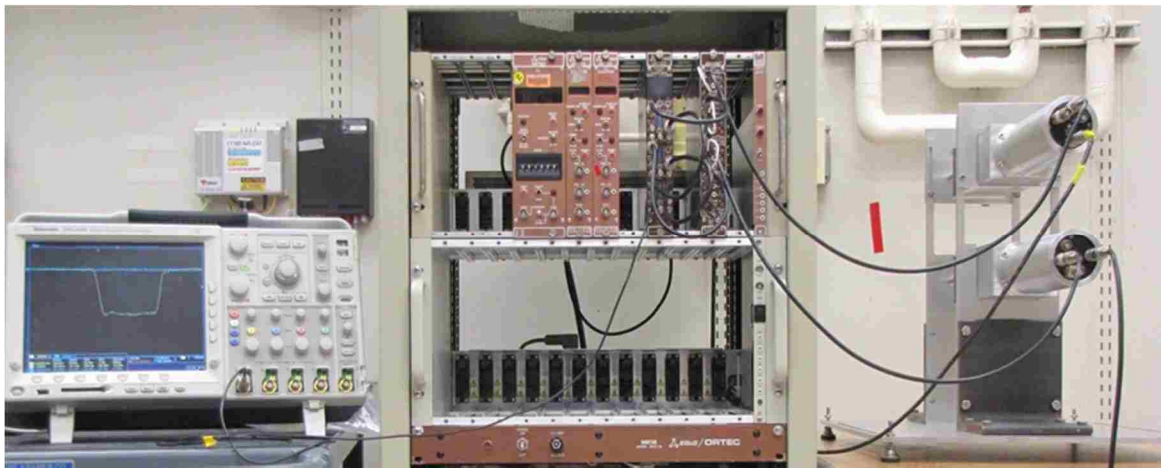

The Coincidence System with Detectors 10 and 11

APPENDIX J: nTOF Detector D1 and D2 Specifications

HAMAMATSU

PHOTOMULTIPLIER TUBE
R5946

Stable Operation in High Magnetic Fields beyond 1 Tesla
38mm(1–1/2 Inch) Diameter, Proximity Photocathode and Fine Mesh Dynodes

GENERAL

Parameter		Description/Value	Unit
Spectral Response		300 to 650	nm
Wavelength of Maximum Response		420 ± 50	nm
Photocathode	Material	Bialkali	–
	Minimum Effective Area	27	mm dia.
Window	Material	Borosilicate glass	–
	Shape	Plano–plano	–
Dynode	Secondary Emitting Surface	Bialkali	–
	Structure	Fine mesh	–
	Number of Stages	16	–
Base		19–pin glass base	–
Suitable Socket		E678–19D (supplied)	–

MAXIMUM RATINGS (Absolute Maximum Values)

Parameter		Value	Unit
Supply Voltage	Between Anode and Cathode	2300	Vdc
	Between Anode and Last Dynode	200	Vdc
Average Anode Current		0.01	mA

CHARACTERISTICS (at 25°C)

Parameter		Min.	Typ.	Max.	Unit
Cathode Sensitivity	Luminous (2856K)	–	80	–	μA/lm
	Blue (CS–5–58 filter)	–	9.5	–	μA/lm–b
	Quantum Efficiency at 390nm	–	23	–	%
Anode Sensitivity	Luminous (2856K)	–	80	–	A/lm
Gain	At 0 tesla	–	1.0×10^6	–	–
	At 1 tesla	–	2.9×10^4	–	–
Anode Dark Current (after 30min. storage in darkness)		–	5.0	30	nA
Time Response	Anode Pulse Rise Time	–	1.9	–	ns
	Transit Time	–	7.2	–	ns
	Transit Time Spread (FWHM)	–	0.35	–	ns

NOTE: Anode characteristics are measured with the voltage distribution ratio shown below.

VOLTAGE DISTRIBUTION RATIO AND SUPPLY VOLTAGE

Electrodes	K	Dy1	Dy2	Dy3	Dy4	Dy5	Dy6	•••••••••••••	Dy16	P
Ratio	2	1	1	1	1	1	1	•••••••••••••	1	1

Supply Voltage : 2000Vdc, K : Cathode, Dy : Dynode, P : Anode

PHOTOMULTIPLIER TUBE R5946

Figure 1: Typical Spectral Response

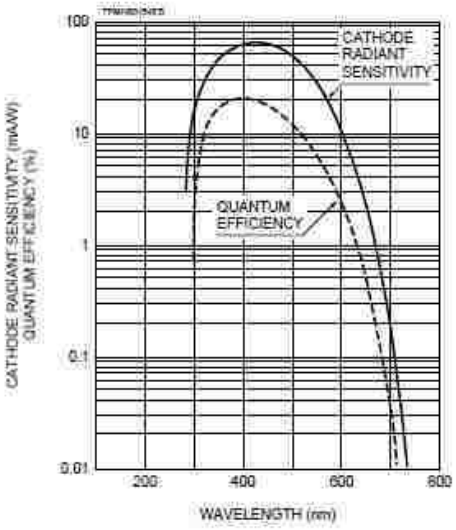

Figure 2: Typical Gain in Magnetic Fields (Parallel to Tube Axis)

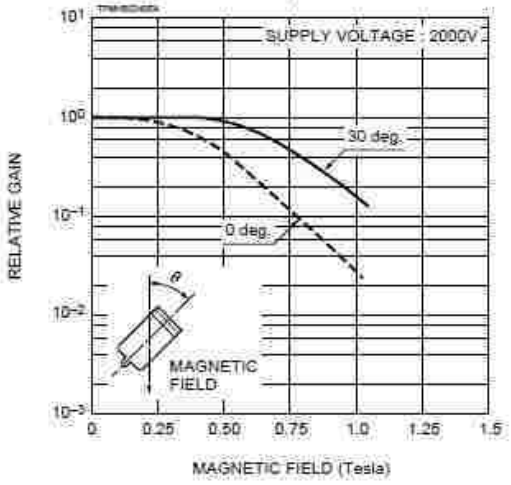

Figure 3: Dimensional Outline and Basing Diagram (Unit : mm)

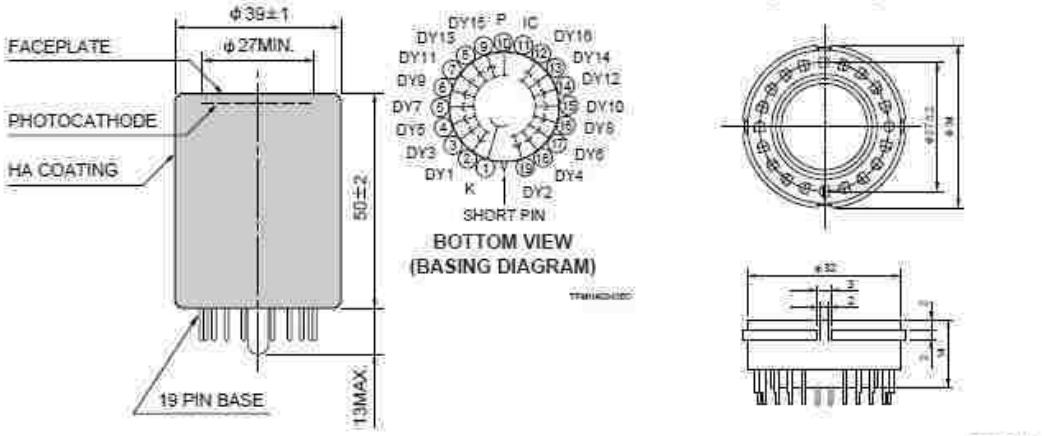

HAMAMATSU

HAMAMATSU PHOTONICS K.K., Electron Tube Center
314-5, Shimokanzo, Toyooka-village, Iwata-gun, Shizuoka-ken, 438-0193, Japan, Telephone: (81)539/62-5248, Fax: (81)539/62-2205

TPMH1097E04
JUL. 1994

BC-422Q
Ultra-fast Timing Plastic Scintillator

BC-422Q premium plastic scintillator is intended for use in ultra-fast timing and ultra-fast counting applications. It is quenched with various weight percentages of benzophenone (specified at time of order) to improve timing properties. The faster timing comes at the expense of total light output, however.

Scintillation Properties –

	Weight % Benzophenone					
	None*	0.5	1.0	2.0	3.0	5.0
Light Output, %Anthracene	55	19	11	5	4	3
Rise Time, ps	350	110	105	100	100	100
Decay Time , ns	1.6	0.7	0.7	0.7	0.7	0.7
Pulse Width, FWHM, ps	1300	360	290	260	240	220

*BC-422

General Technical Data –

Base ..... Polyvinyltoluene

Density ..... 1.032 g/cc

Refractive Index 1.58

Ratio H:C Atoms ..... ~1.1

Coefficient of Linear Expansion ..... 7.8×10^{-5} below 67°C

Light Output Temperature Dependence ..... at +60°C ~ 95% of that at +20°C; independent of temperature from -60°C to +20°C

Vapor Pressure ..... May be used in a vacuum

Solubility ..... Soluble in aromatic solvents, chlorine, acetone, etc.. Insoluble in water, dilute acids, lower alcohols, silicone fluid, grease and alkalis.

Softening Point ..... 70°C

SAINT-GOBAIN
CRYSTALS

Scintillation Products
Organic Scintillators

SAINT-GOBAIN
CRYSTALS

USA

Saint-Gobain Crystals
17900 Great Lakes Parkway
Hiram, OH 44234
Tel: (440) 834-5600
Fax: (440) 834-7680

Europe

Saint-Gobain Crystals
104 Route de Larchant
BP 521
77794 Nemours Cedex, France
Tel: 33 (1) 64 45 10 10
Fax: 33 (1) 64 45 10 01

P.O. Box 3093
3760 DB Soest
The Netherlands
Tel: 31 35 60 29 700
Fax: 31 35 60 29 214

Japan

Saint-Gobain KK, Crystals Division
3-7, Kojimachi, Chiyoda-ku,
Tokyo 102-0083 Japan
Tel: 81 (0) 3 3263 0559
Fax: 81 (0) 3 5212 2196

China

Saint-Gobain (China) Investment Co., Ltd.
15-01 CITIC Building
19 Jianguomenwai Ave.
Beijing 100004 China
Tel: 86 (0) 10 6513 0311
Fax: 86 (0) 10 6512 9843

www.detectors.saint-gobain.com

BC-422Q
Ultra-fast Timing Plastic Scintillator

Emission Spectra –

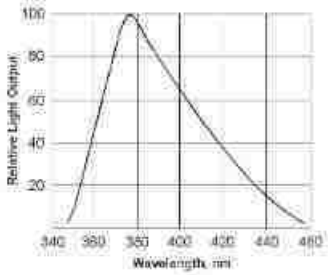

Atomic Particles Response –

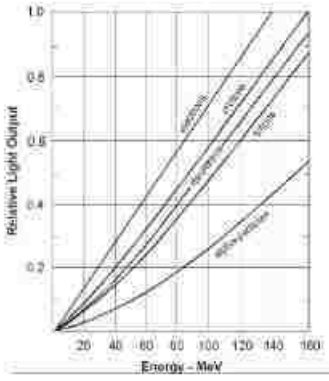

Premium Plastic Scintillators Response to Atomic Particles

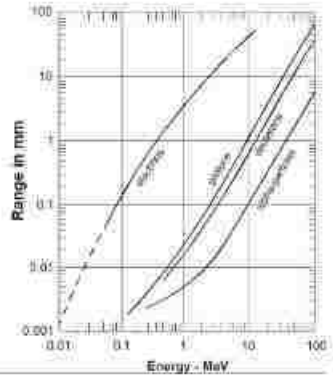

Range of Atomic Particles in Premium Plastic Scintillators

(07-08)

APPENDIX K: PeakFit Peak and Data Summary

Peak Summary

Measured Values

Peak	Type	Amplitude	Center	FWHM	Asym50	FW Base	Asym10
1	EMG	0.08060789	2.29994062	3.19697630	0.86981121	6.90292432	0.73058916
2	EMG	0.04835695	4.89994086	3.19697630	0.86981122	6.90292432	0.73058916
3	EMG	0.08869980	8.69994073	3.19697630	0.86981123	6.90292432	0.73058917
4	EMG	1.02362943	12.8581262	3.73463696	0.97297900	7.54486572	0.94477715
5	EMG	0.08706586	17.0999414	3.19697631	0.86981123	6.90292432	0.73058917

Peak	Type	Anlytc Area	% Area	Int Area	% Area	Centroid	Moment2
1	EMG	0.28515127	5.51844017	0.25329160	4.93425727	2.33504601	1.35000757
2	EMG	0.17106323	3.31053136	0.16918430	3.29580147	4.62151792	2.12390634
3	EMG	0.31377650	6.07241503	0.31366255	6.11031591	8.36301717	2.42780584
4	EMG	4.08925659	79.1380587	4.08925649	79.6609253	12.7921263	2.59560399
5	EMG	0.30799640	5.96055470	0.30793294	5.99870009	16.7586212	2.45492457
	Total	5.16724399	100.000000	5.13332788	100.000000		

Parameter Statistics

Peak 1 EMG

Parm	Value	Std Error	t-value	95	
Area	0.28515127	52.3401392	0.00544804	-103.78107	104.351370
Ctr	3.07419319	73.0735800	0.04206983	-142.21566	148.364047
Wid	1.10318049	34.4101702	0.03205972	-67.313457	69.5198176
Dstn	-1.1145817	50.9092198	-0.0218935	-102.33575	100.106586

Peak 2 EMG

Parm	Value	Std Error	t-value	95	
Area	0.17106323	53.0563081	0.00322418	-105.31909	105.661218
Ctr	5.67419344	257.225435	0.02205922	-505.75888	517.107270
Wid	1.10318049	82.5102188	0.01337023	-162.94924	165.155601
Dstn	-1.1145817	1085.59158	-0.0010267	-2159.5615	2157.33232

Peak 3 EMG

Parm	Value	Std Error	t-value	95	
Area	0.31377650	6.02061503	0.05211702	-11.656819	12.2843721
Ctr	9.47419331	24.0681294	0.39364062	-38.379696	57.3280825
Wid	1.10318049	14.3907110	0.07665921	-27.509408	29.7157694
Dstn	-1.1145817	88.4966701	-0.0125946	-177.06967	174.840507

Peak 4 EMG

Parm	Value	Std Error	t-value	95	
Area	4.08925659	3.53242788	1.15763342	-2.9341564	11.1126696
Ctr	13.3990799	6.67349854	2.00780443	0.13037695	26.6677829
Wid	1.49238526	2.38952490	0.62455313	-3.2586304	6.24340093
Dstn	-0.6069536	9.93222935	-0.0611095	-20.354886	19.1409793

Peak 5 EMG

Parm	Value	Std Error	t-value	95	
Area	0.30799640	2.69595407	0.11424394	-5.0522826	5.66827537
Ctr	17.8741940	10.0660308	1.77569435	-2.1397720	37.8881600
Wid	1.10318049	3.73340108	0.29548941	-6.3198211	8.52618203
Dstn	-1.1145817	33.9942469	-0.0327874	-68.704252	66.4750884

Baseline Linear Bg

Parm	Value	Std Error	t-value	95	
a0	-0.0917951	1.17540754	-0.0780964	-2.4288202	2.24523000
a1	0.00486306	0.05589685	0.08700053	-0.1062749	0.11600097

Analysis of Variance

r^2 Coef Det	DF Adj r^2	Fit Std Err
0.98405468	0.97987853	0.04517631

Source	Sum of Squares	DF	Mean Square	F
Regr	10.705984	21	0.50980874	249.79613
Error	0.17347644	85	0.0020408993	
Total	10.87946	106		

Details of Fit

Set Convergence	State	Iterations	Minimization	Extent
1E-6	Not Fitted	0	Least Squares	1/1

Curvature Matrix	Constraints			Violated
Sparse-Roots	25.0000	-5.00000	-50.0000 - None - None	0

Data Summary

XY	*	X Value	Y Value	Y Predict	Residual	Residual%	95% Confidence Limits		95% Prediction Limits		Weights
1		0.1000078	-0.039216	-0.061834	0.0226182	-57.67651	-0.134325	0.0106571	-0.177259	0.0535916	1
2		0.3000078	-0.039216	-0.055749	0.0165336	-42.16065	-0.104631	-0.006867	-0.158011	0.0465129	1
3		0.5000078	-0.058824	-0.049053	-0.009771	16.610712	-0.093211	-0.004894	-0.149143	0.0510377	1
4		0.7000078	-0.019608	-0.041795	0.0221873	-113.1554	-0.085778	0.0021875	-0.141808	0.0582177	1
5		0.9000078	-0.039216	-0.034083	-0.005132	13.087708	-0.077392	0.0092252	-0.133801	0.0656350	1
6		1.1000079	-0.039216	-0.026084	-0.013131	33.484676	-0.068562	0.0163932	-0.125445	0.0732758	1
7		1.3000078	-0.019608	-0.018029	-0.001579	8.0539009	-0.059862	0.0238043	-0.117115	0.0810577	1
8		1.5000078	0.0392157	-0.010199	0.0494151	126.00843	-0.051530	0.0311316	-0.109075	0.0886761	1
9		1.7000078	0.0196078	-0.002915	0.0225225	114.86476	-0.044219	0.0383895	-0.101779	0.0959496	1
10		1.9000077	0.0000000	0.0035024	-0.003502	0.0000000	-0.038377	0.0453814	-0.095603	0.1026081	1
11		2.1000077	0.0000000	0.0087599	-0.008760	0.0000000	-0.033576	0.0510954	-0.090540	0.1080594	1
12		2.3000077	0.0000000	0.0126364	-0.012636	0.0000000	-0.029391	0.0546641	-0.086532	0.1118051	1
13		2.5000078	0.0000000	0.0150145	-0.015015	0.0000000	-0.026474	0.0565028	-0.083927	0.1139558	1
14		2.7000078	0.0000000	0.0159031	-0.015903	0.0000000	-0.025852	0.0576581	-0.083150	0.1149565	1
15		2.9000078	0.0196078	0.0154419	0.0041659	21.246212	-0.027198	0.0580819	-0.083988	0.1148716	1
16		3.1000078	0.0000000	0.0138858	-0.013886	0.0000000	-0.029022	0.0567940	-0.085659	0.1134308	1
17		3.3000078	-0.019608	0.0115698	-0.031178	159.00589	-0.030692	0.0538320	-0.087699	0.1108381	1
18		3.5000078	0.0000000	0.0088611	-0.008861	0.0000000	-0.033042	0.0507646	-0.090255	0.1079772	1
19		3.7000079	-0.019608	0.0061059	-0.025714	131.13992	-0.036506	0.0487181	-0.093312	0.1055237	1
20		3.9000079	-0.039216	0.0035815	-0.042797	109.13281	-0.039764	0.0469275	-0.096153	0.1033160	1
21		4.1000079	-0.019608	0.0014633	-0.021071	107.46258	-0.041515	0.0444413	-0.098112	0.1010384	1
22		4.3000079	0.0000000	-0.000189	0.0001885	0.0000000	-0.042380	0.0420025	-0.099427	0.0990495	1
23		4.5000079	-0.019608	-0.001419	-0.018189	92.764407	-0.043828	0.0409905	-0.100750	0.0979122	1
24		4.7000079	-0.019608	-0.002348	-0.017259	88.023193	-0.045676	0.0409792	-0.102075	0.0973781	1
25		4.9000080	-0.019608	-0.003132	-0.016476	84.025782	-0.046536	0.0402720	-0.102892	0.0966276	1
26		5.1000080	0.0196078	-0.003912	0.0235202	119.95319	-0.046405	0.0385800	-0.103279	0.0954541	1
27		5.3000080	-0.019608	-0.004778	-0.014830	75.634395	-0.046902	0.0373467	-0.103987	0.0944321	1
28		5.5000080	-0.019608	-0.005734	-0.013874	70.755070	-0.048654	0.0371859	-0.105285	0.0938159	1
29		5.7000080	-0.039216	-0.006696	-0.032520	82.925628	-0.050158	0.0367660	-0.106481	0.0930891	1
30		5.9000080	-0.039216	-0.007489	-0.031727	80.903609	-0.050231	0.0352535	-0.106962	0.0919849	1
31		6.1000080	-0.058824	-0.007875	-0.050948	86.612300	-0.049726	0.0339753	-0.106969	0.0912186	1
32		6.3000081	-0.058824	-0.007584	-0.051239	87.106485	-0.049788	0.0346193	-0.106828	0.0916590	1
33		6.5000081	-0.039216	-0.006350	-0.032865	83.806984	-0.049443	0.0367424	-0.105975	0.0932745	1
34		6.7000077	-0.039216	-0.003944	-0.035271	89.941878	-0.046844	0.0389551	-0.103486	0.0955969	1
35		6.9000077	-0.058824	-0.000205	-0.058619	99.651655	-0.041976	0.0415660	-0.099265	0.0988552	1
36		7.1000077	-0.039216	0.0049462	-0.044162	112.61279	-0.036459	0.0463512	-0.093960	0.1038526	1
37		7.3000077	-0.039216	0.0114970	-0.050713	129.31727	-0.030776	0.0537702	-0.087776	0.1107700	1
38		7.5000077	-0.019608	0.0193518	-0.038960	198.69432	-0.023464	0.0621681	-0.080154	0.1188573	1
39		7.7000077	-0.019608	0.0283505	-0.047958	244.58754	-0.013681	0.0703823	-0.070820	0.1275209	1
40		7.9000078	0.0196078	0.0382991	-0.018691	-95.32528	-0.002715	0.0793134	-0.060444	0.1370426	1
41		8.1000078	0.0196078	0.0490119	-0.029404	-149.9606	0.0077502	0.0902735	-0.049835	0.1478583	1
42		8.3000078	0.0196078	0.0603614	-0.040754	-207.8433	0.0181194	0.1026035	-0.038898	0.1596211	1
43		8.5000078	0.0196078	0.0723320	-0.052724	-268.8932	0.0300322	0.1146318	-0.026952	0.1716163	1
44		8.7000078	0.0392157	0.0850699	-0.045854	-116.9281	0.0438350	0.1263047	-0.013765	0.1839051	1
45		8.9000078	0.0000000	0.0989219	-0.098922	0.0000000	0.0583636	0.1394803	0.0003670	0.1974769	1
46		9.1000079	0.0392157	0.1144539	-0.075238	-191.8575	0.0732684	0.1556395	0.0156392	0.2132687	1
47		9.3000079	0.0588235	0.1324403	-0.073617	-125.1485	0.0904493	0.1744313	0.0332872	0.2315935	1
48		9.5000079	0.0980392	0.1538219	-0.055783	-56.89836	0.1121991	0.1954448	0.0548241	0.2528197	1
49		9.7000079	0.0980392	0.1796308	-0.081592	-83.22345	0.1391647	0.2200969	0.0811138	0.2781479	1
50		9.9000079	0.1568627	0.2108880	-0.054025	-34.44110	0.1708272	0.2509488	0.1125367	0.3092392	1
51		10.100008	0.1960784	0.2484828	-0.052404	-26.72621	0.2076660	0.2892995	0.1498212	0.3471443	1
52		10.300008	0.2941177	0.2930470	0.0010706	0.3640184	0.2516357	0.3344583	0.1941380	0.3919560	1
53		10.500008	0.3529412	0.3448377	0.0081035	2.2959939	0.3040445	0.3856308	0.2461858	0.4434895	1
54		10.700008	0.4705882	0.4036408	0.0669474	14.226322	0.3640489	0.4432328	0.3054796	0.5018020	1
55		10.900008	0.5098039	0.4687082	0.0410957	8.0610858	0.4294560	0.5079604	0.3706835	0.5667329	1
56		11.100008	0.6078431	0.5387341	0.0691090	11.369544	0.4987270	0.5787412	0.4404047	0.6370635	1
57		11.300008	0.6470588	0.6118775	0.0351813	5.4371130	0.5712975	0.6524575	0.5133136	0.7104414	1
58		11.500008	0.7058823	0.6858299	0.0200524	2.8407625	0.6458275	0.7258323	0.5875024	0.7841574	1
59		11.700008	0.7647059	0.7579272	0.0067787	0.8864442	0.7191246	0.7967298	0.6600817	0.8557727	1
60		11.900008	0.8431372	0.8252993	0.0178378	2.1156517	0.7869782	0.8636205	0.7276438	0.9229549	1
61		12.100008	0.9019608	0.8850486	0.0169122	1.8750445	0.8460790	0.9240183	0.7871368	0.9829605	1
62		12.300008	0.9607843	0.9344434	0.0263409	2.7416082	0.8947343	0.9741525	0.8362349	1.0326519	1
63		12.500008	0.9607843	0.9711122	-0.010328	-1.074938	0.9316440	1.0105804	0.8730008	1.0692235	1
64		12.700008	0.9999999	0.9932210	0.0067789	0.6778943	0.9548278	1.0316142	0.8955371	1.0909049	1
65		12.900008	0.9999999	0.9996165	0.0003834	0.0383424	0.9619782	1.0372548	0.9022269	1.0970062	1
66		13.100008	0.9999999	0.9899204	0.0100796	1.0079586	0.9519296	1.0279111	0.8923939	1.0874468	1
67		13.300008	0.9607843	0.9645641	-0.003780	-0.393402	0.9256803	1.0034479	0.8666863	1.0624418	1
68		13.500008	0.9411764	0.9247601	0.0164163	1.7442353	0.8855999	0.9639203	0.8267722	1.0227480	1
69		13.700008	0.8627451	0.8724110	-0.009666	-1.120371	0.8339820	0.9108400	0.7747131	0.9701090	1
70		13.900008	0.8039216	0.8099664	-0.006045	-0.751916	0.7725131	0.8474197	0.7126481	0.9072847	1
71		14.100008	0.7450980	0.7402414	0.0048566	0.6518045	0.7029269	0.7775560	0.6429764	0.8375064	1
72		14.300008	0.6862745	0.6662163	0.0200582	2.9227631	0.6280911	0.7043415	0.5686374	0.7637952	1

73	14.500008	0.5882353	0.5908353	-0.002600	-0.441995	0.5519371	0.6297334	0.4929518	0.6887187	1
74	14.700008	0.4901961	0.5168235	-0.026627	-5.431997	0.4780792	0.5555678	0.4190011	0.6146459	1
75	14.900008	0.4117647	0.4465363	-0.034772	-8.444543	0.4087106	0.4843621	0.3490741	0.5439986	1
76	15.100008	0.3529412	0.3818502	-0.028909	-8.190899	0.3446648	0.4190356	0.2846347	0.4790657	1
77	15.300008	0.2745098	0.3240999	-0.049590	-18.06496	0.2865114	0.3616884	0.2267295	0.4214703	1
78	15.500008	0.2156863	0.2740604	-0.058374	-27.06435	0.2354831	0.3126377	0.1763040	0.3718167	1
79	15.700008	0.1568627	0.2319702	-0.075107	-47.88103	0.1929244	0.2710161	0.1340280	0.3299125	1
80	15.900008	0.1176471	0.1975882	-0.079941	-67.94996	0.1590736	0.2361027	0.0998565	0.2953198	1
81	16.100008	0.0784314	0.1702753	-0.091844	-117.1011	0.1326510	0.2078997	0.0728911	0.2676596	1
82	16.300009	0.0588235	0.1490951	-0.090272	-153.4617	0.1116478	0.1865424	0.0517791	0.2464111	1
83	16.500008	0.0196078	0.1329221	-0.113314	-577.9025	0.0947098	0.1711344	0.0353092	0.2305350	1
84	16.700008	0.0392157	0.1205532	-0.081338	-207.4107	0.0815349	0.1595715	0.0226220	0.2184845	1
85	16.900008	0.0588235	0.1108130	-0.051989	-88.38205	0.0718651	0.1497608	0.0129098	0.2087162	1
86	17.100009	0.0784314	0.1026455	-0.024214	-30.87299	0.0645706	0.1407203	0.0050863	0.2002047	1
87	17.300009	0.0392157	0.0951866	-0.055971	-142.7259	0.0578225	0.1325508	-0.002097	0.1924707	1
88	17.500009	0.0392157	0.0878102	-0.048595	-123.9161	0.0502323	0.1253882	-0.009556	0.1851766	1
89	17.700009	0.0196078	0.0801447	-0.060537	-308.7378	0.0417983	0.1184910	-0.017521	0.1778101	1
90	17.900009	0.0588235	0.0720602	-0.013237	-22.50236	0.0334093	0.1107111	-0.025725	0.1698456	1
91	18.100009	0.0000000	0.0636303	-0.063630	0.0000000	0.0256335	0.1016271	-0.033898	0.1611591	1
92	18.300009	0.0196078	0.0550744	-0.035467	-180.8794	0.0181810	0.0919677	-0.042030	0.1521786	1
93	18.500009	0.0196078	0.0466920	-0.027084	-138.1293	0.0103850	0.0829990	-0.050191	0.1435749	1
94	18.700009	0.0392157	0.0387986	0.0004171	1.0636401	0.0022015	0.0753956	-0.058193	0.1357906	1
95	18.900009	0.0000000	0.0316719	-0.031672	0.0000000	-0.005455	0.0687985	-0.065521	0.1288649	1
96	19.100009	0.0196078	0.0255155	-0.005908	-30.12884	-0.011506	0.0625374	-0.071638	0.1226686	1
97	19.300009	-0.039216	0.0204412	-0.059657	152.12509	-0.015601	0.0564832	-0.076343	0.1172251	1
98	19.500009	0.0000000	0.0164696	-0.016470	0.0000000	-0.018280	0.0512189	-0.079840	0.1127796	1
99	19.700009	0.0196078	0.0135436	0.0060642	30.927625	-0.020439	0.0475258	-0.082492	0.1095795	1
100	19.900009	0.0196078	0.0115503	0.0080575	41.093313	-0.022497	0.0455978	-0.084509	0.1076093	1
101	20.100009	0.0196078	0.0103453	0.0092626	47.239118	-0.024100	0.0447901	-0.085855	0.1065458	1
102	20.300009	0.0196078	0.0097741	0.0098337	50.151910	-0.024695	0.0442428	-0.086435	0.1059832	1
103	20.500009	0.0000000	0.0096898	-0.009690	0.0000000	-0.024360	0.0437397	-0.086370	0.1057497	1
104	20.700009	0.0196078	0.0099634	0.0096444	49.186458	-0.024320	0.0442471	-0.086180	0.1061064	1
105	20.900009	0.0196078	0.0104893	0.0091185	46.504334	-0.026764	0.0477423	-0.086752	0.1077307	1
106	21.100009	0.0392157	0.0111861	0.0280296	71.475511	-0.033441	0.0558135	-0.089112	0.1114842	1
107	21.300009	0.0196078	0.0119940	0.0076138	38.830631	-0.044423	0.0684114	-0.094077	0.1180649	1

APPENDIX L: Detailed Analytical Process

Step 1: Copy wave form data file into the analysis folder

Step 2: Cut out the 107 points of time and amplitude data that start with the first positive time value
(usually cell 5000)

Step 3: Divide the time cell of the resulting 107 data points by $1*10^{-9}$ to put the time into nanoseconds

Step 4: Multiply the amplitude data by -1 to invert the waveform

Step 5: Divide the amplitude by the max amplitude to normalize the waveform

Step 6: Copy the resulting time in ns and the normalized amplitude data and save it in a text file

Step 7: Open that text file in PeakFit

Step 8: Choose autofit III in Peakfit

Step 9: Choose the Chromatography button from the drop down menus and the EMG button from the drop down menus. Also choose the no baseline option from the baseline drop down window

Step 10: Click the autoscan functions of vary width and vary shape

Step 11: Move the EMG curve to fit the data as closely as you can to optimize the fit

Step 12: Capture the screen using the save function and save it as a bitmap

Step 13: Click review on the screen and it will analyze the curve fit

Step 14: Click the Export button and save the PeakFit curve data

Step 15: Click the numeric data and save it

Step 16: Click the data summary and save it

Step 17: Linearly interpolate the data to discover the through-put delay at the 10% amplitude mark

APPENDIX M: The Detector D1 Raw and Analyzed Data

Detector D1 2500 V Raw Data

run	Centroid	r^2	SE	FWHM	Through-Put
1	12.2	0.997844	0.0142558	3.2357	9.354
2	12.8	0.984055	0.0451763	3.73463696	8.913882
3	11.716	0.989888	0.0349613	5.0136	11.716
4	10.897	0.990264	0.0312092	3.10365894	7.964969
5	10.5	0.981159	0.0437652	3.75171892	7.704
6	11.3	0.990683	0.0313135	3.29112479	8.290719
7	10.454	0.991825	0.0280929	2.8478765	8.158916
8	10.5	0.997999	0.013773	3.05251433	8.108005
9	12.96	0.98717	0.0352682	3.17190633	10.51958
10	10.368	0.98283	0.0424457	3.18901506	7.834678
11	9.9	0.995403	0.0207567	3.00137733	7.602316
12	10.982	0.989864	0.032248	3.13777931	8.364144
13	11.016	0.989211	0.0332714	3.12074989	8.356263
14	11.306	0.990375	0.0303535	2.77967602	8.798677
15	11.613	0.981114	0.0398555	2.79670976	9.510427
16	12.006	0.991849	0.0267004	3.01839793	9.552235
17	10.829	0.985999	0.0345167	2.89906746	8.604407
18	11.085	0.982611	0.0421406	3.2743266	8.635231
19	11.1	0.987094	0.0360826	3.37654896	8.630033
20	10.999	0.990605	0.0322602	4.50203167	7.907787

Detector D1 2500 V Analysis

	Mean	Standard Deviation of the Mean	Range	Minimum Value	Maximum Value
Centroid	11.22655	0.796188121	3.06	9.9	12.96
R^2	0.988892	0.004971	0.16885	0.981114	0.997999
SE	0.0324	0.008727	0.031403	0.013773	0.045176
FWHM	3.314921	0.56313	2.233924	2.779676	5.0136
Through-Put	8.726313	1.011333	4.113684	7.602316	11.716

Detector D1 2400 V Raw Data

run	Centroid	r^2	SE	FWHM	Through - Put
1	11.75	0.98036	0.0478513	4.02437463	8.773961
2	11.016	0.991302	0.0302979	3.63235321	8.29835
3	10.965	0.991113	0.0307558	3.06958035	10.965
4	11.75	0.997139	0.0166565	3.71670049	8.794766
5	12.091	0.987247	0.0379842	3.53927566	9.30554
6	14.1	0.992762	0.0380212	4.23329417	10.30618
7	12.7	0.982203	0.0407003	3.27422541	9.654061
8	10.5	0.990669	0.0302066	3.61707172	7.819989
9	10.897	0.99188	0.0291193	3.03549081	8.241918
10	10.88	0.98502	0.0377796	3.13779633	8.443027
11	10.027	0.995587	0.0200661	2.98429196	7.603211
12	11.2	0.985869	0.0362232	2.96727819	8.61376
13	11.272	0.980915	0.0468105	3.63243982	8.215609
14	10.368	0.989163	0.0329834	3.37653361	7.719766
15	10.897	0.983573	0.0417924	3.7005423	8.275909
16	11.3	0.988618	0.0337252	3.18892878	8.70904
17	12.892	0.974634	0.0219218	4.16098288	10.35947
18	11.272	0.952626	0.0685007	3.44477637	8.589575
19	12.7	0.986738	0.0361625	3.25716715	9.178466
20	11.477	0.982084	0.045166	3.96175682	8.589138

Detector D1 2400 V Analysis

	Mean	Standard Deviation of the Mean	Range	Minimum Value	Maximum Value
Centroid	11.5027	0.983269	4.073	10.027	14.1
R2	0.9985475	0.009523	0.044513	0.952626	0.997139
SE	0.036136	0.011345	0.051844	0.016657	0.068501
FWHM	3.497743	0.391163	1.266016	2.967278	4.233294
Through-Put	8.82837	0.903336	3.361789	7.603211	10.965

Detector D1 2300 V Raw Data

run	Centroid	r^2	SE	FWHM	Through-Put
1	11.971	0.989144	0.032491	3.773755	9.360854
2	11.187	0.972844	0.053906	3.956965	8.119913
3	12.3	0.992519	0.028453	4.14394	9.127977
4	11.357	0.986691	0.038639	3.83695	8.312684
5	10.5	0.986698	0.034876	3.32539	7.959812
6	11.204	0.97176	0.052774	3.39630333	8.829112
7	11.5	0.982109	0.043135	3.34241926	9.153992
8	10.948	0.986925	0.035114	3.50529059	8.464569
9	11.9	0.98976	0.031424	3.75160516	9.201395
10	10.454	0.979293	0.047478	3.61540807	7.762231
11	12.1	0.997092	0.017759	4.28037622	8.852413
12	11.92	0.981639	0.044066	3.63238129	9.10249
13	10.778	0.978723	0.052767	3.88037149	7.301227
14	12.858	0.977128	0.056114	4.12692427	9.283881
15	11.494	0.979856	0.044366	2.93322554	9.101732
16	12.261	0.970521	0.058244	3.50083	9.147138
17	12.329	0.972192	0.056569	3.63227218	9.86045
18	10.93	0.981749	0.045579	3.87109943	8.016915
19	12.398	0.967288	0.058006	3.34240642	9.654476
20	12.159	0.961444	0.071615	4.36571661	8.651631

Detector D1 2300 V Analysis

	Mean	Standard Deviation of the Mean	Range	Minimum Value	Maximum Value
Centroid	11.6274	0.689619	2.404	10.454	11.858
R2	0.980269	0.009062	0.035648	0.961444	0.997092
SE	0.045169	0.012811	0.053856	0.017759	0.071615
FWHM	3.710681	0.361424	1.432491	2.933226	4.365717
Through-Put	8.763245	0.670975	2.559223	7.301227	9.86045

Detector D1 2200 V Raw Data

run	Centroid	r^2	SE	FWHM	Through-Put
1	11.681	0.989068	0.031728	3.37655006	9.117453
2	11.903	0.97638	0.054317	3.68348063	8.761883
3	11.272	0.977153	0.054202	4.02457442	8.250823
4	14.137	0.936346	0.09302	4.36561848	11.00131
5	10.897	0.88155	0.111192	3.39358105	8.527041
6	11.562	0.975203	0.049465	3.14307207	8.708046
7	13.029	0.965015	0.065213	3.81996132	8.96783
8	11.3	0.981034	0.04629	3.46181369	8.640857
9	11.9	0.979632	0.045387	3.10366336	9.355814
10	12.824	0.972632	0.055752	4.22918562	9.485479
11	11.63	0.94885	0.0707	2.55798651	9.446139
12	12.926	0.960428	0.074835	5.59344704	8.937613
13	11.545	0.96234	0.068658	4.43383614	8.752128
14	11.085	0.955837	0.068294	3.54508668	8.512688
15	11.119	0.984651	0.040934	3.54704442	8.24275
16	12.5	0.964217	0.062185	3.27422479	8.933792
17	11.3	0.97622	0.050381	3.70053248	8.866231
18	11.5	0.986636	0.036578	3.20598625	8.843117
19	12.346	0.95369	0.067095	2.95018985	9.623682
20	12.892	0.969735	0.060006	4.17805628	9.706262

Detector D1 2200 V Analysis

	Mean	Standard Deviation of the Mean	Range	Minimum Value	Maximum Value
Centroid	11.9674	0.844584	3.24	10.897	14.897
R2	0.964831	0.023818	0.107518	0.88155	0.989068
SE	0.060312	0.018736	0.079464	0.031728	0.111192
FWHM	3.679395	0.666766	3.035461	2.557987	5.593447
Through-Put	9.034047	0.625132	2.75857	8.24275	11.00131

Detector D1 2100 V Raw Data

run	Centroid	r^2	SE	FWHM	Through-Put
1	12.1	0.953453	0.066015	2.711277	9.6194
2	11.698	0.983176	0.042772	3.35949793	9.211636
3	11.5	0.989268	0.033308	3.89841739	8.500371
4	11.5	0.986773	0.039134	3.94950695	8.760167
5	11.75	0.990867	0.032226	3.63231111	8.805966
6	11.323	0.980219	0.043212	2.77968787	9.204481
7	11.289	0.979438	0.044049	3.30833463	8.858821
8	13.199	0.993245	0.026878	3.58115385	9.60962
9	11.988	0.947508	0.0828	4.05864096	8.724997
10	13.131	0.971638	0.054791	3.37653003	9.413121
11	11.374	0.953853	0.067664	3.39355431	8.877913
12	10.3	0.969117	0.054436	3.4172426	7.941614
13	12.568	0.975734	0.05137	3.92224828	8.398656
14	10.9	0.972809	0.049633	3.12913578	8.484093
15	11.92	0.945657	0.075076	3.20598207	9.30125
16	12.534	0.89351	0.109047	2.62627381	10.50891
17	11.17	0.988616	0.034343	3.63391939	8.712613
18	12.295	0.95089	0.07877	3.68347076	9.185783
19	11.495	0.980017	0.043795	3.29127516	8.946883
20	11.5	0.976976	0.049695	3.22304989	8.484217

Detector D1 2100 V Analysis

	Mean	Standard Deviation of the Mean	Range	Minimum Value	Maximum Value
Centroid	11.7767	0.71577	2.899	10.3	13.199
R2	0.969138	0.023361	0.099735	0.89351	0.993245
SE	0.053951	0.0205	0.082169	0.026878	0.101047
FWHM	3.409075	0.403928	1.432367	2.626274	4.058641
Through-Put	8.977526	0.560038	2.567296	7.941614	10.50891

Detector D1 2000 V Raw Data

run	Centroid	r^2	SE	FWHM	Through-Put
1	12.824	0.932708	0.081332	2.74562323	10.63188
2	11.5	0.991134	0.031735	4.48498775	8.353801
3	12.159	0.91969	0.095735	3.70053869	9.186905
4	12.33	0.96733	0.068062	4.63845227	9.197041
5	11.903	0.944265	0.078591	3.2301229	9.380488
6	13.319	0.857781	0.137292	3.8369	9.500711
7	12.091	0.87694	0.018031	3.215442	9.694838
8	12.022	0.911711	0.107698	3.32539893	9.049936
9	12.074	0.919539	0.103652	3.63234101	9.304788
10	12.568	0.901039	0.118166	3.2400983	9.61439
11	11.784	0.922015	0.0853	3.41063007	9.11016
12	13.489	0.935319	0.106344	4.43626884	9.3948
13	12.824	0.849651	0.126839	3.41063735	9.05172
14	11.9	0.980079	0.046894	3.25717779	9.506972
15	12.364	0.821878	0.124199	2.67734057	8.974359
16	13.08	0.837235	0.132967	3.46179678	10.18746
17	12.483	0.935866	0.078033	3.51385373	8.671677
18	9.9	0.993997	0.024586	3.42770095	7.23908
19	11.886	0.840032	0.148442	3.66642351	9.353667
20	12.705	0.859461	0.128985	3.47883271	8.391558

Detector D1 2000 V Analysis

	Mean	Standard Deviation of the Mean	Range	Minimum Value	Maximum Value
Centroid	12.26025	0.767756	3.589	9.9	13.489
R2	0.909884	0.052925	0.172119	0.821878	0.993997
SE	0.092144	0.038804	0.130411	0.018031	0.148442
FWHM	3.539528	0.507341	1.961112	2.61112	4.638452
Through-Put	9.189812	0.700649	3.3928	7.23908	10.63188

Detector D1 1900 V Raw Data

run	Centroid	r^2	SE	FWHM	Through-Put
1	11.647	0.811785	0.161088	2.62620698	9.660899
2	12.3	0.904121	0.10514	3.63233557	9.453645
3	12.329	0.92075	0.09499	2.71625986	9.673058
4	12.602	0.619124	0.271824	3.63233416	9.95809
5	12.227	0.810023	0.164797	2.43859451	8.262653
6	12.159	0.933923	0.079029	2.9501966	9.9679969
7	13.881	0.895137	0.119635	3.66640909	10.5773
8	12.7	0.986842	0.039337	4.2377176	9.864794
9	11.886	0.88212	0.115688	2.89903026	9.513453
10	12.091	0.892118	0.1062	2.9672409	9.967024
11	12.858	0.89442	0.109597	2.96723	10.43619
12	12.3	0.979848	0.046956	3.88813023	9.25359
13	12.3	0.906445	0.103064	3.17184042	9.374257
14	13.898	0.98531	0.042668	5.43999416	9.764274
15	12.466	0.949496	0.081963	3.66640909	9.123883
16	11.3	0.939966	0.08154	3.3083453	8.229475
17	11.903	0.93377	0.083551	2.84789923	9.405658
18	12.5	0.902567	0.092722	2.55796417	9.50278
19	13.131	0.91696	0.092975	3.00134709	10.70528
20	13.898	0.935752	0.086915	4.07573895	9.643492

Detector D1 1900 V Analysis

	Mean	Standard Deviation of the Mean	Range	Minimum Value	Maximum Value
Centroid	12.5188	0.718006	2.598	11.3	13.898
R2	0.900024	0.081046	0.367718	0.619124	0.986842
SE	0.103984	0.050985	0.232487	0.039337	0.271824
FWHM	3.334561	0.717237	3.0014	2.438595	5.439994
Through-Put	9.61689	0.629004	2.475805	8.229475	10.70528

Detector D1 1800 V Raw Data

run	Centroid	r^2	SE	FWHM	Through-Put
1	12.585	0.896893	0.873023	3.90515295	7.792432
2	12.381	0.399447	0.286112	3.61528	9.420944
3	15.7	0.751094	0.166286	2.19986	13.83624
4	12.79	0.765939	0.187871	3.17188213	8.858333
5	13.216	0.846292	0.118945	2.6571403	10.96743
6	13.319	0.869058	0.121984	2.93315075	9.763808
7	13.285	0.913197	0.105148	3.57357191	10.29121
8	10.982	0.967984	0.060294	3.60363351	7.27861
9	11.784	0.888849	0.107331	3.29124853	9.147013
10	12.688	0.894884	0.108694	3.71760623	9.8093441
11	11.2	0.93365	0.091893	3.1348224	7.386076
12	13.08	0.839154	0.152404	3.44473154	9.711494
13	12.995	0.901253	0.136405	5.71280098	7.901024
14	12.5	0.990522	0.03278	4.65553482	9.58022

Detector D1 1800 V Analysis

	Mean	Standard Deviation of the Mean	Range	Minimum Value	Maximum Value
Centroid	12.75	1.122887	4.718	10.982	15.7
R2	0.847015	0.144973	0.591075	0.399447	0.990522
SE	0.182084	0.207776	0.840243	0.03278	0.873023
FWHM	3.54403	0.852837	3.512941	2.19986	5.712801
Through-Put	9.410298	1.689935	6.55763	7.27861	13.83624

APPENDIX N: The Detector D2 Raw and Analyzed Data

Detector D2 2500 V Raw Data

run	Centroid	r^2	SE	FWHM	Through - Put
1	12.449	0.994173	0.022998	3.34243602	10.0515
2	11.852	0.956279	0.0680226	3.8369775	9.641013
3	12	0.995469	0.0201689	3.0359208	9.668198
4	12.1	0.99545	0.020074	3.0299109	9.661279
5	12.415	0.991361	0.023195	3.7005291	9.934252
6	12.534	0.994469	0.0236038	3.64221184	9.937534
7	11.8	0.991137	0.0297469	3.7346569	9.130181
9	12.568	0.995829	0.0210624	3.34241816	9.897019
10	12.6	0.979088	0.0478578	3.47886554	10.05075
11	11.784	0.991655	0.0302612	3.80287889	8.980795
12	12.4	0.993568	0.0244884	3.05253534	10.05537
13	12.193	0.971527	0.0562443	4.2051788	9.620569
14	11.136	0.984536	0.040979	3.44399411	8.525341
15	12.074	0.986968	0.0382416	3.85404279	9.047134
16	12.636	0.989268	0.0352686	4.02454832	9.776159
17	12.4	0.987937	0.0341014	3.13777847	10.35238
18	11.2	0.98397	0.0417231	3.42774218	8.547522
19	12.875	0.994098	0.0244496	3.34241053	10.13311
20	11.835	0.99135	0.029293	3.10151991	9.382857

Detector D2 2500 V Analysis

	Mean	Standard Deviation of the Mean	Range	Minimum Value	Maximum Value
Centroid	12.15	0.470161	1.739	11.136	12.875
R^2	0.9807796	0.00987	0.03955	0.956279	0.995829
SE	0.033252	0.013115	0.047949	0.020074	0.0688023
FWHM	3.501924	0.351849	1.175268	3.029911	4.205179
Through-Put	9.59963	0.529132	1.827039	8.525341	10.35238

Detector D2 2400 V Raw Data

run	Centroid	r^2	SE	FWHM	Through-Put
1	12.6	0.971838	0.0527058	3.25717545	10.19945
2	13.063	0.996247	0.019415	3.61247639	10.192
3	12.483	0.995914	0.0207563	3.2060071	9.95277
4	12.278	0.988261	0.033553	3.76874959	9.85333
5	13.37	0.986416	0.0443726	4.58728554	9.187668
6	12.057	0.982579	0.0410068	3.29128349	9.646325
7	12.4	0.987504	0.0335641	3.26815536	9.982623
8	12.466	0.996838	0.0177255	3.25484119	9.979627
9	12.364	0.996917	0.0164352	3.11002515	9.848926
10	12.585	0.979296	0.0473928	4.00751808	9.877991
11	12.824	0.994553	0.023508	3.68351229	10.0852
12	12.2	0.996919	0.0173027	3.31141671	9.479341
13	10.419	0.99275	0.0255373	3.03546516	7.73865
14	11.6	0.994325	0.0231754	3.33332981	8.814545
15	11	0.982646	0.0444046	4.57026966	8.210516
16	13.046	0.976927	0.0537963	4.3650195	10.12103
17	14.2	0.984099	0.0459775	4.72374067	10.50425
18	11.016	0.985534	0.0368914	3.03547074	8.809951
19	13.2	0.995351	0.0211028	3.15482767	10.5302
20	12.312	0.975567	0.0515015	3.85400779	9.706904

Detector D2 2400 V Analysis

	Mean	Standard Deviation of the Mean	Range	Minimum Value	Maximum Value
Centroid	12.37415	0.875126	3.781	10.419	14.2
R2	0.988024	0.008025	0.025081	0.971838	0.99619
SE	0.033506	0.013269	0.037361	0.016435	0.053796
FWHM	3.621529	0.554811	1.688276	3.035465	4.723741
Through-Put	9.636065	0.737227	2.79155	7.73865	10.5302

Detector D2 2300 V Raw Data

run	Centroid	r^2	SE	FWHM	Through-Put
1	12.875	0.994288	0.02521	3.58809891	10.01273
2	12.6	0.996649	0.018183	3.5642668	9.985977
3	13	0.988398	0.034118	3.68831487	10.34857
4	13.2	0.995712	0.020719	3.85833668	9.903497
5	12.04	0.972774	0.052406	2.8514227	9.267327
6	12.892	0.973838	0.050745	3.17188647	10.23636
7	12.8	0.995678	0.020799	4.1335951	9.871477
8	13.387	0.994422	0.024906	3.71363935	10.28882
9	12.551	0.994822	0.021788	3.9931951	9.655814
10	13.301	0.996693	0.018229	3.37655193	13.3618
11	14.325	0.995121	0.023348	4.24624338	10.96073
12	13.4	0.996357	0.019483	3.7925006	9.960445
13	13.114	0.996434	0.019872	3.79116327	9.784375
14	12.398	0.992985	0.027056	3.31645632	9.720228
15	12.392	0.99889	0.02724	3.28236031	9.804598
16	12.517	0.996625	0.017679	3.05253623	10.17297
17	11.392	0.99159	0.028569	3.07308924	8.980899
18	13.36	0.994077	0.024441	3.17190258	10.63303
19	12.8	0.995385	0.022034	3.81993758	9.983835
20	11.4	0.991728	0.030221	3.71759656	8.709422

Detector D2 2300 V Analysis

	Mean	Standard Deviation of the Mean	Range	Minimum Value	Maximum Value
Centroid	12.7872	0.685735	2.933	11.392	14.325
R2	0.992623	0.006992	0.026116	0.972774	0.99889
SE	0.026352	0.009653	0.034727	0.017679	0.052406
FWHM	3.560155	0.382881	1.394821	2.851423	4.24643
Through-Put	10.08215	0.927123	2.311475	8.709422	13.3618

Detector D2 2200 V Raw Data

run	Centroid	r^2	SE	FWHM	Through-Put
1	11.988	0.992817	0.028842	4.1780427	8.735211
2	12.858	0.99391	0.024113	4.06252655	10.42773
3	12.8	0.991488	0.029972	4.00751565	9.898551
4	12.671	0.997051	0.016936	3.37283848	9.856442
5	12.79	0.982127	0.042427	3.59821503	10.30165
6	13.029	0.986748	0.038766	3.4277018	10.50783
7	11.869	0.932049	0.02726	3.14453795	9.156923
8	12.807	0.979346	0.051258	4.48501579	9.413333
9	12.705	0.971804	0.05824	4.41677607	9.823
10	12.4	0.982899	0.043259	4.00575988	9.823129
11	13	0.974651	0.051797	3.57322378	9.719643
12	11.426	0.988053	0.035168	3.75536434	8.4017
13	11.596	0.9841	0.043143	4.21212701	8.734853
14	13.421	0.981243	0.0413	3.10369089	11.033
15	12.6	0.996173	0.019069	3.19776659	9.981679
16	13.08	0.996671	0.018469	3.73466384	10.38054
17	12.671	0.992698	0.028376	3.65053043	9.749093
18	12.585	0.993152	0.026108	3.48249782	10.18365
19	13	0.993506	0.026183	3.50403387	10.18021
20	13	0.989108	0.035669	4.26328359	10.15935

Detector D2 2200 V Analysis

	Mean	Standard Deviation of the Mean	Range	Minimum Value	Maximum Value
Centroid	12.6148	0.518406	1.995	11.426	13.421
R2	0.98498	0.014438	0.065002	0.932049	0.997051
SE	0.034318	0.011736	0.041303	0.016936	0.05824
FWHM	3.758806	0.423322	1.381325	3.103691	4.485016
Through-Put	9.823376	0.659211	2.6313	8.4017	11.033

Detector D2 2100 V Raw Data

run	Centroid	r^2	SE	FWHM	Through-Put
1	12.312	0.991918	0.026684	3.31763142	9.742857
2	12.6	0.986723	0.036818	3.65674305	9.935977
3	12.8	0.992528	0.029333	3.46177863	9.94375
4	12.108	0.987243	0.033001	3.08018142	9.74475
5	13.2	0.971508	0.162359	4.3405704	10.0494
6	13	0.978017	0.048181	3.54706385	10.50125
7	12.756	0.987679	0.036311	3.73465039	10.11803
8	13	0.99107	0.03274	4.87721043	10.31579
9	13.097	0.997297	0.016496	3.43933255	10.35156
10	12.909	0.997182	0.017297	3.90520392	9.953355
11	13.404	0.98803	0.037114	3.56409914	10.37713
12	13	0.993381	0.025692	3.5003128	10.40226
13	12.2	0.99444	0.022215	3.29127131	9.632416
14	13.4	0.994972	0.023402	3.61529158	10.61633
15	12.193	0.983004	0.041751	3.8028592	9.532961
16	13.2	0.981235	0.047466	4.09278422	10.22857
17	13.6	0.994995	0.021899	3.6715058	11.10428
18	12.074	0.992824	0.026513	3.75257602	9.235106
19	14	0.981824	0.048359	4.5872966	10.63
20	13	0.987594	0.035975	3.53002655	10.43412

Detector D2 2100 V Analysis

	Mean	Standard Deviation of the Mean	Range	Minimum Value	Maximum Value
Centroid	12.89265	0.52454	1.926	12.074	14
R2	0.988673	0.00681	0.025789	0.971508	0.997297
SE	0.03848	0.030725	1.797029	0.016496	0.162359
FWHM	3.738419	0.441736	1.869174	3.080181	4.81121
Through-Put	10.14249	0.441577	2.567296	9.235106	11.10428

Detector D2 2000 V Raw Data

run	Centroid	r^2	SE	FWHM	Through-Put
1	13.097	0.971453	0.057925	4.15546804	10.26316
2	13.387	0.991598	0.02903	3.34244415	10.83886
3	13.506	0.990487	0.03204	4.1818554	10.78792
4	13.4	0.99333	0.025607	3.51062886	10.74327
5	13.2	0.989539	0.035065	4.99177329	9.654671
6	12.6	0.978859	0.047583	3.47887068	10.0213
7	13.6	0.994455	0.023867	3.47884441	10.69091
8	12.671	0.980431	0.045731	3.95634496	10.18841
9	14.069	0.959674	0.069251	4.6022425	10.32562
10	13.319	0.992328	0.028505	3.89330524	10.29375
11	13.114	0.980501	0.046235	4.21212446	10.33739
12	12.8	0.993525	0.026103	4.48498827	9.951807
13	13.37	0.989859	0.034355	4.09277276	9.739442
14	12.8	0.986803	0.036636	3.81993949	9.95
15	11.8	0.988098	0.03643	3.66645052	8.66667
16	13.591	0.993476	0.026571	4.06839077	10.90426
17	13.6	0.996081	0.020047	3.85403408	10.825
19	13	0.988496	0.036544	4.34858831	9.816568
20	14	0.992087	0.029643	4.35508291	10.33281

Detector D2 2000 V Analysis

	Mean	Standard Deviation of the Mean	Range	Minimum Value	Maximum Value
Centroid	13.20653	0.530029	2.269	11.8	14.069
R2	0.986899	0.009154	0.036407	0.959674	0.996081
SE	0.036169	0.012431	0.049204	0.020047	0.069251
FWHM	4.026008	0.4298	1.649329	3.342444	4.991773

Detector D2 1900 V Raw Data

run	Centroid	r^2	SE	FWHM	Through-Put
1	13.2	0.974789	0.054348	4.00447514	10.33981
2	11.988	0.984101	0.042858	3.78582531	9.061111
3	13.387	0.978903	0.050351	3.9734026	10.51765
4	13.8	0.979697	0.048888	4.50705075	10.59672
5	13.182	0.993055	0.02724	3.63234134	10.56951
6	12.8	0.97902	0.049296	3.74893539	9.946
7	13.267	0.988021	0.036126	3.93927823	10.55882
8	13.8	0.981545	0.042153	3.12071855	11.28144
9	12.6	0.984466	0.039078	3.2230681	10.40884
10	13.574	0.980907	0.048813	3.93930598	10.62222
11	13.6	0.964596	0.061159	3.65897396	10.58621
12	12.8	0.975963	0.049838	3.1036631	10.26189
13	13.046	0.980667	0.04882	3.512945	10.21443
14	13.4	0.987174	0.034863	3.23313099	10.81443
15	12.2	0.982227	0.048195	5.29780253	9.25641
16	13.182	0.992082	0.028932	3.4276995	10.26857
17	11.92	0.970258	0.060685	4.12013153	9.217778
18	13	0.986273	0.037927	3.6323488	11.35882
19	13.2	0.986518	0.037567	3.90516716	10.58824
20	14	0.972082	0.05847	3.90317563	11.23871

Detector D2 1900 V Analysis

	Mean	Standard Deviation of the Mean	Range	Minimum Value	Maximum Value
Centroid	13.0973	0.579478	2.08	11.92	14
R2	0.981117	0.007164	0.028459	0.964596	0.993055
SE	0.04528	0.009753	0.033919	0.061159	0.905604
FWHM	3.783472	0.506441	2.194139	3.103663	5.297803
Through-Put	10.38538	0.631283	2.297709	9.061111	11.35882

Detector D2 1800 V Raw Data

run	Centroid	r^2	SE	FWHM	Through-Put
1	13.984	0.962219	0.065983	3.47885306	11.49831
2	13.404	0.974909	0.005301	3.7516917	12.98077
3	13.93239	0.919515	0.11188	4.2974313	10.54815
4	14.615	0.964949	0.06502	3.51364424	12.0382
5	13.199	0.969112	0.061403	3.93928993	10.69091
6	13.387	0.981076	0.047876	3.71760623	10.47429
7	13	0.968335	0.062939	4.38266938	10.20488
8	13.216	0.929185	0.091316	3.0354888	10.56972
9	12.6	0.97717	0.005104	3.93927081	9.79872
10	13.6	0.993458	0.025866	3.52091818	10.76129
11	13.2	0.986251	0.038467	3.97339053	10.06875
12	13.6	0.979443	0.047155	3.58116209	11.26166
13	13.267	0.966519	0.059128	3.47967422	10.90952
14	13.6	0.951076	0.071656	2.8820069	11.46531
15	12.995	0.957962	0.067314	3.00138163	10.38788
16	14.785	0.980814	0.057617	3.63230292	11.54815
17	13.8	0.974202	0.05876	4.02455407	10.61143
18	14.597	0.898651	0.039992	4.14395221	11.47879
19	13.83	0.98397	0.042167	4.19508069	10.87222
20	13.8	0.981397	0.046211	3.93930248	10.76622

Detector D2 1800 V Analysis

	Mean	Standard Deviation of the Mean	Range	Minimum Value	Maximum Value
Centroid	13.62057	0.571231	2.185	12.6	14.785
R2	0.965011	0.024032	0.094807	0.898651	0.993458
SE	0.053156	0.025096	0.106776	0.005104	0.11188
FWHM	3.721484	0.422553	1.500662	2.882007	4.382669
Through-Put	10.94676	0.738889	3.18205	9.79872	12.98077

APPENDIX O: Ortec NIM Model 771 Timer-Counter Specifications

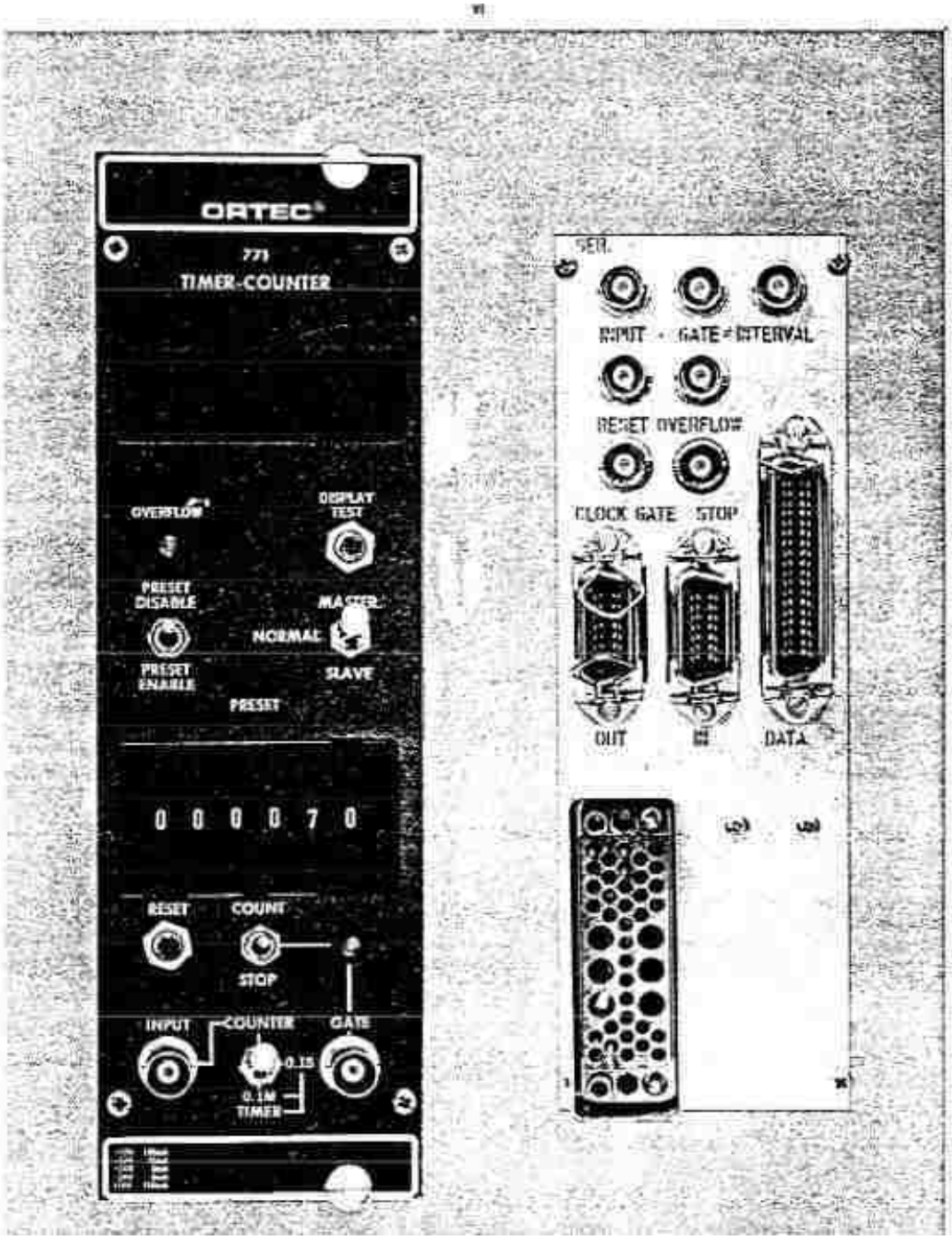

2. SPECIFICATIONS

2.1. PERFORMANCE

Count Capacity 6 decades, for 000 000 through 999 999.

Time Base 0.1-sec or 0.1-min counting increments, time base derived from 100-kHz crystal-controlled oscillator. Dead-time gating at oscillator output through a rear panel connector.

Counting Rate (Scaler) 20 MHz.

Time Base Accuracy Within <0.005%.

Time Base Stability Within <0.002%/°C.

Synchronizing Error <0.2 μsec.

Automatic Clear Generated when power is turned on initially or after a power failure.

2.2. INDICATORS

Readout Display 6 direct-reading 7-segment LED digits and a decimal point with automatic blanking of insignificant zeros.

Overflow LED illuminated from first overflow until reset.

Gate LED illuminated while unit is in the counting condition.

2.3. CONTROLS

Display Test Push-button switch lights all 7 segments of each digit in the display when it is pressed for a reading of 888 888.

Master/Slave/Normal 3-position locking toggle switch selects system control of the unit in a printing loop. Master selects control over all Slaves in the system by furnishing signals through the system gate and reset lines. Normal isolates this module from system control through gate and reset lines. Slave selects control from some other module, operating as the Master, that furnishes system gate and reset signals.

Preset Disable/Preset Enable Toggle switch selects whether the preset signal will or will not be generated.

Preset Six thumbwheel switches select any count level within the capacity of the unit as a preset signal generation level.

Reset Push-button switch resets display and internal logic to an initial condition when pressed.

Count/Stop Toggle switch manually selects counting or noncounting condition for the module.

Counter/Timer 3-position locking toggle switch selects the source of pulses to be counted; Counter selects the logic pulses through the adjacent input connector or its equivalent on the rear panel; 0.1 S selects the timer pulses that are furnished from the internal timing system at 0.1-sec intervals; 0.1 M selects the internal timer pulses that are furnished at 0.1-min intervals.

2.4. CONNECTORS

Input Front and rear panel type BNC connectors accept NIM-standard slow positive logic signals; ≥+3 V to count or ≤+1.5 V to not count, ±25 V maximum, ≥25-nsec width, Z_{in} <2 kΩ, dc-coupled.

Gate Front and rear panel type BNC connectors accept NIM-standard slow positive logic signals to control the gate to the counting register and the associated Gate indicator lamp. ≥+3 V or open circuit permits counting, ≤+1.5 V inhibits counting, ±25 V maximum. Driving source must be capable of sinking 0.5 mA of positive current.

Interval Rear panel type BNC connector furnishes a +5-V output level whenever the 771 is in a counting condition. Nominally 0 V for noncounting.

Stop Rear panel type BNC connector furnishes a nominal +5-V logic pulse, 0.5 μsec wide, each time a preset condition is sensed. Z_o <10Ω dc-coupled.

Clock Gate Rear panel type BNC connector permits gating of internal timing oscillator output. ≥+3 V gates the timer off, ≤+1.5 V or open circuit gates timer on. Z_{in} <2 kΩ, dc-coupled.

Reset Rear panel type BNC connector accepts standard positive logic signal to reset the unit to an initial zero condition. ≥+3 V resets; ≤1.5 V does not reset; ±25 V maximum; 100 nsec minimum width. Z_{in} 2 kΩ dc-coupled to ground.

Overflow Rear panel type BNC connector furnishes standard positive logic output, +5 V for 2 μsec, whenever the counting register overflows to zero. Driving source impedance <10Ω, dc-coupled.

In/Out Rear panel Amphenol type 57-40140 connectors for use with the ORTEC standard printing system logic and data interconnections.

Data Rear panel output accommodates the connector for the Parallel Data Output option.

APPENDIX P: Ortec Model 425A

ORTEC®

425A
Nanosecond Delay

- **Aligns fast-timing channels that incorporate coincidence circuits or TACS**
- **50-Ω calibrated delay cable for linear or logic signals**
- **2- to 65-ns delay in 1-ns steps**

The ORTEC Model 425A Nanosecond Delay provides a calibrated delay for any type of signal in 1-ns steps from 0 to 63 ns. Longer delays can be obtained by cascading several Model 425As. The delays are accomplished with RG-58A/U coaxial cables that are interconnected by stripline sections. No power is required to operate the instrument.

The Model 425A has many uses. For example, it can be used for aligning fast-timing channels to operate coincidence circuits or time-to-pulse-height converters. And, because of the high accuracy of the delays, it can be used to calibrate that equipment.

The input and output impedances of the Model 425A are 50 Ω, making it fully compatible with related signal sources and loads in other NIM-standard modular nuclear instruments.

Specifications

PERFORMANCE

DELAY ACCURACY ±100 ps or ±1% for each delay section used.

MINIMUM DELAY (All Switches Out) 2.0 ns.

IMPEDANCE MISMATCH REFLECTION ≤±2% from any of the delay switches.

CONTROLS

Six slide switches, each with an Out position and an In position, permit selection in any combination for total delay; switches select 1, 2, 4, 8, 16, and 32 ns.

INPUT

BNC connector accepts signal of either polarity to ±600 V maximum; impedance, 50 Ω.

OUTPUT

BNC connector furnishes input signals with the delay selected by the switches that are set at IN; impedance, 50 Ω.

ELECTRICAL AND MECHANICAL

POWER REQUIRED None.

WEIGHT
Net 1.0 kg (2.2 lb).
Shipping 1.4 kg (3.0 lb).

DIMENSIONS NIM-standard single-width module 3.43 X 22.13 cm (1.35 X 8.714 in.) per DOE/ER-0457T.

Ordering Information

To order, specify:

Model	Description
425A	Nanosecond Delay

Specifications subject to change
011108

ORTEC®
www.ortec-online.com
Tel. (865) 482-4411 • Fax (865) 483-0396 • ortec.info@ametek.com
801 South Illinois Ave., Oak Ridge, TN 37831-0895 U.S.A.
For International Office Locations, Visit Our Website

AMETEK®
ADVANCED MEASUREMENT TECHNOLOGY

REFERENCES

Bartl, W. and P. Weinzierl. ñExperimental Investigation on the Limits of Time Resolution of Scintillation Counters.ò *The Review of Scientific Instruments* 34 (1963): 252-255.

Bengtson, B. and M. Moszynski. ñTiming Properties of Scintillation Counters.ò *Nuclear Instruments and Methods* 81 (1970): 109-120.

Birks, J. B. *The Theory and Practice of Scintillation Counting.* New York: Pergamon Press, 1964.

Bray, A. D., et al. ñResponse of Plastic Scintillators to Cosmic Ray Air Showers.ò *The Review of Scientific Instruments* 36 (1965): 587-591.

Chen, J. B., et al. ñCalibration of the time response functions of a quenched plastic scintillator for neutron time of flight.ò *Nuclear Instruments and methods in Physics Research A* 491 (2002): 474-477.

El-Wahab, M. A. and J. V. Kane. ñAn Analytic Treatment for Scintillation Counter Time Resolution Functions.ò *Nuclear Instruments and Methods* 15 (1962): 15-22.

Fallu-Labruyere, A. and H. Tan, W. Hennig, W. K. Wardurton. ñTime resolution studies using digital constant fraction discrimination.ò *Nuclear Instruments and Methods in Physics Research A* 579 (2007), 247-251.

Gatti, E. and V. Svelto. ñTime resolution in scintillation counters.ò in *Proceedings of the Symposium on Nuclear Instruments,* edited by J. B. Birks. Manchester: Victoria University of Manchester, 1962.

Gedcke, D.A. and W.J. McDonald ñA Constant fraction of pulse height trigger for optimum time resolution.ò *Nuclear Instruments and Methods* 55 (1967): 377-380.

Harms, A. A., *et. al*. *Principles of Fusion Energy: An Introduction to Fusion Energy for*

Students of Science and Engineering. London: World Scientific, 2000.

Harvey, J. A. and N.W. Hill. ñScintillation Detectors for Neutron Physics Research.ò *Nuclear Instruments and Methods* 162 (1979): 507-529.

Idaho State University Accelerator Center. ñFacilities and Capabilities.ò Accessed on 24 March 2014. http://iac.isu.edu/facilities.html.

Jacobsson, David. ñCalibration of plastic-scintillator detectors at MAX-lab in preparation for (ɔ, ´ $^{+}$) experiments.*"* MS thesis, Lund University, 2009.

Johnson, M. Gatu, *et al.* ñNeutron spectrometry- An essential tool for diagnosing implosions at the National Ignition Facility.ò *The Review of Scientific Instruments* 83, number 10 (2012): 10D308.

Keefe, Denis. ñInertial Confinement Fusion.ò *The Annual Review of Nuclear Particle Science* 32 (1982): 391-441.

Knoll, Glenn F. *Radiation Detection and Measurement,* 4th ed. New York: John Wiley & Sons, Inc., 2010.

Leo, W. R. *Techniques for Nuclear and Particle Physics Experiments: A how to Approach,* 2nd ed. New York: Springer-Verlag, 1994.

Lyons, P. B. and J. Stevens. ñTime Response of Plastic Scintillators.ò *Nuclear Instruments and Methods* 114 (1974): 313-320.

Mitrica, Bogdan. ñ20 years of cosmic muons research performed in IFIN-HH.ò *Exotic Nuclei and Nuclear/Particle Astrophysics (IV) From Nuclei to Stars AIP Conference Proceedings* (2010): 291-303.

Murphy, T. J. and R. A. Lerche. ñDevelopment of a geometrically-compensated neutron time-of-flight detector for ICF applications with approximately 200 ps time

response,ò *The Review of Scientific Instruments* 63, (1992): 4883-4885.

Murphy, T. J. and R. A. Lerche, C. Bennett, G. Howe. ñIon Temperature Measurements of Indirectly Driven Implosions Using a Geometry Compensated Neutron Time-of-Flight Detector.ò *The Review of Scientific Instruments* 66, (1995), 930-932.

Murphy, T.J. *et. al,* ñNeutron Time-of-Flight and Emission Time Diagnostics for the National Ignition Facility,ò *The Review of Scientific Instruments* 72 (2001): 850-853.

Nelson, A. J., *et al.* ñA novel method for modeling the neutron time of flight detector response in current mode to inertial confinement fusion experiments.ò *The Review of Scientific Instruments* 83, number 10 (2012): 10D915.

Ortec. *Fast-Timing Discriminator Introduction.* Oak Ridge: Ametek Advanced Measurement Technology.

Peter K. and F. Grieder. *Cosmic Rays at Earth: Researcher's Reference Manual and Data Book*. New York: Elsevier, 2001.

Platino, M., et. al. ñFabrication and testing system for plastic scintillator muon counters used in cosmic showers detection.ò *32nd International Cosmic Ray Conference, Beijing* vol. 4 (2011): 330-333.

Post, R. F. and L. I. Schiff. ñStatistical Limitations on the Resolving Time of a Scintillation Counter.ò *Physical Review* 80 (1950): 1113.

Ruiz, C. L. and R. W. Huggett, P. N. Kirk. ñResponse of Plastic Scintillation Counters to Relativistic Heavy Ions.ò *Nuclear Instruments and Methods* 159 (1979): 55-60.

SASfit Manual. ñExponentially Modified Gaussian.ò Accessed 17 March 2014. http://sasfit.ingobressler.net/manual/Exponentially_Modified_Gaussian.

SAS/STAT® 9.2 Userôs Guide, Second Edition, ñMean Squared Error,ò accessed 11 March 2014, https://support.sas.com/documentation/cdl/en/statug/63033/HTML/default/viewer.htm#statug_intromod_sect005.htm .

Stanev, Todor. *High Energy Cosmic Rays*, 2nd edition. Chichester: Springer, 2010.

SYSTAT Software Inc., *PeakFit: Peak Separation and Analysis Software,* 2002.

Taylor, John R. *An Introduction to Error Analysis: The Study of Uncertainties in Physical Measurements,* 2nd ed. Sausalito: University Science Books, 1997.

Thomas, D. J. ñNeutron spectrometry.ò *Radiation Measurements* 45 (2010): 1178-1185.